DESIGN AND ANALYSIS OF MAC PROTOCOLS FOR WIRELESS MULTI-HOP SENSOR AND TERAHERTZ NETWORKS

A Dissertation
Presented to
The Academic Faculty

By

Jian Lin

In Partial Fulfillment
of the Requirements for the Degree
Doctor of Philosophy
in
Electrical and Computer Engineering

School of Electrical and Computer Engineering
Georgia Institute of Technology
May 2015

DESIGN AND ANALYSIS OF MAC PROTOCOLS FOR WIRELESS MULTI-HOP SENSOR AND TERAHERTZ NETWORKS

Approved by:

Dr. Mary Ann Weitnauer, Advisor
Professor, School of ECE
Georgia Institute of Technology

Dr. Gregory David Durgin
Professor, School of ECE
Georgia Institute of Technology

Dr. Chuanyi Ji
Professor, School of ECE
Georgia Institute of Technology

Dr. Ellen Witte Zegura
Professor, School of CS
Georgia Institute of Technology

Dr. Ian F. Akyildiz
Professor, School of ECE
Georgia Institute of Technology

Date Approved: February 04, 2015

To my parents and my wife.

ACKNOWLEDGMENT

It is my pleasure to thank many people who have helped through this process. First and foremost, I wish to express my deepest gratitude to my PhD advisor, Prof. Mary Ann Weitnauer (Ingram), for her guidance, inspiration, encouragement, and continuous support. With her passion, immense knowledge, and insightful coaching, she has made every bit of discussion an exciting learning process for me. Not only I am deeply indebted to her for providing me with insightful technical advice during my doctoral study, but also I appreciate her genuinely kindness and excellent personal rapport for me. It has been a real honor and privilege to be her student and work with her.

My special thanks go to the members of my thesis committee, Prof. Chuanyi Ji, Prof. Douglas Blough, and Prof. Ian F. Akyildiz for being on my thesis reading committee. Their enlightening suggestions have greatly improved my research and the quality of this dissertation. I express my deep appreciation to Prof. Gregory Durgin and Prof. Ellen Zegura for being on my dissertation committee and their helpful discussions in improving this dissertation.

My grateful thanks also extend to the Professors at NYU Polytechnic School of Engineering, Prof. Shivendra Panwar, Prof. David Goodman, and Prof. Thanasis Korakis for writing recommendations for my PhD study and giving me tremendous advice and encouragement. I also owe a great deal to my friend and alumnus Dr. Feilu Liu at Qualcomm, one of the kindest men I have ever known. His guidance and encouragement have been leading me towards my Ph.D research.

I thank my awesome friends and colleagues at the Smart Antenna Research Lab, Dr. Haejoon Jung, Dr. Jin Woo Jung, Dr. Yongjun Chang, Dr. Aravind Kailas, Dr. Syed Ali Hassan, Dr. Lakshmi Thanayankizil, Alper Akanser, Qiongjie Lin, Wang Feng, Abdul Javaid, Van Nguyen, and Gaurav Pradhan, for their everlasting friendship and unlimited

support, and for making SARL a lively home. I also thank the visiting scholars, Prof. Zhihao Yun, Dr. Xia Nan, Dr. Wensi Wang, Dr. Hongzhi (Jason) Jiao, Dr. Nikolaj Marchenko, Dr. Gao Zhen, Zhenzhe (Stephen) Sun, Lakshmikanth Guntupali, Mingxi Zhang and Dr. Bing Xie, for enjoying the life together at Atlanta and making lasting memories. To many others go my gratitude for valuable discussions and conversations, some of which were directly related to this dissertation, others of which were helpful to me personally and/or professionally along the way. To Dr. Xiong Cong, Chong Han, Cen Lin, Yun Wei, Qingsong Wen, and many others at GT ECE, to Dr. Yi Gai and Dr. Yiting Liao at Intel, thank you for the many interesting and enlightening discussions and for your support, encouragement, and insights.

To my wife Siming goes all the gratitude of my heart. Without her love, I would never finish my Ph.D. She is always believing in me no matter where I am in ups and downs, and is willing to cook my favorite meals everyday even she works full-time like me. I don't have room in this dissertation to express my appreciation for her; however, I owe all my achievement to her.

Last but not the least, to my parents, remotely in China, go many special gratitude for their perpetual love and support. From my birth they have raised me with whatever they can afford, and sacrificed many things so that I may pursue the best education possible. The success in my education and career, that I had, have, and will have, is impossible without them. I am eternally indebted to them.

CONTENTS

LIST OF TABLES

LIST OF FIGURES

SUMMARY

The contributions of this thesis include designing and analyzing novel medium access control (MAC) protocols for two types of wireless networks: (1) duty-cycling cooperative multi-hop wireless sensor networks (MHWSNs), and (2) single-hop Terahertz networks (TeraNets).

For MHWSNs, the specific contributions are two new scalable MAC protocols for alleviating the "energy-hole" problem with cooperative transmission (CT). The energy-hole is known to limit the life of battery-powered MHWSNs. The hole occurs when nodes near the Sink exhaust their energy first because their load is heavier: they must transmit packets they originate and relay packets from and to other nodes farther from the Sink. Effective techniques for extending lifetime in MHWSNs include duty cycling (DC) and, more recently introduced, cooperative transmission (CT) range extension. However, a scalable MAC protocol has not been presented that combines both. From the MAC perspective, conducting CT in an asynchronous duty-cycling network is extremely challenging. On the one hand, the source, the cooperators and the destination need to reach consensus about a wake-up period, during which CT can be performed. This dissertation develops novel MAC protocols that solve the challenge and enable CT in an asynchronous duty-cycling network. On the other hand, the question arises, "Does the energy cost of the MAC cancel out the lifetime benefits of CT range extension?" We show that CT still gives as much as 200% increase in lifetime, in spite of the MAC overhead.

The second contribution of this dissertation is a comprehensive analytical framework for MHWSNs. The network performance of a MHWSN is a complex function of the traffic volume, routing protocol, MAC technique, and sensors' harvested energy if sensors are energy-harvesting (EH) enabled. The optimum performance provides a benchmark for heuristic routing and MAC protocols. However, there does not exist such an optimization

framework that is able to capture all of these protocol aspects. The problems and performance metrics of non-EH networks and EH networks are different. Because the non-EH nodes depend on a battery, a suitable performance metric is the lifetime, defined as the number of packets delivered upon the first or a portion of nodes' death. Thus, the lifetime is governed by the absorbing states in a controlled dynamic system with finite decision horizon. On the other hand, the lifetime of an EH network is theoretically infinite unless the sensors are broken or destroyed. Therefore, an infinite horizon problem is formulated towards the performance of EH networks. The proposed model departs significantly from past analyses for single-hop networks that do not capture routing and past analyses for multi-hop networks that miss MAC aspects. To our knowledge, this is the first work to model the optimal performance of MHWSNs, by jointly considering MAC layer link admission, routing queuing, energy evolution, and cooperative transmission.

The third contribution of this dissertation is a novel MAC protocol for Terahertz (THz) Band wireless networks, which captures the peculiarities of the THz channel and takes advantage of large antenna arrays with fast beam steering capabilities. Communication in THz Band (0.1-10THz) is envisioned as a key wireless technology in the next decade to provide Terabits-per-second links, however, the enabling technology is still in its infancy. Existing MAC protocols designed for classical wireless networks that provide Megabits-per-second to Gigabits-per-second do not scale to THz networks, because they do not capture the peculiarities of the THz Band, e.g., the very high molecular absorption loss or the very high reflection loss at THz Band frequencies. In addition, to overcome the high path loss and extend communication range, the proposed MAC design takes advantage of fast beam steering capabilities provided by the large antenna arrays, in particular, beam-switching at the pulse level.

CHAPTER 1

INTRODUCTION

1.1 Network Lifetime of Multi-hop Wireless Sensor Networks

Multi-hop wireless sensor networks (MHWSNs) usually consist of a vast number of integrated system-on-a-chip devices (nodes) that are powered by batteries and equipped with less capable micro-controllers and limited memory. These nodes make local measurements and send the data through multiple hops to the remote gateway, i.e., the Sink node. It is desirable that the energy constrained network operates unattended for a long period of time, especially when those networks are deployed in human-prohibited areas where replacing nodes is infeasible or too costly. Therefore, the network lifetime is among the paramount considerations when designing medium access control (MAC) protocols. Various data gathering applications that favor long lifetime include, among others, environmental monitoring, animal habitat tracking and border intrusion detection [1].

The network lifetime is often defined as the number of packets delivered to the Sink when the first node or a portion of nodes deplete their energy. The *energy-hole* is a known problem to limit the lifetime of multi-hop WSNs, in which an intermediate node that is carrying heavier traffic has to spend more energy and consequently exhausts earlier [2]. If this node is the only node connecting two parts of a network, then a network partition or energy hole occurs when the node dies. Generally, the nodes near the Sink are heavily burdened and are prone to the energy-hole. Consequently, energies outside of the holes are trapped and unused.

Besides data transmission and reception, the major sources of a node's energy consumption inherent to MACs include idle listening, overhearing, and collision [3]. Idle listening means that nodes keep listening to the channel while there are no incoming packets at all - a condition that still exists in many MAC protocols such as IEEE 802.11 [4] wherein WIFI stations must listen for possible traffic. Notably, idle listening is disastrous in WSNs

based on the fact that nodes in this mode consume the same magnitude of power as in receiving [3]. Overhearing means that nodes decode packets that are destined to others. Collisions result in corrupted packets and the following MAC layer retransmissions consume extra energy. From the network perspective, while these factors reduce an individual node's lifetime, the network lifetime is more critically limited by the "energy holes" near the Sink leaving ample energy outside of the holes.

Duty cycle (DC) MAC is a popular energy conserving mechanism [3]. By allowing nodes to switch between active and sleep modes by turning the radio on and off periodically, nodes save substantial energy by reducing the periods of idle listening and overhearing. In particular, DW-MAC [5] has been shown to have superior energy saving for individual nodes. Unfortunately, DW-MAC and the others do not solve the energy hole problem in multi-hop WSNs, due to their inability to balance energy consumption.

Cooperative transmission (CT) range extension is a particular promising energy-balancing method [6]. CT is a mixture of physical layer combining techniques and communication protocols that allows spatially separated single-antenna nodes to collaborate to form a virtual multiple-input-single-output (VMISO) array [7]. The source node first multi-casts a packet to the neighboring cooperators, which then send the packet in orthogonal and in-band diversity channels. The destination receiver obtains a significant signal-to-noise ratio (SNR) advantage through physical layer combining. The SNR advantage can be used to increase transmission rate, reduce transmission power or achieve a longer transmission range. The range extension property of CT has been shown, in concert with routing, to correct the energy imbalance and extend network lifetime by factors of two or more, as in [6] [8]. In particular, in the Residual-Energy-Activated Cooperative Transmission (REACT) protocol introduced in [6], a node on the primary route, instead of forwarding the packet to the next-hop node that has lower residual energy, can transmit to the Sink directly by recruiting cooperators, and therefore the bottleneck nodes in the network are protected. However, the increased control overhead (OH) from CT was not considered in [6] [8]. Also, [6] [8]

did not consider how CT could be merged with duty cycling, which is a popular way to conserve energy and extend the life of a WSN. From the MAC perspective, conducting CT in an asynchronous duty-cycling network is extremely challenging, because the source, the cooperators and the destination need to reach consensus about a wake-up period, during which CT can be performed. Also, the question arises, "Does the energy cost of the MAC cancel out the lifetime benefits of CT range extension?" Therefore, a part of this thesis addresses this challenge and answers this question.

For MHWSNs, this dissertation addresses designing MAC protocols to alleviate the "energy-hole" problem and extend the network lifetime [2] by jointly considering cooperative transmission and duty cycling and properly accounting for the control packet overhead. In particular, ours is the first work to solve the spatial challenges that the source, cooperators and the destination are not located in one collision domain (i.e., within transmission range of each other), and the temporal challenges that all nodes should be scheduled stay active when CT is performed.

1.2 Modeling of Multi-hop Wireless Sensor Networks

The network performance of a MHWSN is a complex function of sensors' energy, traffic volume, routing protocol, and medium access (MAC) technique. An analytical approach that is suitable for WSN traffic and that derives the optimal performance would serve as a valuable benchmark for heuristic MAC and routing protocols. However, such a multi-hop framework has not been presented. In this dissertation, we consider such an approach for both energy constrained (EC) networks and energy harvesting (EH) networks.

In the context of non-CT based WSNs, existing analyses have mainly focused on a single node [9], a single link [10] or a single-hop network [11]. Departing from the literature, we address the general multi-hop network with neither assumptions on node distribution nor assumptions on total traffic pattern, motivated by the following reasons. First, since the communication range of a single node is limited, single-hop deployment cannot meet the

requirements of many applications, such as environmental and structural monitoring, security and defense, and wireless body area networks. Second, the traffic pattern of nodes in a MHWSN is unbalanced, invalidating the homogeneous or deterministic traffic assumptions, which are widely assumed for wireless ad-hoc or mesh networks. Therefore, the works based on these assumptions cannot capture the "energy hole" problem for EC networks, as introduced in Section 1.1. Moreover, the traffic unbalance is not known a priori, and is actually determined by a routing protocol. Therefore, towards quantifying the network performance, careful consideration should be taken to capture the peculiarity of the traffic pattern. Third, because the network's energy consumption rate is closely related to nodes' interaction in various aspects including channel access, routing and cooperation, the optimal solution obtained by focusing only on a point-to-point link does not imply the global optimum for the network-wide objective. In fact, quantifying the latter problem is fairly challenging.

On another track, cooperative transmission (CT) range extension, as introduced in Section 1.1 and experimentally demonstrated in [12], has shown significant impact on Layer Two and Layer Three of a WSN by eliminating the "energy hole" in EC networks [13] and providing better Quality of Service in EH networks [14], necessitating a network analysis that also incorporates CT. From the Layer Two perspective, though existing heuristic CT MAC protocol designs, such as [13] [15], show notable lifetime improvement over other non-CT based MAC protocols, the performance gap between the CT protocols and the optimal performance is unresolved. From the Layer Three perspective, it is noted that the analysis in [14], among others, assumes perfect link scheduling, which contrasts with the practical situation wherein link activities are subject to MAC constraints and packet collisions occur. All the above discussions have further motivated our analysis to comprehensively consider energy harvesting, routing, MAC and Cooperation, from the network perspective.

Therefore, this dissertation addresses presenting a comprehensive analytical framework

for MHWSNs to capture all of those protocol aspects, for both EC networks and EH networks. In particular, the EC network is modeled as a controlled dynamic system with finite decision horizon, and an infinite horizon problem is formulated towards the performance of EH networks. Another distinctive feature of the proposed model is the inclusion of CT, which is in stark contrast to most analytical works that consider only non-CT networks. The proposed model departs significantly from past analyses for single-hop networks that do not capture routing and past analyses for multi-hop networks that miss MAC aspects. To our knowledge, ours is the first work to model the optimal performance of MHWSNs, by jointly considering MAC layer link admission, routing queuing, energy evolution, and cooperative transmission.

1.3 MAC Design for Terahertz Networks

Wireless data traffic has drastically increased accompanied by an increasing demand for higher speed wireless transmission. In particular, wireless data rates have doubled every 18 months over the last three decades and are quickly approaching the capacity of wired communication systems according to Edholm's law of bandwith [16]. Following this trend, Terabit-per-second (Tbps) short-range communication in the Terahertz (THz) Band (0.1-10 THz) is envisioned as a key wireless technology in the next decade [17] [18] [19] [20]. Enabling THz Band communication will address the spectrum scarcity and capacity limitations of the current cellular system, and will boost a plethora of applications in biomedical, environmental, industrial and military fields [17] [18]. Much research has been recently performed towards channel modeling, antenna design and transceiver design [18]. However, the enabling technology is still in its infancy. Moreover, the protocol design in the system level is still unsolved. Existing MAC protocols designed for classical wireless networks that provide Megabits-per-second to Gigabits-per-second do not scale to THz networks, because they do not capture the peculiarities of the THz Band, e.g., the very high molecular absorption loss or the very high reflection loss at THz Band frequencies. In

addition, to overcome the high path loss and extend communication range, the new MAC designs need to take advantage of fast beam steering capabilities provided by the large antenna arrays. Also, existing research mainly focuses on nano-scale applications [21]. In this dissertation, we propose the first MAC protocol that is suitable for THz Band communication in the indoor picocell.

The extensive transmission loss necessitates very large antenna arrays with electronic beam-steering capability, and the communication over line-of-sight LOS or directed NLOS. However, the study of directional networking must be distinguished from the existing designs for cellular [22], broad-band [23], and WIFI based multihop wireless networks [24] operating at lower radio frequency (RF) bands, for the following reasons. First, the fact that the directivity achieved in THz Band is much higher gives a "pseudo-wired" abstraction of the wireless link and switches the role of the MAC to "coordination and scheduling" from the conventional "fighting for access." Second, most of existing protocols rely on omni-directional or sector-directional mode to solve neighbor discovery or the deafness problem. This dual-mode is not appropriate for THz because fully directional transmission is required to simply achieve the desired distance. For example, the only existing MAC protocol PHLAME [25] designed for nano-network operating in Terahertz can work only in micro-scale, because PHLAME is in the "omni" category. Third, direct paths could be completely blocked by obstacles between a transmitter and its receiver. The blockage foresees and necessitates directed non-line-of-sight (NLOS) paths reflected from walls, ceilings or a dedicated reflective mirror [18], requiring new MAC solutions.

Our approach is motivated by the advancements in Graphene-based electronics, including the novel plasmonic nano-antennas [26], compact plasmonic pulse generators and detectors [27] [28], and nano-antenna arrays with scanning capability [29]. On the other hand, the feasibility of carrier-based modulation is limited by the lack of compact transceivers able to generate carriers at THz Band frequencies. Recently, femtosecond-long pulse-based modulation has been proposed to capture the expected capabilities of THz signal generator

and detectors [30]. However, for the time being, pulse-based directional transmission has not been explored in system design in THz networks. Aimed to fill this gap, building on Time Spread On-off Keying (TS-OOK) [30], this dissertation presents the MAC design to capture the peculiarity of THz channel and the expected THz transceiver capabilities, as well as analytical studies to quantify the system capacity at macro-scale ranges.

Therefore, the third contribution of this dissertation is on designing a novel MAC protocol for Terahertz (THz) Band wireless networks, which captures the peculiarities of the THz channel and takes advantage of large antenna arrays with fast beam steering capabilities. With pulse-based communication, we are the first to also optimize the inter-pulse separation (IPS) and inter-pulse separation (ISS), and present a MAC protocol that explores the IPS and ISS.

CHAPTER 2

ORIGIN AND HISTORY OF THE PROBLEM

In this chapter, we review some of the works that are related to the topics addressed in this dissertation. In Section 2.1, we overview the popular lifetime enhancement techniques for multi-hop wireless sensor networks (MHWSNs). The duty cycling MAC protocols and cooperative MAC protocol are discussed in Section 2.1.1. Moreover, some particular methods for attacking the "energy hole" problem are introduced in Section 2.1.2. In Section 2.2, we highlight the challenges in modeling MHWSNs in the presence of unbalanced traffic, and review the existing analytical models for WSNs and their limitations. In Section 2.3, we introduce the motivation of communications in Terahertz (THz) Frequency Bands, and emphasize the design direction of a new MAC that operates in THz Bands and captures the peculiarities of the THz wireless channel.

2.1 Lifetime Enhancement for Wireless Sensor Networks

In general, network longevity can be achieved from two strategies: energy *conservation* and energy *balancing*, which are individual node oriented and network oriented, respectively. Duty cycle (DC) MAC, e.g., [3], is a popular energy conserving mechanism that alternates each node between active and sleep modes by turning the radio on and off periodically. Cooperative transmission (CT) range extension [7] is recently proposed as an energy balancing scheme to solve the "energy hole."

2.1.1 Duty Cycling and Cooperative MAC Protocols

Duty cycling has been widely investigated as an essential component in MAC protocols to save energy consumption [3] [5] [31] [32] [33]. By cycling between active and dormant modes, nodes reduce idle-listening and thus conserve energy substantially in sleep periods. Duty cycle MAC protocols fall mainly into two categories: synchronous and asynchronous protocols. Synchronous protocols such as S-MAC [3] and DW-MAC [5] align nodes to

wake up and sleep at the same time. However, these protocols require network-wide synchronization, which consumes extra energy to maintain and introduces more packet collisions. Asynchronized approaches including B-MAC [31] and X-MAC [32] allow nodes to maintain active-sleep schedules independently; these protocols rely on low power listening (LPL), which requires appending a long preamble before each data transmission, which is energy inefficient. Moreover, the channel utilization efficiency is low, because the channel is excessively occupied by the preamble, preventing neighboring nodes to transmit. RI-MAC [33] switches the burden of the sender to the the receiver, which transmits a packet upon waking up, to poll the senders. However, senders still need to stay awake to listen for the polling packet. Although duty-cycling techniques save energy for individual nodes, none of the the reported studies solves the "energy hole" problem due to their inability to balance energy in MHWSNs.

Cooperative transmission (CT) [7] is a physical layer communication scheme, in which spatially separated users or nodes collaborate to form a virtual antenna array. The collaborating nodes transmit the same source message through multiple independently faded channels to the receiver, which decodes the message through physical layer combining. CT has been deeply explored in the physical layer [7] [34] [35] [36]. According to the synchronization requirements at the cooperative node, there are three types of CT schemes: coherent beamforming (CB), time division CT (TDCT) and concurrent CT (CCT). In addition to the physical layer, there is also increasing interest in Layer Two and Layer Three supporting CT [37] [38] [39], and some cross-layer design [40]. Nevertheless, three limitations exist in the current literature. First, though many authors have considered how the SNR gains may benefit a wireless network in terms of increasing link reliability [38] and reducing transmit power [41], relatively less attention has been given to the benefits of CT range extension. Second, while the improvements in single-hop networks have been studied through diverse examples [38] [39], the studies on cooperative multi-hop networks that provide explicit MAC signaling procedure are limited. Third, as ad-hoc network oriented,

none of these works considers duty cycling, and thus the lifetime issue is not addressed. Although some work such as LC-MAC [42] demonstrates energy efficiency of CT, without duty cycling, no noticeable lifetime benefits can be derived. Cooperative transmission (CT), when used as a range extension forwarding scheme, is shown in [6] to overcome the energy hole problem; however, the analysis in [6] includes neither MAC nor duty cycling.

Though many other authors have proposed MACs to support CT [7] [38] [41] [42], these works pay less attention to the range extension property of CT, and thus none of them addresses network lifetime or alleviates the *energy hole* problem. Further, all these CT protocols make the spatial assumption that the source, cooperators and the destination are located in one collision domain (i.e. within transmission range of each other), and the temporal assumption that all nodes stay active when CT is performed. The spatial assumption is not generally true for multi-hop networks, and the temporal assumption is not generally satisfied in asynchronous duty-cycle networks.

While most of the CT MACs pay less attention for the range extension aspect of CT, to the best of our knowledge, the only works that explicitly consider MAC design with CT range extension are [43] [40] [44]. Again, [43] and [40] do not address the lifetime issue as they do not consider duty cycling and do not alleviate the "energy hole" problem. CDC-MAC [44] is mostly related as it also considers CT in a duty cycle context; unfortunately, it addresses only the two-hop networks and lacks scalability to the multi-hop networks.

2.1.2 Methods of Attacking Energy Hole

The energy hole is a known problem that limits the lifetime of a multi-hop WSN. Existing solutions for the energy-hole problem focus mainly on the network-layer protocols, such as (i) the non-uniform node deployment [45] [46] [47] and (ii) the mobile-relay strategy [48] [49]. In the non-uniform deployment scheme, additional nodes are placed in the area close to the Sink, and routes are selected so that nodes can evenly consume the energy. The downside of this strategy is that it can drastically increase the cost of deployment

because of the required additional nodes [45]. On the other hand, when the number of available nodes in the network is fixed, the non-uniform strategy decreases the sensing/coverage area of the network because the extra nodes deployed near the Sink node could have been used to cover other areas. The mobile-relay strategy determines the movement of mobile nodes and routes (to send packets via mobile node) to mitigate the energy-hole problem. However, as noted in [48], mobile relays may be hard to operate in certain environments such as under a bridge, on water, and in an unpaved area. Last, a common issue is that these routing strategies look at only transmission and receiving, while overlooking the energy consumption in idle listening and overhearing whose magnitude is comparable to transceiving [3].

2.2 Analysis of Wireless Sensor Networks

Many analytical investigations are limited to a single transmission link or single-hop networks. In [9] , the focus is on energy management of a single node for achieving maximum throughput and minimizing delay assuming a linear rate-power curve. The optimal power management for sensor nodes is studied in [50], assuming a leaky-bucket type property for the harvested energy. In [11], the stochastic shortest path as a special case of Markov decision process (MDP) [51] is used to formulate the lifetime of a *single-hop* network, which considers sensor scheduling in a scenario where only a fraction of sensors collect information and communicate directly with a one-hop Sink. In [52], considering nodes that are equipped with a hybrid energy storage system, the authors provide a MDP model for *single-hop* energy-harvesting (EH) network. [53] studies the game-theoretic approach to obtain the equilibrium for saving energy at a sensor node. [54] gives a general model for wireless interference, which is more accurate than a pure analytical model because it is based on measurements; however, [54] focuses only on one-hop traffic demands, instead of multi-hop traffic demands. Since the transmission range of sensors is limited, single-hop

deployment cannot meet the requirements of many applications, such as structural monitoring, security and defense, and wireless body area networks. Further, analyses based on single-hop traffic cannot capture load difference of nodes when the traffic must go through multiple hops. Moreover, none of these works considers cooperative transmission. Therefore, the applications of the analyses in aforementioned works are limited.

Analyses of multi-hop networks have been treated with various approaches. The optimal lifetime of a multi-hop WSN is derived in [55] using linear programming (LP) formulation based on traffic balance conditions. In [56], the authors provide a Lyapunov analysis for multi-hop EH WSNs, which considers the dynamics of energy and queue, to maximize the utility. [57] studies the upper bound on the lifetime of data gathering sensor networks, while [58] derives the upper bound on the lifetime of large-scale networks using the theory of coverage processes. Both [57] and [58] are based on the assumption that the data sources are deployed with a particular probability density function or process. Note that all the aforementioned works fail to consider MAC constraints, as they assume perfect link scheduling, and thus ignore packet losses and retransmissions, which contrasts the practical situation wherein link activities are subject to MAC constraints and packet collisions occur. Moreover, none of these works considers cooperative transmission.

The past analyses of cooperative networks are typically limited to single-hop networks. In [59], the authors consider the lifetime maximization in an amplify-and-forward cooperative network and model the energy dissipation of nodes as a Markov chain. In [60], the authors develop a general probability model to study the outage performance of the best-relay selection with adaptive decode-and-forward cooperative network. Relatively less works have focused on analysis of multi-hop cooperative networks. The LP model in [55] has been recently extended to multi-hop CT networks [61] by considering all single-input-single-output (SISO) and virtual multiple-input-single-output (VMISO) links. Again, none of these works has considered MAC layer link constraints, and therefore the bounds that they provide are somewhat over-optimized. Moreover, because the interference range has

significant effect on the performance of the MAC, and the interference range of CT could differ from that of a SISO transmission, a complete evaluation of multi-hop cooperative networks is hard to obtain without the inclusion of MAC constraints.

2.3 Communications in Terahertz Networks

Over the last few years, wireless data traffic has drastically increased accompanied by an increasing demand for higher speed wireless transmission. In particular, wireless data rates have doubled every eighteen months over the last three decades and are quickly approaching the capacity of wired communication systems [16]. Following this trend, communication in the Terahertz Band (0.1-10 THz) is envisioned as a key wireless technology in the next decade [62] [17] [18] [19] [20] [63]. Teraherts (THz) Band communication that escalates the frequency and will deliver unprecedented data rates is becoming a reality in the next decade. Networks operating in THz Band ("TeraNets") will enable a plethora of long-awaited applications, such as uncompressed high-definition media transfers, and ultrafast massive data transfers among nearby devices. The THz Band is not yet regulated. Recently, the IEEE 802.15 Wireless Personal Area Networks (WPAN) Terahertz Interest Group (IGthz) [64] has been created.

Several reasons have motivated the research of the THz Band to increase the capacity of wireless networks: (1) Wireless technologies below 100 GHz cannot currently support Terabit-per-second (Tbps) links. Although advanced modulations and sophisticated schemes, e.g., OFDM and Massive MIMO, can achieve very high spectrum efficiency at frequencies below 5 GHz, the available bandwidth is very scarce. The Long-Term Evolution Advanced (LTE-A) targets the peak rate of 1 Gbp, and the current systems in the 60 GHz band can currently achieve only bit rates up to 10 Gbps within one meter [65], both of which are well below the target rates in TeraNets. (2) Wireless technologies above 10 THz do not currently support Tbps links. On the one hand, IR technologies achievable data-rates that are limited to a few hundreds of Megabit-per-second (Mbps), because of

the poor sensitivity in incoherent receivers, high diffuse reflection losses, and high ambient noise [62] [63]. On the other hand, free-space optical wireless communication systems [66] [67] must solve challenges for developing compact and energy efficient sources and broadband modulators. Only 10 Gbps have been demonstrated for the free-space optical system. (3) THz Band communication can contribute to major energy savings. The very short bit transmission time and very simple modulation and demodulation contribute to energy savings for the transceivers. Also, the high direction beam transmissions are more energy efficient than omni or sector transmissions, and the directivity is much higher than other communication systems due to the very large number of antennas that can fit on chips or boards [68] [69].

The bigger project "TeraNets" aims to establish the foundations of ultra-broadband communication addressing several research challenges including transceiver design, antenna design, channel modeling, modulation and coding, and medium access control (MAC) protocol. This dissertation considers the MAC layer design and analysis. The reason that existing MAC protocols and their simple modifications designed for lower frequency bands do not apply to TeraNets is, existing protocols do not capture the peculiarity of THz channel characteristics and expected capability of THz transceivers. Fig. 1 depicts the path loss in the THz Band for different transmission distances [70]. The path loss consists of spreading loss and molecular absorption loss. The spreading loss accounts for the attenuation due to the expansion of the wave as it propagates in the medium. The absorption loss accounts for the molecular absorption. From Fig. 1, we can make three observations. First, contrary to classical wireless networks, there are multiple transmission windows, which are several tens of Gigahertz wide each and which support the transmission at very high bit-rates (up to a few Tbps). Second, the bandwidth is not a fixed value, but there is a unique dependence between the transmission distance, the 3dB bandwidth of each transmission window and the achievable bit rate. Third, very high directivity antennas are needed to overcome the very high path-loss of the THz Band. Therefore, it is clear that novel MAC layer solutions

are required for TeraNets.

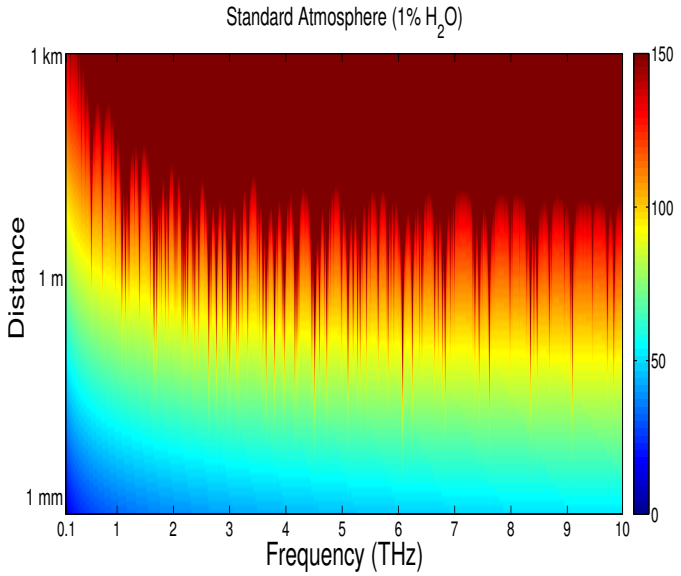

Figure 1. Path loss (in dB) in THz Band v.s. distances and frequencies. The peaks are caused by molecular absorption.

To overcome the extensive transmission loss, it is essential to utilize very electronically large antenna arrays with electronic beam-steering capability [18]. Many studies on directional protocols operating at lower radio frequency (RF) bands have been done for cellular [22], broad-band [23], and WIFI based multi-hop wireless networks [24]. However, these MAC designs for lower RF bands cannot be reused for TeraNets with simple modifications, due to the peculiarity of THz channel, large antenna arrays, and expected capabilities for modulation and demodulation. Most importantly, the directivity achieved in THz Band using very large antenna array is much higher; this renders a "pseudo-wired" [71] abstraction of the wireless link. In this case, traditional carrier sensing multiple access (CSMA) based MAC schemes (in both non-directional and directional networks) are not suitable for TeraNets. On the other hand, transmission failure due to collisions are very rare even under uncoordinated transmissions, as pointed in [71]. Therefore, the mainly functionalities of the MAC should focus on "coordination and scheduling," instead of channel contention and interference management, as seen in MAC protocols in lower RF bands. In

this context, time division multiplexing access (TDMA) seems an efficient choice for high-rate high-directional TeraNets. The promise of femtosecond-long pulses [27] [30] and ultra fast beamscanning capability of graphene-based antennas [29] at THz suggests the novel idea of pulse-level beamswitching, which will require new TDMA schemes for TeraNets. Though multi-band carrier-based modulation is possible theoretically, there does not exist a practical transceiver due to the lack of a supportive digital processor.

So far, the only works that study the MAC in THz bands are [72] and [73]. Both of these works are designed for nano-networks and also assume TS-OOK. First, these protocols work only in very short ranges (up to only a few millimeters), because none of the works takes advantage of large antenna arrays. Second, although they manage the reception at a common receiver from different transmitters at different time slot, these works assume omni transmission and reception, and do not explore beam steering capability of large antenna arrays, leaving the interference problem for omni transceivers unsolved. In addition, the assumed carrier sensing based access [72] is not appropriate for high directional picocell TeraNets. Moreover, none of these works solves the neighbor discovery problem.

Therefore, in this dissertation we present the first system design for picocell TeraNets by utilizing both the large antenna arrays and the pulse-level beam-switching capability. Tailoring to the peculiarities of THz channel and building on the assumed transceiver capabilities, we provide complete solutions for user discovery and acquisition, transmission scheduling, and, energy control for long range users.

CHAPTER 3

SCHEDULING DUTY CYCLE MAC: A DESIGN FRAMEWORK FOR COOPERATIVE WIRELESS SENSOR NETWORKS

In this chapter, we provide a systematic solution to enable cooperative transmission in a duty-cycle multi-hop wireless sensor network (WSN). The proposed MAC protocol, SCT-MAC, serves as a design framework, which to our knowledge is the first work that incorporates both CT and duty cycling to enhance the lifetime of multi-hop WSNs.

The key contributions of this chapter are as follows. A simple duty cycle scheduling algorithm is proposed to establish a semi-synchronized network on the fly, and to provide the wake-up rendezvous for cooperators to reach a CT agreement. The staggered nature of the scheduling also alleviates channel contention and collisions while reducing end-to-end latency. A scheduling cooperative MAC protocol (SCT-MAC) is designed in this context to prolong network lifetime using cooperative diversity. We introduce a seamless contention and transmission scheduling scheme in SCT-MAC to support both direct transmission and dynamic cooperative transmission. The protocol is evaluated for random networks with 50 nodes using NS-2 simulations.

In the rest of the chapter, first we will give the network system overview, then we will present the detailed design of SCT-MAC protocol. The results from NS-2 simulations will show the efficacy of the proposed protocol in terms of network lifetime and packet delivery ratio.

3.1 Distributed duty cycle scheduling

In this section we describe the network model and the proposed duty cycle scheduling algorithm.

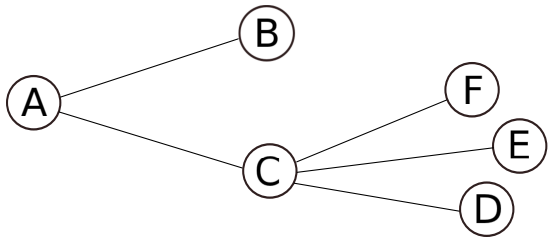

Figure 2. An illustrative 2-hop topology

In WSNs, data gathering from sensor nodes to one or more sink nodes is seen in numerous applications such as environmental monitoring, industrial monitoring, asset tracking and intrusion detection. A data gathering tree is formed by routing protocols. Such protocols include the emerging IPv6 Routing Protocol for Low Power and Lossy Networks (RPL) [74], which is currently under development by the Internet Engineering Task Force (IETF) for low power and lossy networks (LLN). In such a converge-cast tree, we call nodes that have no children the leaf nodes, and nodes that have at least one child the parent nodes. Although routes may change during network operation, we assume a primary route that is durable for a reasonable length of time.

In SCT-MAC, we use the concept of superframe that is bounded by network beacons sent by parent nodes, same as in IEEE 802.15.4 beacon mode. The beacon interval comprises an active period (superframe) and a sleep period. The lengths of the beacon interval and the superframe are defined as:

$$BI = aBaseSuperframeDuration \times 2^{BO} \tag{1}$$

$$SD = aBaseSuperframeDuration \times 2^{SO} \tag{2}$$

where BO and SO are the beacon order and the superframe order, respectively.

We require that each parent node should transmit beacons periodically to delimit its own superframe and deliver the residual energy information. We assume that one-hop and two-hop neighbors can interfere. Similar to [75], we assign the superframe of interfering parent nodes in the sleep period of each other, so that beacon and data transmission are collision free over adjacent flows. For example in Fig. 2, the beacons of Nodes B and C if

sharing the same schedule would collide at an intermediate node, such as A. All the leaf nodes upon joining the network follow the schedule of their parent nodes. The available number of time slots is determined by $N_s = 2^{BO/SO}$. Here BO and SO can be adjusted to fit for different network densities and traffic loads.

The network initialization is triggered at the sink. Each node around the sink first retrieves the time slots that have already been occupied by interfering parent nodes, and then selects a free slot based on the collected information. After that, a beacon is transmitted for the scheduling procedure to propagate over the rest of the network. Instead of randomly selecting a superframe slot, the active schedule slots of nodes on the path towards the sink are arranged in a cyclic increasing order within $[1, N_s]$, as shown in Alg. 1. To adapt for dynamic topology variation, a fixed broadcast slot with sufficient duration can be inserted periodically for beacon packets exchange.

Algorithm 1: Superframe scheduling

```
input:
p_t = Direct parent of Node t
I_t = Interfering parent set of Node t
S_a = {s ∈ [1, Ns] : s ≠ s_i ∀ i ∈ I_t,  s_i is the schedule of Node i}
output: s_t
begin
    S_a^d ← sort S_a in descending order
    for s ∈ S_a^d do
        if s < s_{p_t} then s_t ← s,   break ;
        if s = min S_a^d then
            s_t ← max S_a^d;
        end
    end
    return s_t
end
```

3.2 The Proposed SCT-MAC protocol

3.2.1 Overview

In this section, we present the details of the proposed SCT-MAC Protocol. The SCT-MAC is a semi-synchronized duty cycle MAC protocol, where each node maintains a brief wakeup at the start of the superframe of its direct parent and two-hop parent node. We

denote the two wakeups as $Sched_1$ and $Sched_2$. The superframe duration is divided into two periods: Scheduling and Data. We denote the duration of each period by T_{Sch} and T_{Data}, respectively. The main idea of SCT-MAC is to wake up nodes on demand during the data period, to support both direct transmission and cooperative transmission, which would otherwise be a mandatory active period as specified in IEEE 802.15.4. Different with DW-MAC, in which the sleep period is used to transmit and receive data, we keep the whole sleep period inactive. The reason comes from the intrinsic staggered beacon schedules.

Fig. 2 shows a two-hop multi-hop wireless network where the solid lines represent the routes toward a remote sink. A node talks to its direct parent (using non-CT) or the two-hop parent (using CT) in their scheduled active period; thus neighboring nodes can communicate even they have different schedules. For example, Node B and Node C can transmit to Node A during A's active period using non-CT, while Node D and Node E can transmit to Node A during A's active period using cooperative transmission. Unlike S-MAC where the latency could be as long as multiple duty cycles, the nature of the distributed beacon scheduling in our scheme enables multiple superframe allocation in a single beacon interval, thus ensuring lower latency.

As stated above, during the superframe of a receiving node, two types of incoming traffic are anticipated: the non-CT transmission from one-hop children and the CT transmission from two-hop children. To avoid collisions, these two types of traffic must contend for the channel. Note that in CT scenario, the source node and the helper are able to talk to the two-hop away receiver if and only if they transmit in a cooperative manner. In contrast, many existing works on CT assume the *one-hop contention* scenario in which the source, helper and destination are in one collision domain. Instead we address the contention scenario that involves both one-hop non-CT and two-hop CT, which we refer to as *two-hop contention*. We propose a seamless contention and scheduling scheme to support both one-hop non-CT and two-hop CT transmissions.

As IEEE 802.15.4 does not use virtual carrier avoidance (RTS/CTS), we introduce short

scheduling frames (SF) in the scheduling period, similar to DW-MAC. The time at which the pending packet will be transmitted in the data period, is specified by the SF sent from the receiver, which contains the number of transmissions that have already been reserved in the following data period. It is noted that the receiver has the knowledge of the number of non-CT and CT transmissions that have been scheduled, from the SF exchange with the senders.

3.2.2 Non-CT and CT transmission

In this section, we discuss protocol details using the network of Fig. 2.

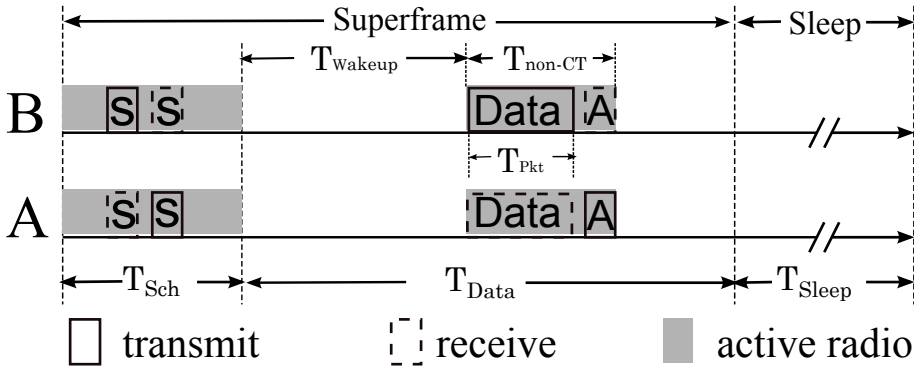

Figure 3. One-to-one Mapping for Non-CT Transmission

1) Non-CT case: When Node B has a pending packet for A, it first contends for channel access and transmits a SF during the scheduling period. As illustrated in Fig. 3, A after receiving, sends to B a SF which includes the number of non-CTs and CTs that have already been reserved, denoted as N_{non-CT} and N_{CT}, respectively. Both A and B determine the corresponding wakeup time instance T_{Wakeup} from the beginning of the subsequent Data period, according to:

$$T_{Wakeup} = T_{non-CT} \times N_{non-CT} + T_{CT} \times N_{CT} \tag{3}$$

where, $T_{non-CT} = T_{Pkt} + T_{Ack} + SIFS$ and $T_{CT} = 2T_{Pkt} + 2T_{Ack} + 3SIFS$. It is easy to see that for a particular receiver, no schedule conflicts will occur during the subsequent data period, and so data collision from different transmitters is avoided. When both A and B wake up at the scheduled time T_{Wakeup} in the data period, B immediately transmits the data packet to

A. If the packet is successfully decoded, A sends an ACK to B after short interframe space (SIFS).

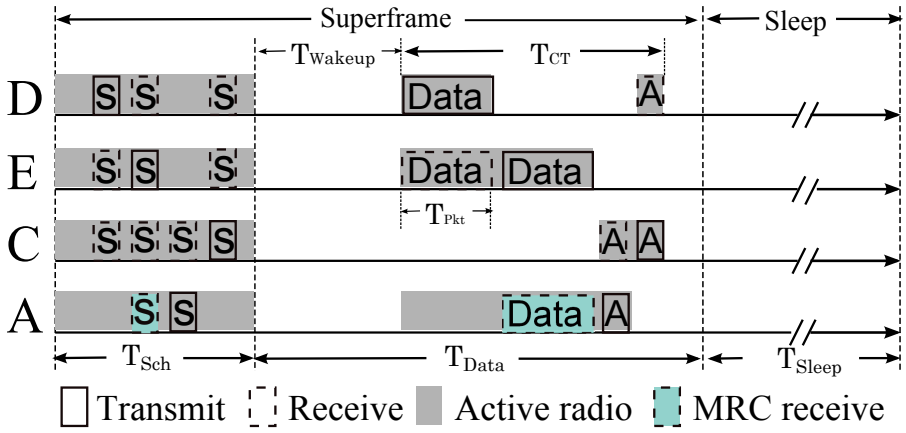

Figure 4. Cooperative Range Extension Case

2) CT case: Conducting CT for range extension in an asynchronous network is very challenging as the source, the cooperators and the destination need to wake up at a common rendezvous. The idea in the section is for the source and the cooperators to reach a CT agreement and complete the CT during the active period of the two-hop parent, which they have locked to as shown in last section.

The source node D: As shown in Fig. 4, when D decides to hop over its one-hop parent using cooperative transmission, it initializes CT by firstly sending a cooperative schedule frame (CSF) destined to the two-hop parent. The CSF also specifies the ID of the selected helper (such as E). Many measures can be applied to select the best helper such as best link quality, minimum distance, minimum load, etc, or a combination of those metrics. Inspired by REACT [6], we use a simple helper selection criterion by considering residual energy requirement as discussed in the following subsection.

The helper node E: If E receives the CSF from Node D which enlists itself as the potential helper, if it is available it sends a CSF the same as the incoming CSF to D to indicate its availability to help. Note that the CSF frames from D and E are transmitted in two orthogonal time slots, and can not be decoded separately by A which is the two-hop parent, however, they can be decoded jointly at A using Maximum Ratio Combining

(MRC) [36]; A then replies a SF to D and E in a two-hop manner, through the intermediate node C. Also A schedules a wakeup time instance T_{Wakeup} in the Data period according to Eq. (3), to receive the cooperative data transmission from Nodes D and E. If D and E receive the SF (A's reply) forwarded by C, then they schedule the same wakeup time, to proceed the data transmission in the data period.

As shown in Fig. 4, at time T_{Wakeup} Node D sends the data packet in the first time slot, which is decoded and forwarded by Node E in the next time slot. Node A, upon receiving the two independent copies of packets, decodes the original packet using MRC. Then it sends an ACK back to D in two hops through C. Note that D should go to sleep after sending its packet, to avoid overhearing the retransmission from the cooperator, and wake up again right before the expected ACK which is forwarded by C on behalf of A.

The intermediate node (one-hop parent C): As stated above, the role of Node C is to forward the control packets sent from Node A, such as SF and ACK. The SF is an acceptive reply for the cooperative transmission request initiated by Node D. The ACK is an acknowledgement of the correct reception of the cooperative data transmission from Node D and E. Both of the CSF frames from D and E can be overheard by their one-hop parent C; if C decodes either of the CSF it then anticipates to receive the SF replied from Node A. If SF is received, C forwards it to D and E. Also C schedules a wakeup time at $T_R = T_{Wakeup} + 2T_{Pkt} + SIFS$ to receive a possible ACK from A which is destined to Node D. Note that the goal of REACT is to hop-over the energy constrained node (e.g. Node C), however, completely avoiding the usage of Node C requires cooperative transmission at A's side, which adds extra energy cost with an increase in complexity of the protocol. Therefore, we let Node C forward only two control packets which are much shorter than the data packet, and allow C to sleep otherwise.

3.2.3 Triggering CT in REACT

After waking up at the beacon time of the parent, a node reads the residual energy of the parent from the beacon. According to REACT, it first compares the residual energy of the

parent E_p with its own energy E_t. If $E_p < E_t$, the node tries to initialize CT, by sending a Cooperation Request (CSF) during the superframe ($Sched_2$) of the two-hop parent, after Clear Channel Assessment (CCA) and Backoff. The CSF includes the ID of the selected cooperator and the ID of its two-hop parent. The cooperator, whose residual energy should be larger than the parent's, is selected from its sibling nodes and the siblings of its direct parent. Otherwise, if $E_p > E_t$ the data packet will be delivered directly to its direct parent during $Sched_1$.

Note that because a node has to wait for $Sched_2$ to initialize CT, the CT decision might be changed during the waiting. Similarly, a non-CT decision made at the moment when the packet is generated may need to switch to CT when $Sched_2$ arrives. So we provide a policy to handle this dynamic CT decision adjustment during the network operation based on energy information. The policy, summarized in Alg. 2, is designed to gain the balance between the benefits of CT and the avoidance of long latency.

Algorithm 2: Dynamic decision adjustment

```
input:
S_c = Current schedule ID
D_p = Previous decision on transmission method
output: Decision of CT or non-CT
begin
    D_n ← CTdecsion( )
    if S_c = 1 then
        if D_p = non-CT & D_n = CT then
            Wait for Sched_2 to do CT;
            Go to sleep if possible;
        end
        if D_p = CT & D_n = non-CT then Do non-CT now;
    else if S_c = 2 then
        if D_p = non-CT & D_n = CT then Do CT now;
        if D_p = CT & D_n = non-CT then Do CT now ;
    end
    return
end
```

Table 1. Simulation Parameters

Bandwidth	20 Kbps	Channel Enc. Ratio	2
Tx Power	31.2 mW	Tx Range	250 m
Rx Power	22.2 mW	CS Range	550 m
Idle Power	22.2 mW	Superframe Length	3071 ms
Sleep Power	3 uW	Cycle Length	24.58 s
State Transition Power	31.2 mW	Size of ACK	10 B
DIFS	2 ms	Size of SF/CSF	14 B
SIFS	0.6 ms	Size of Data	100 B
Contention Window	16 ms	Retry limit	5

3.3 Simulation Results

To show the effectiveness of the proposed protocol, we compare SCT-MAC with DW-MAC using NS-2.29. We generate 100 random network topologies where 50 nodes are distributed in a 1000 m $\times$ 1000 m area. The sink node is located in the center. The transmission range is 250 m and the carrier sensing range is 550 m. Although different devices would have different transmission range and carrier sensing range, the similar ratio between them is observed by measurements [76]. Same as DW-MAC, the Random Correlated-Event (RCE) traffic is assumed to simulate the burst traffic triggered by spatially-correlated events observed in detection and tracking applications. The event location is randomly picked every 100 seconds, and each node within the circle centered at the event location with radius R can sense the event and generates a packet destined to the sink. The radius R ranging from 100 m to 500 m is used to reflect different traffic loads. The initial energy is set to 50 $Joules$. Other simulation parameters are summarized in Table 2, in which DIFS means distributed interframe space. We use the default parameters in [5] for DW-MAC. The routing for SCT-MAC and DW-MAC is based on minimum distance.

Fig. 5 depicts the average number of packets successfully delivered to the sink with 95% confidence intervals, when the first node has depleted its energy. We observe that SCT-MAC doubles the network lifetime of DW-MAC for a variety of traffic loads.

Fig. 6 shows the average delivery ratio with 95% confidence intervals. Although both protocols have similarly high delivery ratio, SCT-MAC has a smoother curve with smaller

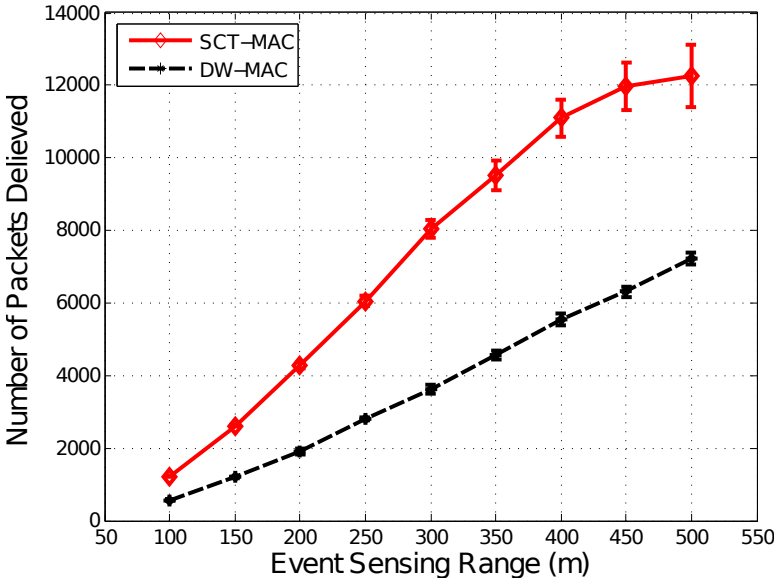

Figure 5. Network lifetime v.s. Event sensing range

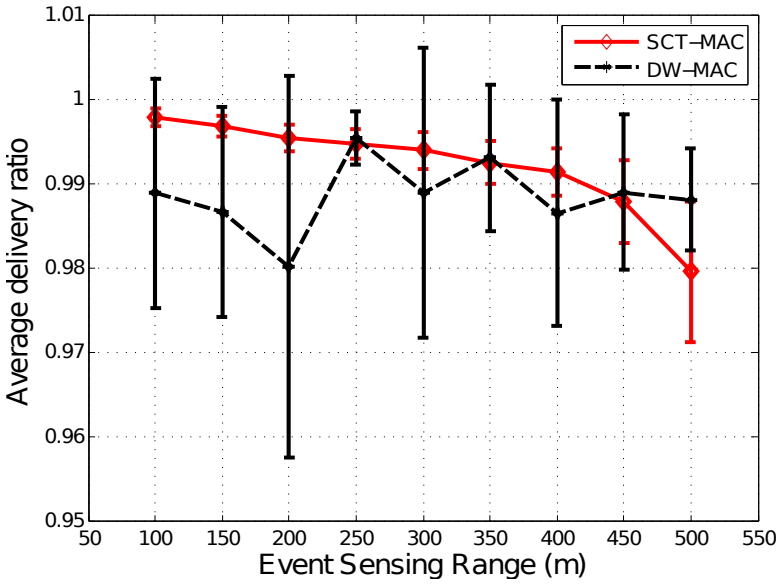

Figure 6. Delivery ratio v.s. Event sensing range

confidence intervals for all but the largest sensing range. Our results show that the average latency of SCT-MAC is approximately twice of that in DW-MAC, which is predictable because a CT transaction has to be done in $Sched_2$. The reward for increasing the latency is the very good lifetime extension.

The residual energy profile for each node when the first node has depleted its energy (with $R = 250m$) is presented in Fig. 7. Higher node IDs indicate nodes that are farther from

the sink. We observe that neither protocol depletes the energy around the sink, therefore they both avoid the energy hole problem. We also observe that even though SCT-MAC renders a doubled network lifetime when the first node dies, it still leaves a significant amount of energy trapped in the network. The relatively higher energy remaining near the sink suggests that the nodes surrounding the sink are somewhat overprotected by SCT-MAC; we will address this in Chapter 4.

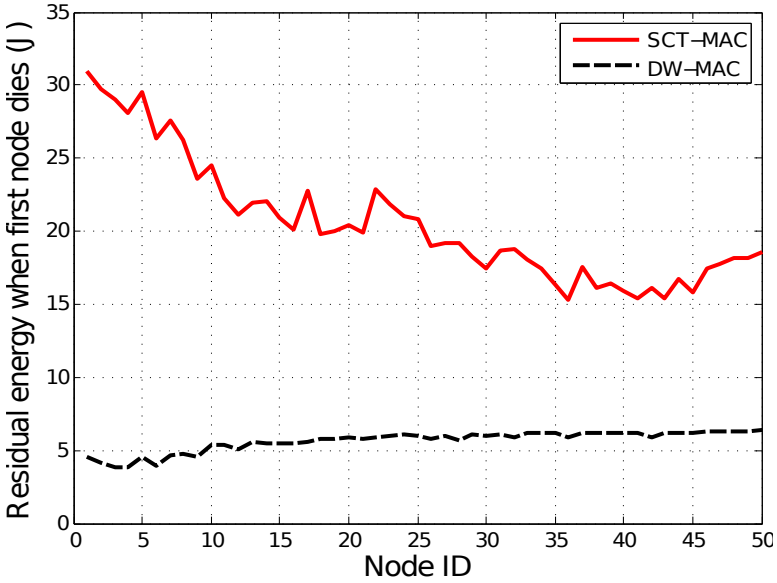

Figure 7. Residual energy profile when the first node has depleted its energy with event sensing range of 250 m

3.4 Conclusions

In this chapter, we propose a design framework to enable cooperative transmission in a duty cycle context. Specifically, a novel scheduling cooperative transmission MAC protocol (SCT-MAC) for multi-hop wireless sensor network is presented, which can extend the network lifetime significantly. A distributed duty-cycle scheduling algorithm is introduced to let nodes wake up on demand in the data period. The duty cycle scheduling algorithm provides a wake-up rendezvous for cooperators and their destination to reach a CT agreement and reduces contention over adjacent flows. The on-demand wake-up further reduces

idle listening in the data period. SCT-MAC, with CT range extension strategy and staggered duty-cycling, alleviates the energy hole problem and improves the network lifetime by approximately 100% compared with DW-MAC.

CHAPTER 4

ON-DEMAND DUTY CYCLE SCHEDULING AND COOPERATION IN MULTI-HOP WIRELESS SENSOR NETWORK

In Chapter 3, we have presented the first design framework that enables cooperative transmission in duty-cycling multi-hop WSNs. However, the idle listening has not been sufficiently reduced due to the fixed scheduling scheme in SCT-MAC. In this chapter, we propose on-demand wake-up scheduling and completely solve challenges regarding this matter. We also show extended NS-2 simulation results for random networks, grid networks, and networks with and without a mobile Sink.

Summarizing, the contributions presented in this chapter are as follows:

- A novel and scalable solution to enable CT in a duty-cycle multi-hop WSN. Unlike most papers on MAC that focus on either an *energy-conserving* or an *energy-balancing* strategy, we propose an On-demand Scheduling Cooperative MAC (OSC-MAC) to incorporate both heuristics in the MAC design.

- A simple and effective DC scheduling algorithm embedded in the MAC is proposed to enable on-demand CT, and to provide the wake-up rendezvous for cooperators to reach a CT agreement. The staggered and orthogonal nature of the scheduling also alleviates channel contention and collisions.

- A seamless contention and transmission scheduling scheme to support both direct transmission and CT range extension. The CT range extension scheduling and on-demand wakeup scheme have relaxed the spatial-tempo assumptions made in previous CT protocols.

- Extensive NS2 simulations are performed that show significantly prolonged lifetime compared with other efficient MAC protocols, under different static network topologies. The superiority of OSC-MAC is also shown in a mobile scenario of WSN

wherein the Sink has the mobility.

4.1 Network Model and Duty Cycle Design

A data gathering tree is formed by routing protocols. Such protocols include the emerging IPv6 Routing Protocol for Low Power and Lossy Networks (RPL) [74], which is currently under development by the Internet Engineering Task Force (IETF) for low power and lossy networks (LLN). In such a converge-cast tree, it is customary to call nodes that have no children the leaf nodes, and nodes that have at least one child the parent nodes. Although routes may change during network operation, we assume a primary route that is durable for a time that is long compared with a frame or several frames, with a tree-based routing structure. We assume Time Division CT (TDCT), which includes a multi-cast phase and several uni-cast phases [7]. In the first multi-cast phase, the source shares one copy of the packet to the cooperators. Subsequently, the cooperators forward the the packet to the destination in orthogonal time slots. In order to achieve TDCT range extension, the radio of the source node, cooperators and the destination must be on at the time when the source firstly multi-casts the packet to the cooperators that are within one SISO hop of the source. Note that the destination needs to be on during each transmission so that it can sample and store the signal received from the source, to combine later with copies received from the cooperators. Due to explicit control packets, we only allow two SISO-hops range extension in our MAC design. Our previous work, SCT-MAC [13], provides the wakeup rendezvous by letting a node wake up during its parent's and two-hop parent's schedule, namely $Sched$ 1 and $Sched$ 2, and initiating CT during $Sched$ 2. However, in SCT-MAC the nodes far from the Sink usually have to maintain more schedules than the nodes near the Sink, and therefore consume more energy in idle listening. In addition, the candidate helpers are limited to the siblings who share a common parent or the parent's siblings, because of the schedule. In this study, we present a different approach to bring the cooperating nodes into temporary synchrony in an on-demand fashion. Specifically, each

node shall maintain a permanent schedule (PS) of its own to receive incoming packets, and wake up only on demand to support CT, which we call temporary schedules (TS). Different TS will be described in the next section.

One *duty-cycle* is composed of the scheduling period, the data period, and the sleep period. The *superframe* is defined as the concatenation of the scheduling period and the data period. We define the length of a *cycle* to be N_s superframes. During a superframe, the scheduling period is used for cooperation wakeup request and transmission reservation. The non-CT data transmissions and CT data transmissions are performed in the data period according to the scheduling information obtained in the preceding scheduling period. Nodes sleep during the entire sleep period, and also sleep in the "unused" portion of the data period. The permanent schedules are achieved using the same greedy algorithm and broadcast procedure at network initialization phase as SCT-MAC, as in Alg.1.

The network initialization is triggered at the Sink. Each node around the Sink first retrieves the time slots that have already been occupied by interfering parent nodes, and then selects a free slot based on the collected information. After that, a beacon is transmitted for the scheduling procedure to propagate over the rest of the network. The resulting schedules in a path from a low-level node towards the Sink are sorted in a cyclic increasing order. The pipelined feature is similar to [77]. Unlike [77], the schedules of interfering nodes appear orthogonal in time (i.e., the superframe of a node lies in the sleep period of its interfering nodes). Here we assume the interference range is twice of SISO transmission range, which has been validated by measurements [76]. The introduced orthogonality guarantees that different traffic flows in the network are collision-free. Same as DW-MAC [5], a separate network time synchronization protocol is assumed to achieve the "coarse" synchronization. Note that a node does not need to wake up at the exact time of a schedule, instead, it needs only wake up a little earlier with a small margin time. Fig. 8 shows an instance of the scheduling algorithm for a random topology of 50 nodes and a deterministic 7×7 grid topology with $N_s = 12$. The number represents the permanent schedule (PS). Note that a

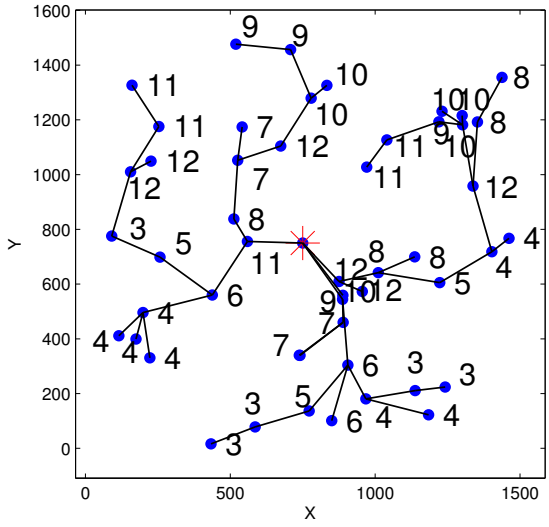

(a) Random Topology

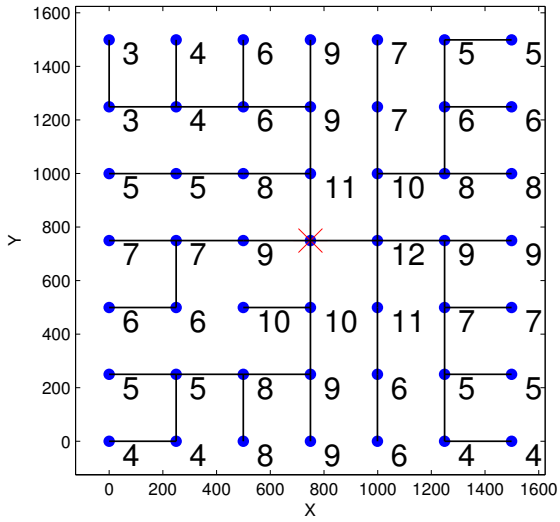

(b) Grid Topology

Figure 8. Examples of the scheduling instance of random and grid topologies ($N_s = 12$)**.**

leaf node follows its parent's schedule.

As aforementioned, conducting CT range extension in an asynchronous network is extremely challenging, because the source, the cooperators and the destination (which may be two SISO-hops from the source) need to reach consensus about a wake-up period, during which CT can be performed, and also because the collaborating nodes may have distinct

individual schedules. To address this challenge, in this section, we explore an explicit requesting procedure to gather the cooperators and the one-hop parent to a common wakeup rendezvous; the method will be described in the next section.

4.2 On-demand Scheduling Cooperative MAC

4.2.1 Overview

In OSC-MAC, each node maintains one permanent schedule (PS) and decides temporary schedules (TSs) on the fly. The TSs are activated on demand to support CT and deactivated afterwards. It is assumed that each node is aware of the PS of its one-hop neighbors and the PS of its two-hop parent. Because every node can be a receiver, it always keeps awake during its own PS to receive either CT data or non-CT data. When a node decides to transmit a non-CT data packet directly to its parent, it wakes up in its parent's PS and proceeds to transmit using the procedure in Section 4.2.5. On the other hand, when the source node decides to do CT, as shown in Fig. 9, it tries to filter the candidate cooperators applying the criteria in Section 4.2.3 . Here we use the same simple criterion for CT decision as in REACT, which compares the source node's residual energy E_i and its parent's energy E_p. If $E_p > E_i$, a non-CT transmission will be performed. Otherwise, a CT decision will be made to protect the parent. Then the cooperating nodes will decide TSs on the fly, during which they will wake up. An algorithm is provided in Section 4.2.4 to achieve this. To support the scheduling in OSC-MAC, three classes of active schedule are defined, and the responsibility of the corresponding nodes are listed as follows:

- *PS (Class 1)*: Set by each node to listen for incoming packets.
- *TS (Class 2)*: Set by source node that initializes CT, to perform wakeup request to cooperators.
- *TS (Class 3)*: Set by cooperating nodes as wakeup rendezvous, to perform CT.

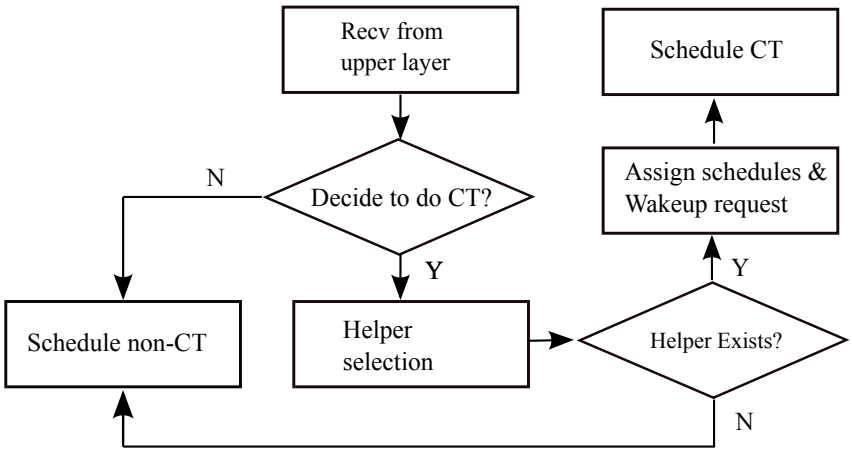

Figure 9. CT decision and wake-up scheduling at the source

4.2.2 Physical Layer Consideration

We take the following physical-layer approach, which is similar to that of [78]. In Rayleigh fading, when spatially separated cooperators transmit encoded symbols across space and time, the receiver that executes diversity combining can decode the symbols with much lower bit error rate (BER) than conventional SISO transmission. This diversity gain leads to a smaller average SNR requirement, i.e., the average E_b/N_o requirement, where E_b refers to the average bit energy and N_o is the power spectral density of white noise. For instance, for a target BER of 10^{-3}, the E_b/N_o required for uncoded BPSK modulation is 25dB [79] [80], whereas with a 2×1 virtual MISO link, the required E_b/N_o is 10dB, and with a real MISO it is around 15dB because each branch has half power. Thus, with cooperation, the reduction of SNR requirement is 15dB for VMISO and 10dB for MISO. For a given target BER, the reduced SNR requirement can be translated into a longer transmission range. Since the average SNR of a fading channel follows a path loss model, the range extension factor can be obtained as $f_{ext}(N_c) = 10^{(10log_{10}(N_c)+D)/10\gamma}$, where N_c is the number of diversity channels, D is the diversity gain, and γ is the path loss exponent [78]. Also, as in [78], we assume the diversity gain depends only on the number of cooperating nodes and not on the physical location of these nodes (as long as they are all within the SISO range). In our NS-2 simulations, we employ the widely used Two-ray ground reflection model [36] for

all studied protocols, with $\gamma = 4$. The cooperating nodes use the same maximum power as in SISO, and we do not exploit power control. In this power setting, for the cooperative transmission, instead of the ideal 15dB, we use a lower diversity gain $D = 10$dB to leave some margin for other channel effects. With one cooperator ($N_c = 2$), $\gamma = 4$ and $D = 10$dB, the range extension factor is over two. Although more cooperators lead to longer range extension, in our protocol design we consider only two-hop range extension.

4.2.3 Cooperator Selection

In our previous work, SCT-MAC, a cooperator must be the sibling of the source node or the sibling of the parent due to the scheduling design. One disadvantage of such selection constraint is that in some form of grid topologies, such as *non-diagonal* grid as will be discussed later, there lack the available cooperators and thus CT will not be applicable. In contrast, OSC-MAC allows each node to choose the cooperator from its one-hop neighborhood, which may have a distinct schedule. In this study, we consider selecting the helper that has: 1) the maximum residual energy, and 2) energy that is higher than the source node. Energy information of neighbors can be obtained by inserting a common information-sharing broadcast slot periodically and by overhearing control packets in the scheduling period. Energy information of the parent node can also be obtained by letting the parent transmit a beacon during the first slot in the parent's PS. Packets transmitted during the broadcast period can also be used to readjust permanent schedules and update neighbor information, to accommodate possible topology variations.

4.2.4 On-demand Wakeup

In the case of CT, we present the on-demand wakeup scheme to bring cooperating nodes into temporary synchrony, by managing TSs on the fly. Specifically, we require that CT should be performed during the two-hop parent's PS, which would be the schedule had a two-hop non-CT been performed. Thus, the objective is to have all the cooperating nodes locked onto this CT rendezvous.

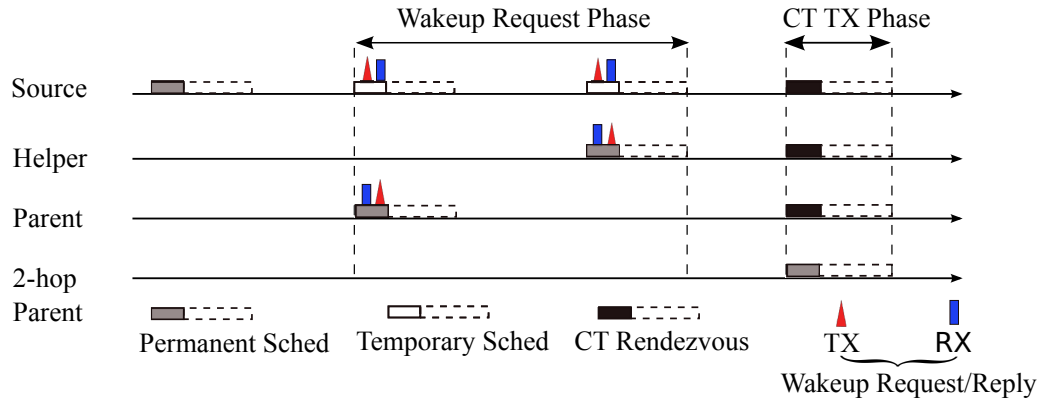

Figure 10. On-demand wakeup scheme.

Because nodes may have distinct PSs, an explicit wakeup request procedure is proposed to set up the wakeup rendezvous for the cooperating nodes. As in Fig. 10, the source Node i sets $Class$ 2 TSs to temporarily wake up in each of the cooperator's and the one-hop parent's PS s_j. Note that each s_j is a concatenation of a scheduling period and a data period. The source node will send a wakeup request packet to the cooperating nodes to indicate the expected slot of CT rendezvous β, and wait for the wakeup replies. Depending on Slot α when the packet is generated and the schedule of the cooperating nodes, a method is provided for the cooperating nodes to self-decide when to wake up to perform CT. Basically, the source node that initiates CT when receiving a packet from the upper layer calculates the start time of future slot that CT can be formed in T_{max} by considering the cooperative nodes' individual PSs, and embeds this information in the wakeup request packet; then, the cooperating node j when receiving the wakeup request calculates the wakeup time on the fly, by first calculating an intermediate variable according to

$$T_{Wake,j} = T_{StartS,j} + d * T_{SF} \tag{4}$$

where, $d = (\beta - s_j) \bmod Ns$, T_{SF} is the superframe length, and $T_{StartS,j}$ is the start time of the current slot. And then $T_{Wake,j}$ is compared with T_{max}. This is necessary because a cooperative node's PS may appear before or after the two-hop parent's PS.

This coordination process falls in the *non-CT* case of the MAC procedure, as will be

described in Section 4.2.5, i.e., with the scheduling period used for exchanging wakeup request/reply. More details of the on-demand wakeup scheme are provided in Alg.3.

Algorithm 3: On-demand Wakeup Schedules

Input: Set of cooperating nodes (including the parent) Γ
The slot when packet arrives, α
The PS of the two-hop parent, β
Output: The schedule of wakeup rendezvous

Source: (do wakeup request)
$T_{max} \leftarrow 0$;
foreach $j \in \Gamma$ **do**
  if $s_j \equiv \beta$ **then** $setWakedStatus[j]$;
  else
    $d_1 \leftarrow (s_j - \alpha) \bmod Ns$;
    $d_2 \leftarrow (\beta - s_j) \bmod Ns$;
    $T_{max} \leftarrow \max\{T_{max}, T_{StartS,j} + (d_1 + d_2) * T_{SF}\}$;
    $scheduleTxRequest[j]$;
  end
end
Each cooperating node: (when receiving wakeup request)
$d \leftarrow (\beta - s_j) \bmod Ns$;
$T_{Wake,j} \leftarrow T_{StartS,j} + d * T_{SF}$;
if $T_{Wake,j} < T_{max}$ **then** $scheduleDelayedWakeup()$;
else
  $scheduleWakeup()$;
end
$sendWakeupReply()$;

Remark: There are two kinds of delay: (a) link delay (from the source to the next-hop, either one-hop parent or two-hop parent); (b) possible "extra" delay resulting from cooperator coordination. Note that there will be no extra delay in the cooperator coordination process if the selected helper's on time happens before the two-hop parent's (referred as *coordination in advance*), because of the pipelined feature of PSs. Indeed, a third criterion can be incorporated into cooperator selection (i.e., $s_j < \beta$), to ensure *coordination in advance*. However, the coordination to perform CT can still incur significant delay comparing with delay optimized protocols, exhibiting the inevitable tradeoff between CT and delay. Thus, our protocol favors applications that can tolerate certain delays [81], but would benefit from a significantly longer lifetime, such as ecology monitoring (e.g. lake water quality, forest temperature monitoring), structural health monitoring or animal habit tracking.

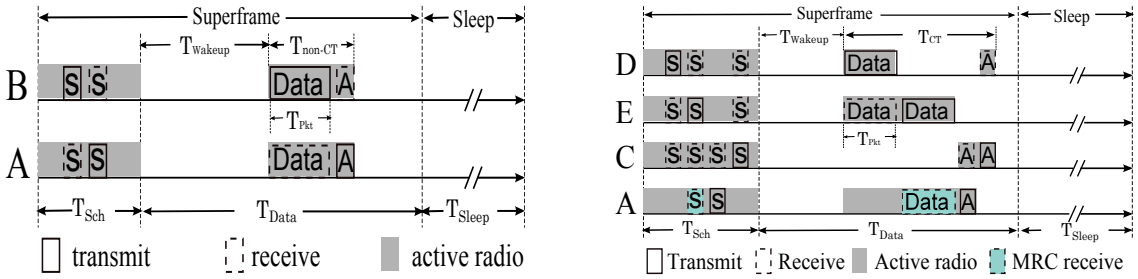

(a) One-to-one Mapping for Non-CT Transmission

(b) Cooperative Range Extension Case (CT TX Phase)

Figure 11. Seamless scheduling and transmission for non-CT and CT packets.

4.2.5 Seamless Scheduling and Transmission for CT and Non-CT

In this subsection, we provide the details for the seamless scheduling and transmission for non-CT during the parent's schedule, and for CT during the CT rendezvous as in Fig. 10. Note that the CT case, Fig. 11(b), is the zoomed-in process in "CT TX Phase" of Fig. 10. Same as SCT-MAC, the scheduling period is used for conducting control handshakes to reserve the data transmission in the following data period. Nodes also sleep during the unreserved portion of the data period. A receiver will keep track of the numbers of non-CT and CT transmissions that have already been granted by itself and thus been reserved in its own data period.Next we will discuss the seamless scheduling and transmission process, using Fig. 12 as an example, wherein Node S is the source, C is the cooperator, P is the parent, and D is the two-hop parent. The process applies to any large network.

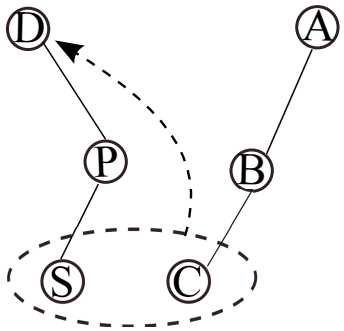

Figure 12. Part of a large network.

1) Non-CT case: During the scheduling period, after random backoff, the source node *S* transmits a scheduling frame (SF) to the destination *P* (one-hop parent), which will reply

with a SF, as in Fig. 11(a). The replying SF includes the numbers of non-CTs (N_{non-CT}) and CTs (N_{CT}) that have already been reserved in the data period. Both Node S and Node P determine the corresponding wakeup time instance T_{Wakeup} from the beginning of the subsequent data period, according to

$$T_{Wakeup} = T_{non-CT} \times N_{non-CT} + T_{CT} \times N_{CT}, \tag{5}$$

where T_{non-CT} and T_{CT} represent channel occupancy time of non-CT packet and CT packet, and thus $T_{non-CT} = T_{Pkt} + T_{Ack} + SIFS$ and $T_{CT} = 2T_{Pkt} + 2T_{Ack} + 3SIFS$. It is easy to see that for a particular receiver, no schedule conflicts will occur during the subsequent data period, and thus data collision from different contending transmitters is avoided. After waking up at the scheduled time T_{Wakeup} in the data period, Node S transmits the data to Node D, which after decoding the packets, replies an ACK. Then both Node S and Node P sleep to avoid idle listening. Note that N_{non-CT} or N_{CT} increments according to whether the scheduled transmission is a non-CT packet or a CT packet.

2) CT case: The CT transmission is performed in the PS of the two-hop parent. This CT TX phase is agreed upon by the on-demand wakeup scheme discussed in Section 4.2.4.

The source S: As shown in Fig. 11(b), when Node S decides to hop over its one-hop parent using cooperative transmission, it initializes CT by firstly sending a cooperative schedule frame (CSF) destined to the two-hop parent D. The CSF also specifies the ID of the selected helper (such as C). Many measures can be applied to select the best helper such as best link quality, minimum distance, minimum load, etc, or a combination of those metrics. Inspired by REACT [6], we use a simple helper selection criterion by considering residual energy.

The cooperator C: If Node C receives the CSF from Node D which enlists itself as the potential helper, if it is available it sends a CSF the same as the incoming CSF to S to indicate its availability to help. Note that the CSF frames from S and C are transmitted in two orthogonal time slots, and can not be decoded separately by D, which is the two-hop parent; however, they can be decoded jointly at D using Maximum Ratio Combining (MRC) [36];

D then replies a SF (including N_{CT} and N_{non-CT}) to S and C in a two-hop manner, through the intermediate node P. Also, D schedules a wakeup time instance T_{Wakeup} in the Data period according to Eq. (5), to receive the cooperative data transmission from Nodes S and C. If S and C receive the SF (A's reply) forwarded by P, then they schedule the same wakeup time, to proceed the data transmission in the data period. As shown in Fig. 11(b), at time T_{Wakeup}, Node S sends the data packet in the first time slot, which is decoded and forwarded by Node C in the next time slot. The two-hop parent D, upon receiving the two independent copies of packets, decodes the original packet using MRC. Then it sends an ACK back to S in two hops through P. Note that S should sleep immediately after sending its packet, to avoid overhearing the retransmission from the cooperator, and wake up again right before the expected ACK which is forwarded by P on behalf of D. Also, the cooperator should also sleep after relaying the packet, and it does not need to wakeup to receive the ACK.

The one-hop parent P (to be protected): As stated above, the role of Node P is to forward the control packets sent from Node D, such as SF and ACK. The SF is a grant for the CT request initiated by Node S. The ACK is an acknowledgement of the correct reception of the cooperative data transmission from Nodes S and C. Both of the CSF frames from S and C can be overheard by their one-hop parent P; if C decodes either of the CSF frames it then anticipates to receive the SF replied from Node D. If SF is received, P forwards it to S and C. Also, P schedules a wakeup time at $T_P = T_{Wakeup} + 2T_{Pkt} + SIFS$ to receive a possible ACK from D which is destined to Node S. Note that the goal of REACT is to hop-over the energy constrained node (e.g. Node P), however, completely avoiding the usage of Node P requires either higher transmit power or cooperative transmission at D's side, which adds extra energy cost (near the Sink) with an increasing complexity of the protocol. Therefore, we let Node P forward only two control packets that are much shorter than the data packet, and allow P to sleep otherwise.

Although we have shown the non-CT and CT contention and scheduling only for one source node, OSC-MAC allows multiple data transmissions from different senders in the

data period. According to Eq. (5), multiple contending nodes contend to execute a control handshake in the scheduling period with their indented (common) receiver and to schedule their data transmissions in the subsequent data periods. Retransmissions for CT and non-CT include the retries of SF handshake and DATA transmission. The former case occurs in the scheduling period which can hold several retries until reaching the boundary of the period. However, if the SF handshake succeeds but the scheduled data transmission fails in the data period, the node has to wait until the next cycle.

4.2.6 Schedule Conflict Detection and Avoidance

As stated above, a receiver does not have a schedule conflict in its data period because it schedules the data transmissions. However, under some conditions the sender may incur a conflict in the scheduled transmission, especially when the sender is both a data source and a cooperator, in the same schedule shared by *different* receivers. We illustrate this in Fig. 12, where Node D is the two-hop parent of Node S, and Node A is the two-hop parent of Node C. Assume D and A (separated over twice the SISO range) happen to have the same PS. In the first control handshake, C acts as the CT initializer to A and receives ($N_{CT} = 1$, $N_{non-CT} = 0$), from A. In the second control handshake (later), S initializes CT to D and enlists C as the cooperator, which then receives ($N_{CT} = 1$, $N_{non-CT} = 0$), from D. Then at the same wakeup time T_{Wakeup}, C must listen to S to receive and transmit its own CT packet, resulting a schedule conflict. To preclude this situation, after a new control handshake, a node checks whether new scheduled wakeup (start time and duration) conflicts with the existing ones; if a conflict is detected, then it sends a *ConFlict* SF (CFSF) to notify the partners to cancel their scheduled wakeup in the data period to avoid unsuccessful data transmission.

4.2.7 First-hop Node Handling and Fast Forwarding to the Sink

Since nodes that are one-hop away from the Sink have orthogonal schedules (because they are within interference range of each other), they receive different Sink transmissions at

different times, which makes it possible for the nodes to reply SF directly to the source, instead of letting the Sink transmit to the source via two hops. There are three kinds of traffic going through a first-hop node as shown in Fig. 13 : the non-CT and CT transmission with itself as MAC layer destination as in (a) and (b), and the CT transmission from its leaf nodes directly to the Sink as in (c). In the first two cases, the node reserves one more T_{non-CT}, which is used to forward the received data immediately to the Sink. In the third case, it replies with SF on behalf of the Sink.

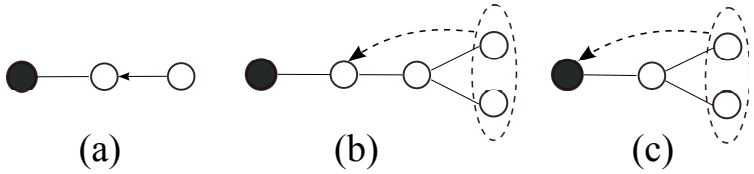

Figure 13. First-hop node traffic.

Table 2. Simulation Parameters

Bandwidth	20 Kbps	Chnl. Enc. Ratio	2
Tx Power	31.2 mW	Tx Range	250 m
Rx Power	22.2 mW	CS Range	550 m
Idle Power	22.2 mW	Superframe	3071 ms
Sleep Power	3 uW	Cycle Length	36.85 s
State Trans. Power	31.2 mW	Size of ACK	10 B
DIFS	8 ms	Size of SF/CSF	14 B
SIFS	4 ms	Size of Data	100 B
Cont. Window	16 ms	Retry limit	5

4.3 Simulation Evaluation

In this section, we present detailed performance results for the proposed OSC-MAC protocol from simulations using NS-2.29 [82]. We consider both random networks and grid networks. Same as SCT-MAC and DW-MAC, OSC-MAC is analyzed using the Random Correlated Event (RCE) traffic model to simulate burst traffic triggered by spatially correlated events, which are commonly observed in detection, monitoring and tracking applications. The event location (x, y) is randomly selected every 200 seconds. Each node within the circle of radius R centered at the event location (x, y) generates a packet to the

Sink. The radius R is gradually increased to input more traffic into the network. The main simulation parameters are listed in Table 2. The SISO transmission range is 250m and the carrier sensing range is 550m, which are modeled after the 914MHz Lucent WaveLAN DSSS radio interference, and which are not typical for a sensor node; but we use these parameters to make our results comparable to those results reported in previous works, e.g., [3] [5] and the reference therein. Moreover, although different devices would have different transmission range and carrier sensing range, the similar ratio between them is observed by measurements [76]. The energy consumption parameters are typical values for Mica2 radios (CC1000) [**?**]. The transition time of CC1000 radio between active and dormant modes is about 2.47ms, however the transition energy is not available from the data sheet. As OSC-MAC requires more state transitions of the radio, to not favor OSC-MAC, we give transition energy the same value as in transmission, although the former normally consumes much lower energy than transmission and reception. The initial energy of node is set to 50J and the Sink has no energy constraint. The routing layer can use different metrics. For random topologies, the minimum-distance metric is used. We compare different metrics in grid topologies. The energy consumption occurring in the routing layer is neglected, for all studied MAC protocols. The performance of OSC-MAC is compared with the cooperative protocol SCT-MAC [13] and the non-cooperative duty-cycle protocol DW-MAC [5].

4.3.1 Random Networks

We consider 100 random topologies, where 50 nodes are randomly distributed in an area of 1000 m * 1000 m. The sink is located in the center. For example, Fig. 8(a) shows one random network.

4.3.1.1 Network Lifetime Evaluation

Fig. 14 - Fig. 16 depicts the CDFs of the network performance of OSC-MAC, SCT-MAC and DW-MAC when the event sensing range, R, is 300m. In particular, Fig. 14 shows

that OSC-MAC significantly outperforms the others in the network lifetime. The improvements attribute to the duty cycle design for reducing contention and congestion, and to the scheduled transmissions for avoiding overhearing and idle listening, as well as to CT range extension for protecting bottleneck nodes. The lifetime is defined as the number of packets delivered to the Sink when the first node exhausts. Fig. 15 indicates that while all the protocols exhibit high delivery ratio (DR) for most random topologies, DW-MAC has relatively lower DR (from the long tail) in occasional cases due to its network-wide synchronization. Fig. 16 shows the energy efficiency in terms of energy consumption per packet. While DW-MAC has much less energy efficiency than OSC-MAC, SCT-MAC is only slightly worse, although the difference in lifetime is noticeable.

To have a quantitative sense, Fig. 17 - Fig. 19 shows average performance. Fig. 17 presents the growth trend of the average lifetime as the event sensing range R increases, with 95% confidence intervals (they are very small). When the first node dies, some fraction of total energy consumed by the network can be attributed to transmission and another fraction can be attributed to idle listening. We note that the fraction attributed to packet transmission increases with event sensing radius (because the packet transmission rate increases) and the fraction due to idle listening will decrease. This explains why the total packets sent at first node death (our definition of lifetime) increases with increasing event radius. In Fig. 17, we see OSC-MAC is superior, for example, it increases the mean network lifetime by 77.8% compared with SCT-MAC when $R = 400m$. This is because OSC-MAC, in spite of CT, spends less time in idle listening. And when traffic increases, the staggered duty-cycles reduce the collisions when many nodes contend for the medium. Fig. 18 shows in very small scale the average delivery ratio of the three protocols, with 95% confidence intervals. Besides having the highest DR, OSC-MAC delivers the smallest confidence intervals for all the event sensing ranges. Together with Fig. 17, Fig. 19 suggests that energy efficiency is only an indirect indicator of network lifetime, because the magnitude of lifetime difference between protocols cannot be projected from the difference in their energy

efficiency.

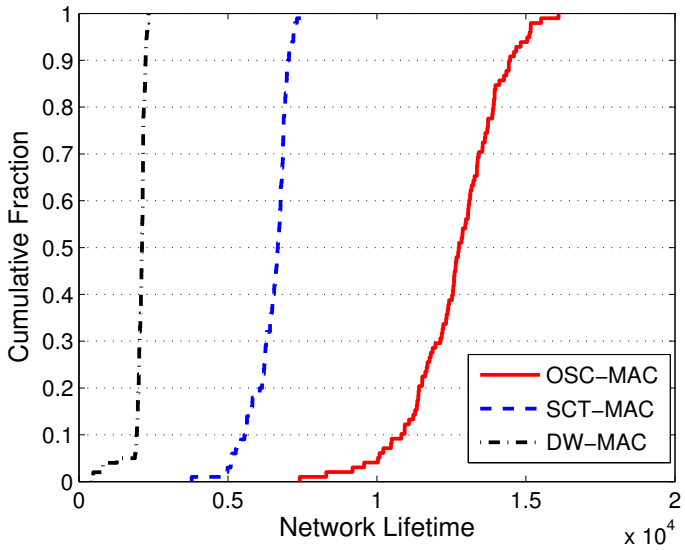

Figure 14. Cumulative distribution function (CDF) of the lifetime of random networks ($R = 300m$).

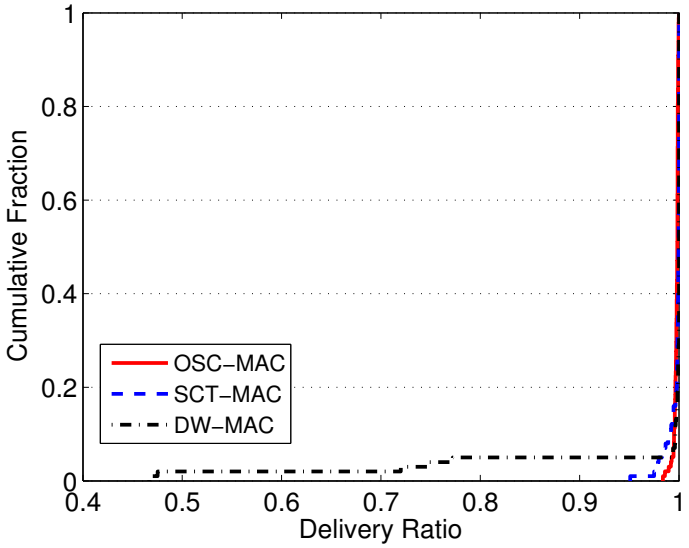

Figure 15. Cumulative distribution function (CDF) of the delivery ratio of random networks ($R = 300m$).

4.3.1.2 Residual Energy Profile

In this subsection, we show the residual energy profile of all the nodes in the network when the first node exhausts, for event sensing ranges of $100m$ and $300m$. Lower ID indicates shortest distance to the Sink. Fig. 20 suggests that SCT-MAC leaves more energy around

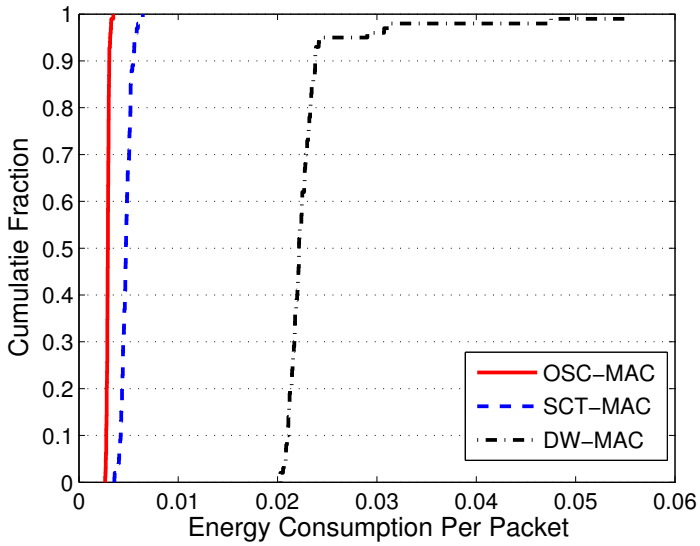

Figure 16. Cumulative distribution function (CDF) of energy consumption per packet of random networks ($R = 300m$).

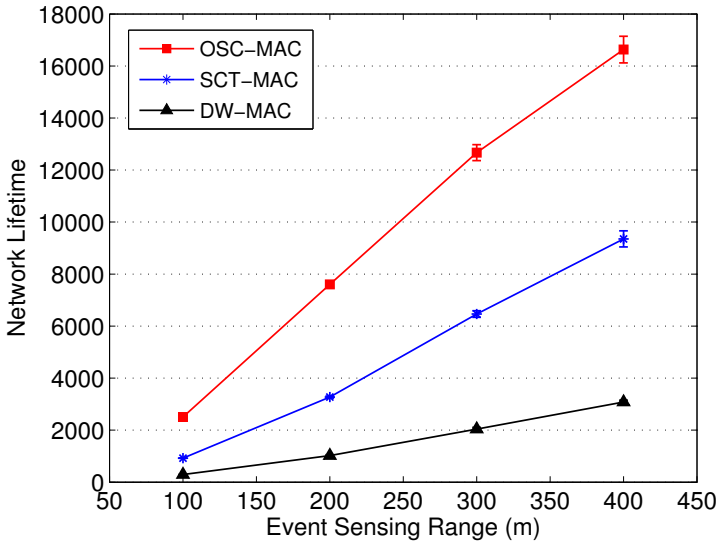

Figure 17. Average lifetime of random networks (Varied R).

the Sink unused. This is because the scheduling in SCT-MAC requires a node to wakeup in the parent's and two-hop parent's schedule to support CT, and thus nodes farther away from the Sink maintain up to three wakeup schedules consuming more energy than necessary in idle listening. From Fig. 20, we also see that DW-MAC obtains a balanced residual energy profile, however, much of the energy is consumed in idle listening in the scheduling period

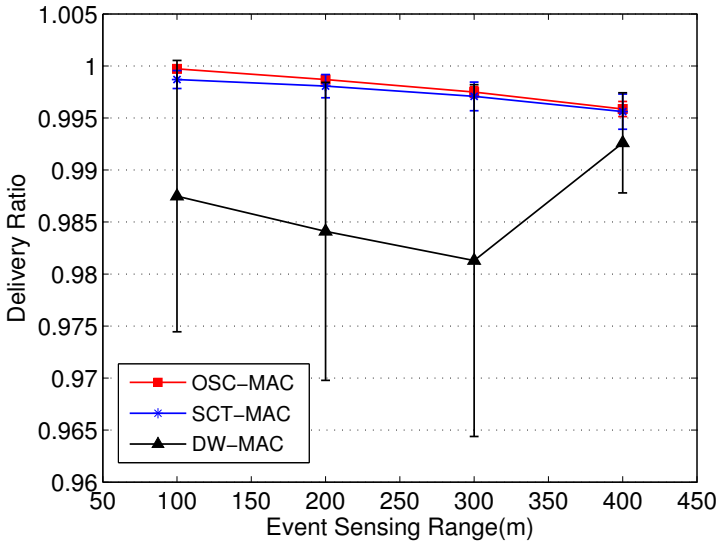

Figure 18. Average delivery ratio of random networks (Varied *R*).

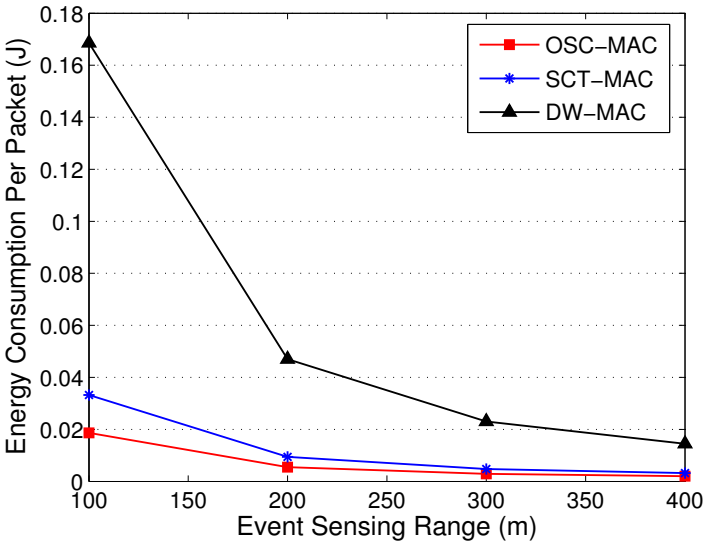

Figure 19. Average energy consumption of random networks (Varied *R*).

and channel contention because of the synchronized schedules of all the nodes. OSC-MAC, on the other hand, achieves more balanced energy than SCT-MAC because nodes are required to maintain one permanent schedule and manage temporary schedules on the fly, and therefore the periods spent in idle listening for possible CT traffic are reduced. However, the energy in OSC-MAC is less balanced than DW-MAC at the nodes near the Sink. Also OSC-MAC still leaves a significant amount of average residual energy at first

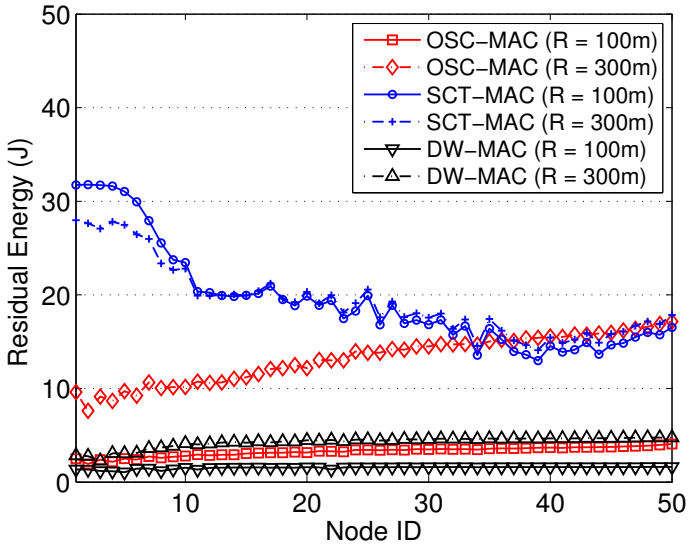

Figure 20. Residual energy v.s. Node ID

node death, suggesting more efficient protocols may be possible. The imbalance is due to the limitation of the two-hop range extension in our scheme, and also the practical failures of CT handshake as will be discussed later. With longer range extension, the energy could be more balanced as shown in REACT [6]. However, longer range extension imposes more challenges in control packets exchange in a duty cycled network.

4.3.1.3 Saturation Lifetime

To quantify the influence of CT in the OSC-MAC protocol, we increase the sensing range from 100m to 1200m and compare the lifetime (with 95% confidence intervals) obtained in OSC-MAC with CT enabled and CT disabled cases, in Fig. 21. "CT disabled" means that the duty cycle assignment as in Section II is held, however every packet is forced to follow non-CT transmission. With sensing range of 1200m almost every node would transmit periodically, and hence there are 50 flows converging to the Sink making the network heavily loaded. We observe in Fig. 21 that after an increasing trend before the sensing range reaches 600m, the lifetime gradually decreases until arriving at a plateau. A similar trend of throughput as traffic increases is also observed by Bianchi [83] in the WIFI network. Similarly, we define the plateau as the saturation network lifetime. Fig. 21 shows that CT

increases the saturation lifetime about 30% compared with non-CT even when both cases are under carefully designed duty cycle schedules and when the communication overhead of CT is considered. We observe that the 30% improvement from CT is much less than was observed in Jung and Ingram [8], because as we will discuss later, idle listening consumes a large part of the energy budget, but the model in [8] did not include idle listening.

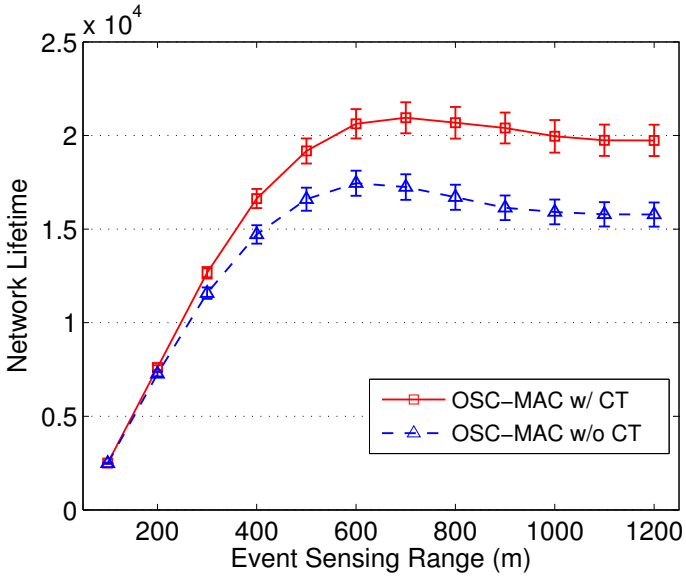

Figure 21. Saturation Lifetime

4.3.1.4 Practical Behavior Due to CT Control Handshake

Ideally, CT should be conducted whenever a CT decision is made according to some criterion, such as REACT. However, this is not always possible due to contention and collisions. We observe that CT is not always being performed as desired. Fig. 22 plots the CT cancellation frequency, for every source node with event sensing ranges of 200m and 600m. Note that the first-hop nodes to the Sink have no need to initialize CT. We observe that when the traffic load in the network is heavy, CT cancellations occur much more frequently. This takes place for two reasons: (1) the SF handshake during CT rendezvous for scheduling CT data transmission suffers more collisions when the network is heavily loaded. The collisions come from the contention with both non-CT an CT handshakes; (2) as we implement

an explicit wakeup request/reply procedure to reach CT rendezvous, this wakeup procedure could fail more frequently due to contentions. Consequently, the CT attempt must be canceled and subsequently the non-CT is pursued.

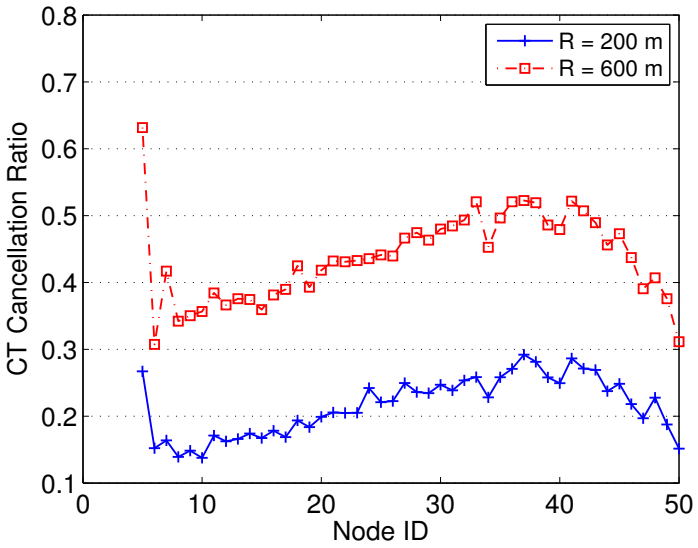

Figure 22. CT cancellation frequency

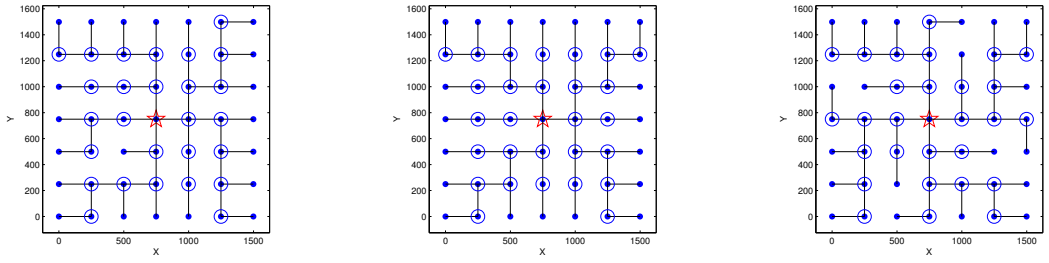

(a) SP (Dijkstra's) (b) Breadth-first search (c) Load balancing

Figure 23. non-Diagonal Case: Routes constructed by different routing algorithms for a 7×7 grid topology.

4.3.2 Grid Networks

We consider two types of grid networks. The first type is the *non-diagonal* grid network, wherein if using SISO transmission nodes can only communicate directly with nodes that are adjacent to them vertically or horizontally. The second type is the *diagonal* grid network, wherein nodes can also communicate directly with nodes that are in the diagonal.

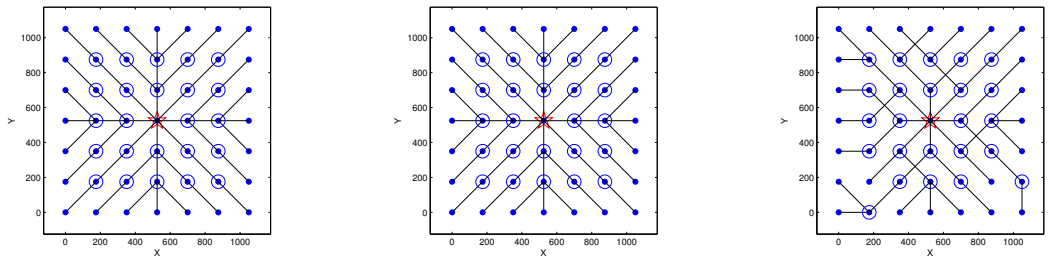

(a) SP (Dijkstra's) (b) Breadth-first search (c) Load balancing

Figure 24. Diagonal Case: Routes constructed by different routing algorithms for a 7×7 grid topology.

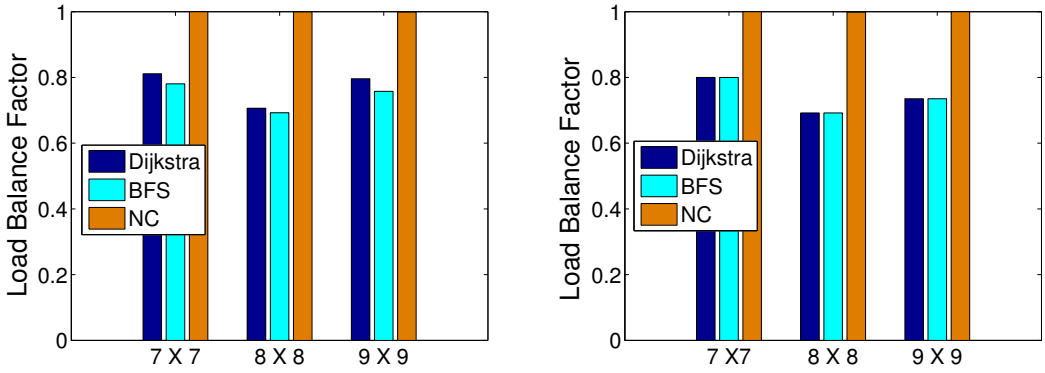

(a) Non-diagnoal network (b) Diagnoal network

Figure 25. Balance factors for a 7×7 grid topology.

These two types of topologies have been considered in the literature and in real applications. Moreover, we remark that SCT-MAC cannot be applied to the *non-diagonal* networks, because due to its schedules SCT-MAC must select a one-hop neighbor that is also a sibling as the cooperator, which is infeasible in the *non-diagonal* networks. In contrast, the proposed on-demand protocol OSC-MAC can be applied to both the *non-diagonal* networks and the *diagonal* networks, because the on-demand feature allows it to select cooperators from one-hop neighbors that are not necessarily sibling nodes.

In this subsection, we evaluate the performance of our proposed MAC protocol under different routing schemes. In particular, different routing protocols cause different loads for the bottleneck nodes, and load balancing schemes, from the routing perspective, have been studied by other authors as a method to balance energy consumption. This motivates us

to evaluate the robustness and performance of OSC-MAC operating under different routing schemes, and to gain some insights of difference when the MAC layer energy consumptions are also captured, beneath the routing layer that typically captures only transmission and receiving. In the *non-diagonal* grid topology, because the source's cooperator is not in the transmission range of the source's one-hop parent, we slightly adjust the transmission of control packet as follows. After receiving the replying SF from the parent, the source node forwards it to the cooperator.

Three routing schemes differing in the load balance factor are considered: the shortest path (SP, Dijkstra's algorithm), breadth-first search (BFS), and node-centric (NC) load balancing routing [84]. To quantify the degree of load balance, the balance factor, θ, is defined as the fairness index among loads in the top subtrees [84]:

$$\theta = \frac{\left(\sum_{k=1}^{n} W_k\right)^2}{n \sum_{k=1}^{n} W_k^2}, \tag{6}$$

where W_k is the aggregate load of each branch, and n is the number of branches. When the weights in each branch converge to the same value, θ tends to be 1 indicating more balanced load. When the imbalance is large, the balance factor approaches $1/n$.

Fig. 25 shows the primary routes constructed from SP, BFS and NC load-balancing algorithms for a 7×7 grid network, and the load balance factors of non-CT networks with different scales. Illustration for the routes in the *diagonal* is omitted due to space limit. For example, for the former network, the balancing factor of SP, BFS and NC are 0.81, 0.78, and 1, respectively. Note that for *diagonal* network, the SP and the BFS produce the same routes. We evaluate 7×7 grid networks in the simulations, while similar trends are observed for networks of other scales. As in the random networks, RCE traffic is generated in the deployment area of the grid networks.

4.3.2.1 Network Lifetime Evaluation

Fig. 26 shows the network performance of OSC-MAC, compared with DW-MAC, for the 7×7 *non-diagonal* network, with 95% confidence intervals in Fig. 26(a)-(c). SCT-MAC

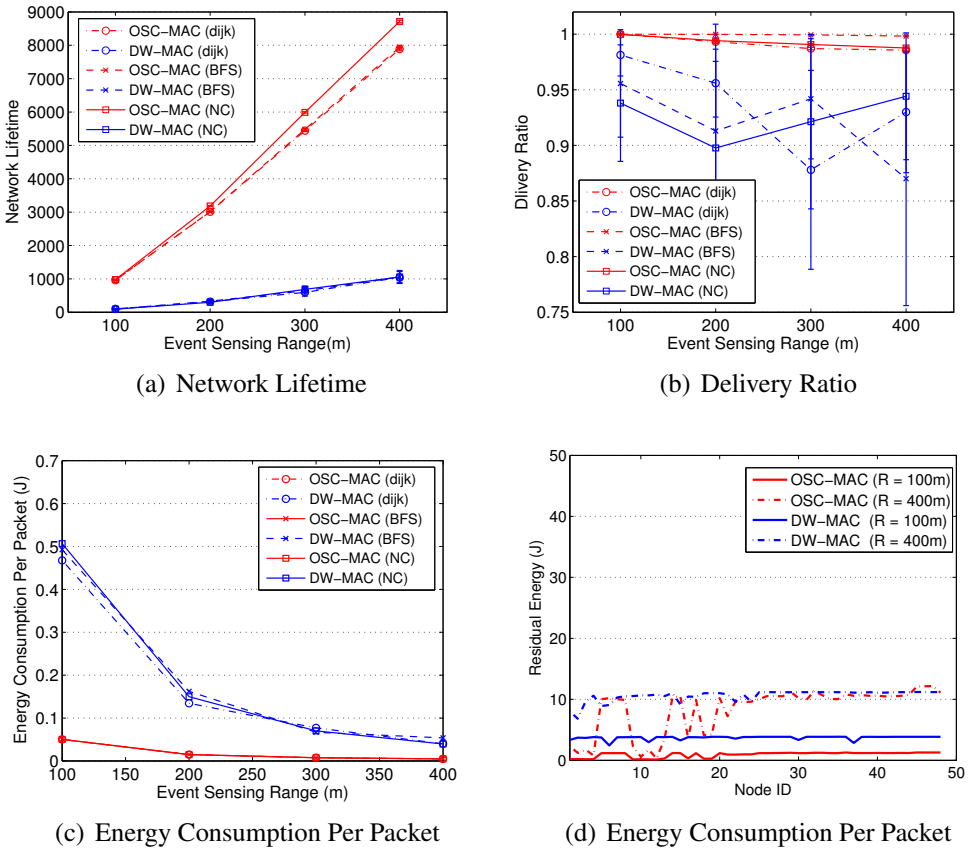

(a) Network Lifetime (b) Delivery Ratio

(c) Energy Consumption Per Packet (d) Energy Consumption Per Packet

Figure 26. non-Diagonal Grid Network

is not shown in the figure, because as mentioned SCT-MAC cannot be applied to *non-diagonal* networks due to its limitation in the cooperator selection. For the same reasons as discussed above, OSC-MAC offers better performance with same trends observed as in the random networks. Specifically, Fig. 26 (a) shows that OSC-MAC outperforms DW-MAC significantly in lifetime, e.g., providing 8−9 times of lifetime of DW-MAC when $R = 400m$. OSC-MAC provides higher average delivery ratio (nearly 100%) with smaller confidence intervals, as in Fig. 26 (b). Fig. 26 (c) demonstrates the high energy efficiency of OSC-MAC, i.e., large gaps with DW-MAC in terms of energy consumption per packet. The gaps in energy efficiency reduce as event sensing range increases, but still render large absolute value. Additionally, we observe that node-centric (NC) load balancing routing favors the lifetime of OSC-MAC. Also, we observe that, for DW-MAC, although the energy efficiency of BFS and NC routing are slightly higher than shortest path, the lifetime of DW-MAC does

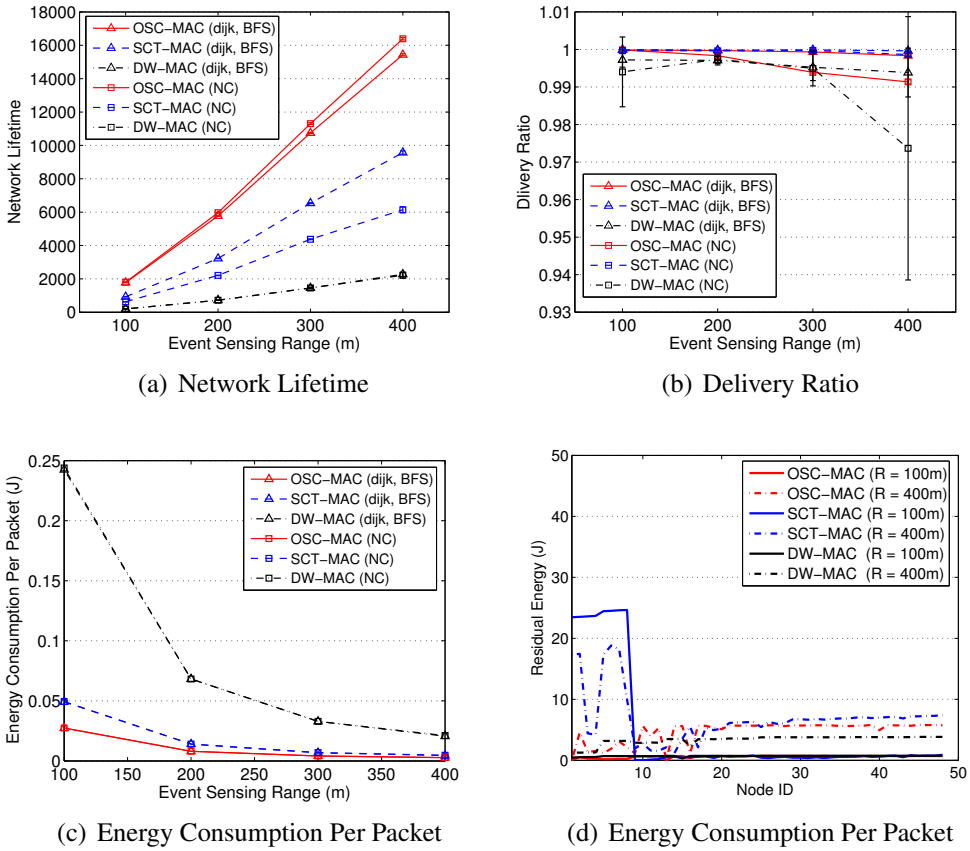

(a) Network Lifetime (b) Delivery Ratio

(c) Energy Consumption Per Packet (d) Energy Consumption Per Packet

Figure 27. Diagonal Grid Network

not benefit noticeably from NC or BFS.

Fig. 27 shows, for the 7×7 *diagonal* network, the network performance of OSC-MAC, compared with both SCT-MAC and DW-MAC, with 95% confidence intervals in Fig. 27(a)-(c). SCT-MAC can be applied because the *diagonal* network can satisfy its cooperator selection criterion. For all the three MAC protocols, the delivery ratios are higher than their counterparts in the *non-diagonal* network as in Fig. 27 (b), because routes in the *non-diagonal* network are more restricted as nodes cannot communicate with a diagonal node. SCT-MAC provides a slightly better delivery ratio than OSC-MAC, at the cost of much less lifetime than OSC-MAC (e.g., OSC-MAC offers over 150% lifetime of SCT-MAC at $R = 400m$), as we can see in Fig. 27 (a). Another observation from Fig. 27 (a) is that while NC routing benefits the lifetime of OSC-MAC compared with shortest path, DW-MAC

gains the greatest lifetime from the shortest path among other routing schemes. This observation suggests that a seemingly "*advantageous*" routing algorithm does not necessarily lead to better lifetime, mainly because the MAC layer captures all complex aspects of energy consumption including collision, overhearing and idle listening besides transceiving, while a routing scheme assessment typically examines only transmission and reception energy. Fig. 27 (c) shows, for each MAC protocol, indistinguishable energy efficiency when different routing protocols are used, although the lifetimes are indeed different, as in Fig. 27 (a). This fact suggests that energy efficiency and lifetime should be jointly considered to quantitatively evaluate a WSN.

4.3.2.2 Residual Energy

The residual energy profiles when the first node dies are shown in Fig. 26(d) and Fig. 27(d), for *non-diagonal* and for *diagonal* networks, respectively. The node ID is sorted according the distance to the Sink, which is in the center of the network; lower ID indicates shorter distance to the Sink. In Fig. 26(d), both OSC-MAC and DW-MAC have balanced residual energy, for both $R = 100m$ and $R = 400m$. We also observe that OSC-MAC has lower residual energy than DW-MAC, indicating better energy utilization towards increasing lifetime. In Fig. 27(d), SCT-MAC is also considered for the *diagonal* network. While OSC-MAC and DW-MAC show relatively balanced residual energy, SCT-MAC leaves significant amount of energy near the Sink, for the same reason for random network that nodes farther from the Sink maintain more schedules than necessary. A common observation from Fig. 26(d) and Fig. 27(d) is that the curve for OSC-MAC has some fluctuation around the Sink, indicating certain nodes around the Sink are not perfectly protected. The reason coincides with our previous observation that, first, CT may be canceled due to collisions and retries; and second, only two-hop CT is conducted due to practical considerations.

4.3.3 The Influence of Mobile Sink

It is uncommon for the nodes in a wireless sensor network to be mobile, however, it is possible that the Sink node(s) can be mobile [85]. Among others, one purpose for the Sink to be mobile could be towards balancing traffic load among nodes. Thus, it is important to evaluate our MAC protocol in the context of mobile Sink. In the mobile scenarios, the Sink node can visit the deployment area following a certain geographical pattern. In this subsection, again we consider the 7×7 diagonal grid network, where a Sink node travels clock-wisely along the borders of the network, in such a way that only the nearest node can directly communicate with it at a time. Therefore, the traffic is more congested than the cases in last section where Sink locates in the middle. There are 24 positions on the border of the network that the Sink can visit, and we determine the level of mobility in terms of the move period of the Sink (traveling time between two positions). Between the times that the Sink moves, nodes follow the schedules as discussed before; when Sink moves to a new position, the same network process as in the network initialization phase is performed to establish new schedules. The shortest path routing algorithm is used. Along with mobile scenarios, we also compare with the static case that the Sink resides still in the "corner" of the network.

Fig. 28 presents the lifetimes of OSC-MAC, SCT-MAC and DW-MAC when the Sink node is static or mobile, with 95% confidence intervals. In the mobile scenario, the Sink traveling period is 600 seconds. Again, the lifetime increases as the event sensing range increases. In the static case, at event sensing range of $400m$, OSC-MAC achieves 182.3% longer lifetime over SCT-MAC, which achieves 71.6% longer lifetime over DW-MAC. As expected, the mobility of Sink releases the burden of the bottle-neck node in the static case, and thus increase the lifetime; however, the increasing rates are different for the three protocols. For example, at event sensing range of $400m$, with mobility the lifetime of OSC-MAC increases (over the static case) by 73.6%, SCT-MAC by 44.3%, and DW-MAC by 25.1%. Another observation that confirms the higher energy efficiency of OSC-MAC and

SCT-MAC is that while OSC-MAC and SCT-MAC benefit from the mobility also in the case of smaller (than 400m) event sensing ranges, DW-MAC improves by the minimum amount.

Fig. 29 shows the packet delivery ratios versus event sensing ranges. For example, at event sensing range of 400m, OSC-MAC achieves the highest delivery ratio (between 92.4% and 95%) among the three protocols, even in the mobile scenario. The delivery ratio of DW-MAC reduces quickly as event sensing range increases, and drops to around 80% at $R = 400m$, due to its requirement of network-wide schedule synchronization and its lower ability to handle congested traffic.

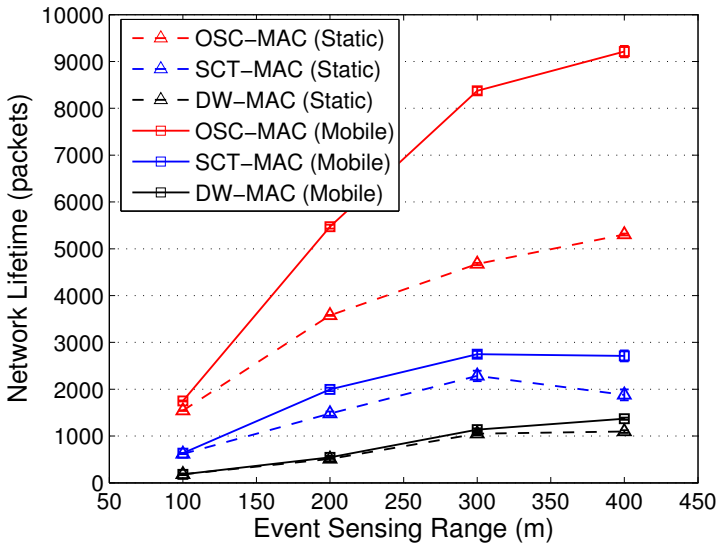

Figure 28. Network lifetime v.s. Event sensing range

In our last experiment, we examine the reaction of the proposed OSC-MAC protocol when the Sink has different levels of mobility. We run the previous 7×7 *diagonal* grid scenario with event sensing range of 200m. The network lifetime versus the mobility level (Sink move period) is depicted in Fig. 30, where larger horizontal axis indicates higher mobility level. We observe that the lifetime reaches the peak value of about 5600 packets when the mobility level is around 400 seconds. As the mobility level decreases, the lifetime

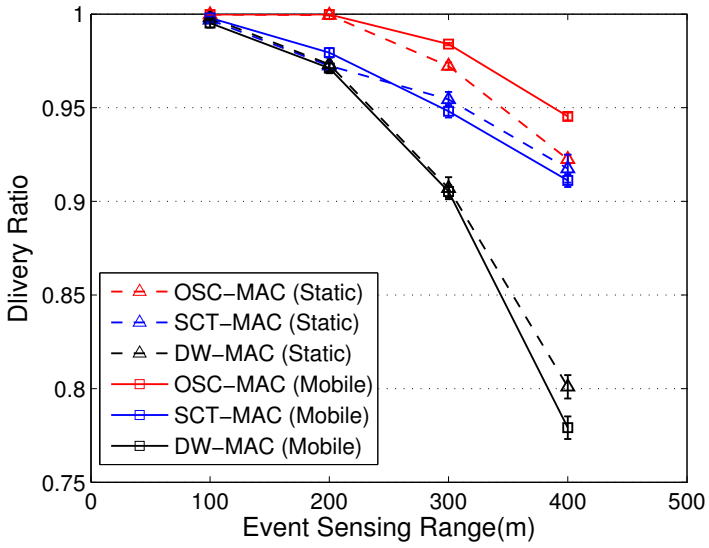

Figure 29. Delivery ratio v.s. Event sensing range

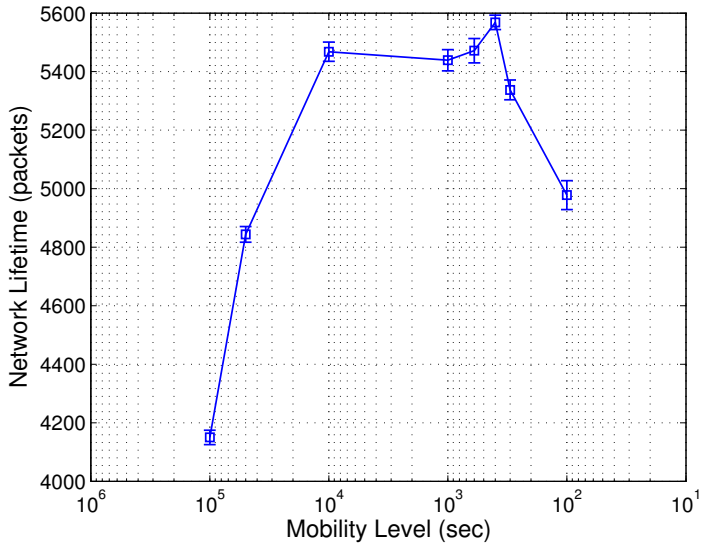

Figure 30. Network lifetime v.s. Mobility Level

reduces towards converging to the static network case. On the other hand, when the mobility level is higher, the network reacts to network schedule changes more frequently and incurs more packet retransmissions. Thus, as we can see from the figure, as the mobility level increases away from the peak point, the lifetime starts to degrade and reaches about 5000 packets when the mobility level is 100 seconds. However, the reduced lifetime due to high mobility still stay almost 90% of its peak value.

4.4 Conclusions

In this chapter, we present a scalable on-demand duty cycling MAC (OSC-MAC) that reduces idle listening and supports cooperative transmission range extension to solve the *energy hole* problem in multi-hop WSNs. By combining an on-demand schedule and CT range extension, we have addressed the spatio-temporal challenges for performing CT in multi-hop duty cycled WSNs, to offer significantly longer lifetime. Even with control packet energy accounted for, OSC-MAC still produces about 80%-200% longer lifetime in various network environments with a static, as well as mobile Sink. OSC-MAC results in an energy-conserving and energy-balancing integrated scheme that can be implemented with sensor nodes equipped with a single antenna.

CHAPTER 5

MODELING OPTIMAL LIFETIME OF ENERGY-CONSTRAINED MULTI-HOP WIRELESS SENSOR NETWORK

This chapter and the next chapter consider modeling the optimal performance of multi-hop wireless sensor networks (MHWSNs), which can be energy constrained (EC) networks or energy harvesting (EH) networks, both with and without relay cooperation. The network performance of a MHWSN is a complex function of sensors' harvested energy, traffic volume, routing protocol, and medium access (MAC) technique. An analytical approach that is suitable for WSN traffic and that derives the optimum serves as a valuable benchmark for heuristics MAC and routing protocols. However, such a multi-hop framework has not been presented previously. In this chapter and the next chapter, we explore the optimum by presenting a unified Markov decision process (MDP) analysis that can analyze both EC and EH networks. We observe that the treatments for both networks fall into two branches of MDP theory, the finite-horizon process and the infinite-horizon process, respectively.

In the remainder of this chapter, we will first describe the system model and assumptions. Then, a Markov decision process (MDP) formulation that considers MAC, routing, energy dynamics, and CT will be presented. We will then propose a computational method that utilizes the stochastic shortest path nature of the problem, and show numerical evaluations for both non-CT and CT networks.

5.1 Problem Statement

5.1.1 System Model and Assumptions

5.1.1.1 Network Model

We consider a general multi-hop WSN whose topology can be modeled as a directed graph $G = (V, E)$, where V is the set of nodes. $V = \{1, \cdots, N\}$. The Sink's ID is 0. Let V^* denote $\{0, 1, \cdots, N\}$. Each Node i (except the Sink) has a set of cooperator groups:

$$\mathbf{H}(i) = \{\mathcal{H}(i)\}, \ i \in V. \tag{7}$$

where $\mathcal{H}(i)$ is a candidate cooperator group (as in Fig. 31(a)), and $E = E^{so} \cup E^{vo}$ denotes the set of links whose end nodes are within transmission range. Specifically, E^{so} includes the links formed by SISO transmission, and E^{vo} includes the long-haul links formed by VMISO transmission.

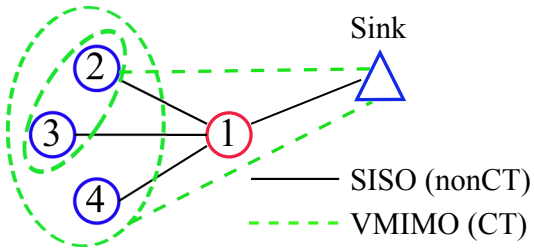

Figure 31. A network example. Node 2 can form a VMISO link to the Sink by cooperating with (i) $\mathcal{H}(2) = \{$Node 3$\}$ or (ii) $\mathcal{H}(2) = \{$Node 3, Node 4$\}$.

$$E^{so} = \{(i, j, \varnothing) : i, j \in V\}, \tag{8}$$

$$E^{vo} = \{(i, 0, \mathcal{H}(i)) : i \in V, \mathcal{H}(i) \in \mathbf{H}(i)\}. \tag{9}$$

A SISO link $(i, j, \varnothing)$ exists if Transmitter i and Receiver j are within direct transmission range. A VMISO link $(i, 0, \mathcal{H}(i))$ means that Sink 0 can be reached by the source node i with its cooperators $\mathcal{H}(i)$. For a link $l \in E$, we denote $s(l)$ as the source of the link and $d(l)$ as the destination of the link.

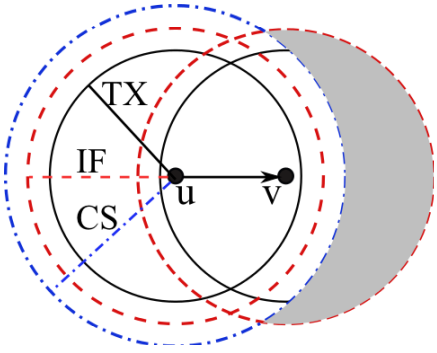

Figure 32. An illustration of interference model. Node v is the receiver of Node u. Node u's hidden nodes in the gray area will interfere v's reception.

5.1.1.2 Interference Model

The interference range (IF) of a link $l \in E$ is denoted as $R(l)$. Note that link $(i, j, \cdot)$ interferes with link $(u, v, \cdot)$ if either the distance $dist(i, v) \leq R(i, j, \cdot)$ or $i = v$, similar to [86] . For instance, in Fig. 32, the Node u and any node in the gray area can start transmission at the same time because they are out of carrier sensing (CS) range of (i.e., hidden from) each other. Also, located in Node v's interference (IF) range, the hidden node's transmission interferes Node v's reception. This phenomenon directly results from the CSMA mechanism of the MAC layer and the relationship between the three ranges (TX, IF, CS) [87][1].

5.1.1.3 MAC Assumptions

Pertaining to the CSMA of MAC, we make the following assumptions, similar to [88]:

(a.1) A node cannot receive and transmit at the same time.

(a.2) A node can transmit if none of its neighbors (in CS range) is transmitting.

(a.3) Link errors result only from collisions due to hidden terminals.[2]

(a.4) Nodes receive with perfect capture, i.e., a packet will be successfully decoded if the receiver and all its neighbors are not transmitting at the start of packet.

We consider a mini-time-slotted system where slots are normalized to integral units $t \in \{1, 2, 3, \cdots\}$. By time slot t, we mean the time duration in between $[t, t + 1]$. Let $\alpha^d(i)$ represent the exogenous packet arrival rate to Node i of *commodity d* (destined to Sink d), which is assumed *i.i.d.* over time slots.

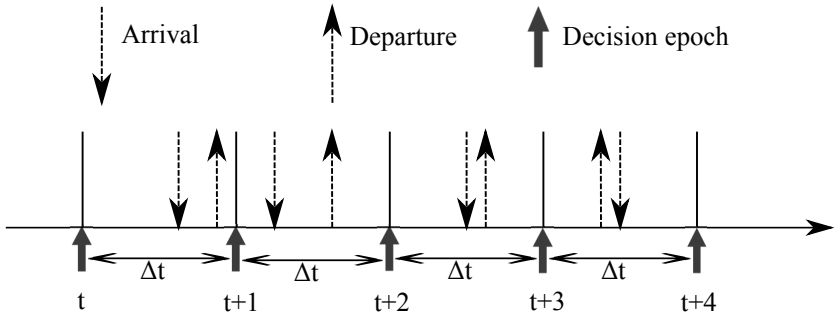

Figure 33. A timeline illustration of the decision process model for the network.

[1]The CTS in CSMA/CA cannot eliminate hidden terminals, because RTS packets can still collide [87].
[2]Our model can be extended to also consider link errors due to channel fading.

5.1.2 Energy Model and Lifetime Definition

Let $\mathbf{e} = (e_1, \cdots, e_N)$ denote the network energy profile at the transmission epoch (which is also the decision epoch). Note that the residual energy of the Node i, e_i, is a random variable conditioned on previous states and decision rules. A node is said to become dead when its energy drops to a predefined threshold e_{th}. The definitions of network lifetime depend on the applications. In this section, we define the lifetime as the number of packets successfully delivered to the Sink when the first node dies.

5.2 Markov Decision Process Formulation

Consider a multi-hop WSN consisting of N sensor nodes each with an initial energy e^{max}. We model the state evolution of the network by an MDP, a controlled Markovian dynamic system. The control model is expressed by the 4-tuple: $\{S, \mathcal{A}(S), q(\mathbf{s}' \mid \mathbf{s}, a), g(\mathbf{s}, a)\}$ (state space, action space, transition kernel, rewards) [51]. A timeline illustration of the MDP process is given in Fig. 33.

Table 3. Parameters of the MDP model

$\Psi(\mathcal{L})$	Collision-free links in the transmission set $\mathcal{L}$
E^{so}, E^{vo}	non-CT and CT links in transmission set $\mathcal{L}$
β^l	Probability that link l finishes transmission
$\alpha(i)$	Exogenous arrival rate of Node i (destined to the Sink 0)
q^{max}, e^{max}	The buffer size, battery capacity of nodes
e_{tx}, e_{rx}	Energy consumption in SISO (source and destination)
$e^{CT}_{init}, e^{CT}_{co}$	Energy consumption in VMISO (source and cooperators)
e_{th}	Threshold of residual energy in lifetime definition

1) Traffic Model: i). We assume that the packet duration of a link l is exponentially distributed with the expectation T^l_{mean}. This assumption is used by several other authors [88] [89]; though inaccurate, it is necessary to make the MDP problem tractable. Due to the memoryless property of the exponential distribution, given that a packet is being transmitted at the beginning of a time slot, it completes within the slot of length Δt with probability $\beta^l(\Delta t) = 1 - e^{-\Delta t / T^l_{mean}}$, regardless of the number of time slots it has already been transmitted. The slot duration Δt is small enough so that we can assume at most one link

can finish transmission during a specific time slot $[t, t+\Delta t], \forall t$, i.e., the probability that more than one link finishes transmission is $o(\Delta t)$. ii). It is also assumed that during one slot, at most one node can self-generate a packet. The probability that only Node i has a new self-generated packet is thus $\alpha(i)\prod_{j\in V, j\neq i}(1-\alpha(j))$, where $\alpha(i)$ is the probability that Node i has a new packet, which is determined by the application. Under uniform exogenous traffic, we have $\alpha(1-\alpha)^{N-1}, \forall i \in V$. The probability that more than one nodes self-generate packets tends to $o(\Delta t)$.

2) Network State Space: The evolution of network states can be modeled by an embedded Markov chain $\{S(t), t \geq 0\}$. We define the network state at the beginning of time slot t as $S(t) \triangleq (\mathcal{L}(t), \mathbf{q}(t), \mathbf{e}(t))$. The state comprises three component processes:

2.1) The transmission set $\mathcal{L}(t) = \mathcal{L}^{so}(t) \cup \mathcal{L}^{vo}(t)$ of links that are active (in transmission) at time t. Denote the space as $\mathfrak{S} = \{\mathcal{L}(t)\}$. $\mathcal{L}^{so}(t)$ and $\mathcal{L}^{vo}(t)$ denote the SISO links and the VMISO links, respectively. This component includes the collisions in the MAC layer. We denote the links that are free of collision as $\Psi(\mathcal{L}) \subset \mathcal{L}(t)$. $\Psi(\mathcal{L})$ is deterministic given $\mathcal{L}(t)$.

Given a graph $G = (V, E)$, a matching $M(G)$ in G is a set of non-adjacent edges (i.e., no two edges share a common vertex). Therefore, $\mathcal{L}(t) \in \{M(G)\}, \forall t \geq 0$. In addition, for any two links $l_1, l_2 \in \mathcal{L}(t)$, the source nodes of the two links $(s(l_1), s(l_2))$ are out of carrier sensing (CS) range of each other, due to CSMA. Therefore, the state space of $\mathcal{L}(t)$ is determined by the graph G and the carrier sensing matrix $\mathbf{H} = [h_{ij}]_{i,j\in V}$ of the network, where the element $h_{i,j} = 1$ if and only if (*iff*) Node i and Node j are within CS range of each other. Finding all the matchings in a graph is *NP-complete*, but despite its hardness many algorithms for finding them have been studied [90].

2.2) The queue length (vector) $\mathbf{q}(t) \in \{0, 1, \cdots, q^{max}\}^N$ of each node, where q^{max} is the buffer size. $\mathbf{q}(t)$ monitors the congestion in the network. The queue backlog contains the packets that arrived both exogenously from the sensing application and endogenously from other nodes.

2.3) The residual energy (vector) $\mathbf{e}(t)$ of each node. $\mathbf{e}(t)$ determines when the network

reaches a termination state (i.e., first node death).

We will show that each component process evolves as a controlled Markov process, and therefore the resulting system state evolution is a controlled Markov process.

3) Action Space: In the beginning of each time slot, t, new link(s) ($a(t)$) may join the remaining *transmission set* $\mathcal{L}(t)$, which comprises those links that did not complete transmission during Slot $t-1$. Note that $\mathcal{L}(t) \subset \mathcal{L}(t-1) \cup a(t-1)$. Again because Δt is small we assume at most one link can join $\mathcal{L}(t)$. Note that link l can join $\mathcal{L}(t)$ iff its source has a non-empty queue and $\mathcal{L}(t) \cup \{l\}$ is also a transmission set. Thus, the candidate links are denoted as

$$\mathcal{A}(S(t)) = \{l \in E : \mathbf{q}_{s(l)}(t) > 0, l \notin \mathcal{L}(t), \mathcal{L}(t) \cup \{l\} \subset \mathfrak{S}\} \tag{10}$$

$\mathcal{A}(S(t))$ represents the action space at time t when the system state is $S(t)$. Note that the null set $\varnothing \in \mathcal{A}(S(t))$, and therefore the action (*link*) can be either a "CT" link, a "non-CT" link or null (no new transmission).

4) Controlled Markovian Dynamics:

4.1) *Transmission set dynamics*: Let $a(t) \in \mathcal{A}(S(t))$ denote the link selected for joining the transmission set. Let $P\left\{z^l(t) \mid \mathcal{L}(t), a(t)\right\}$ denote the probability that only link $l \in \mathcal{L}(t) \cup a(t)$ finishes transmission during Slot t. Let $P\{z^{\varnothing}(t) \mid \mathcal{L}(t), a(t)\}$ denote the probability that no link finishes transmission during Slot t. The time index is dropped when there is no ambiguity. For abbreviation, we denote the transition kernel as $P\{\mathcal{L}' \mid \mathcal{L}, a\} := P\{\mathcal{L}(t+1) \mid \mathcal{L}(t), a(t)\}$. Let $\Delta\mathcal{L} \triangleq \mathcal{L} \cup \{a\} \setminus \mathcal{L}'$, then we have:

$$P\{\mathcal{L}' \mid \mathcal{L}, a\} = \begin{cases} P\left\{z^l \mid \mathcal{L}, a\right\} & \text{if } \Delta\mathcal{L} = l, \\ P\{z^{\varnothing} \mid \mathcal{L}, a\} & \text{if } \Delta\mathcal{L} = \varnothing, \\ 0 & \text{otherwise.} \end{cases} \tag{11}$$

where,

$$P\left\{z^l \mid \mathcal{L}, a\right\} = \beta^l \prod_{\substack{k \in \mathcal{L} \cup \{a\} \\ k \neq l}} \left(1 - \beta^k\right), \forall l \in \mathcal{L} \cup \{a\}. \tag{12}$$

$$P\{z^{\varnothing} \mid \mathcal{L}, a\} = \begin{cases} \prod_{l \in \mathcal{L} \cup \{a\}} \left(1 - \beta^{l}\right) & \text{if } \mathcal{L} \cup \{a\} \neq \varnothing, \\ 1 & \text{if } \mathcal{L} \cup \{a\} = \varnothing. \end{cases} \tag{13}$$

4.2) *Queue length dynamics*: The queue length distribution reflects the loads across the network and directly relates to the first node death. The queue length evolves according to the traffic balance equation in vector form:

$$\mathbf{q}'(t) \triangleq \mathbf{q}(t+1) = \mathbf{q}(t) + \mathbf{R}\mathbf{M}(t)\mathbf{v}(t) + \mathbf{f}(t), \tag{14}$$

where $\mathbf{M}(t)$ is a $|E| \times |E|$ diagonal matrix, whose diagonal element $\mathbf{M}_i(t) = 1$ if the link i's transmission is *completed* and *successful*, and $\mathbf{M}_i(t) = 0$ otherwise (links are numbered to be indexable). Note that a finished transmission is not necessarily successfully decoded by the receiver, because of collision due to hidden terminals; in case of failure, the packet remains in the queue of the transmitter. Also note that under our assumption, at most one diagonal element can be 1, thus $\sum_{i \in E} \mathbf{M}_i(t) \leq 1$. The transmission schedule vector $\mathbf{v}$ is determined by the system state at time slot t, satisfying $\mathbf{v}_i = 1, \forall i \in \mathcal{L}(t) \cup a(t)$ and $\mathbf{v}_i = 0$ otherwise. Matrix $\mathbf{R}$ is the $N \times |E|$ routing matrix. The element of $\mathbf{R}$ in its ith row and lth column is

$$r_{il} = \begin{cases} 1 & \text{if } d(l) = i \text{ and Node } i \text{ is not the sink}, \\ -1 & \text{if } s(l) = i, \\ 0 & \text{otherwise.} \end{cases} \tag{15}$$

$\mathbf{f}(t)$ is a vector with with its ith element $\mathbf{f}_i(t)$ being the number of exogenous packets arriving at Node i during Slot t. Under the assumption that at most one node self-generates a packet, it follows $\sum_{i=1}^{N} \mathbf{f}_i(t) \leq 1$. Let $\mathbf{I}_i$ represent a vector with its ith element being 1 and other elements being 0, $1 \leq i \leq N$, and let $\mathbf{I}_0$ be the zero vector. The probability that only Node i or no node ($i = 0$) self-generates a packet is given by:

$$P\{\mathbf{I}_i\} = \begin{cases} \alpha(i) \prod_{j \in V, j \neq i} (1 - \alpha(j)) & \text{if } i \in V, \\ \prod_{j \in V} (1 - \alpha(j)) & \text{if } i = 0. \end{cases} \tag{16}$$

Case 1 (c1): $\mathbf{q}' = \mathbf{q}$. This can happen for two reasons: (*c1:1*) no link transmission affects the queue state and no new exogenous arrival affects the queues; and (*c1:2*) some link $(i, 0, \cdot)$ destined to the Sink successfully transmits and the source self-generates a new packet.

$$P_{c1:1} = \left(\mathbb{1}\left\{\Delta\mathcal{L} = \varnothing\right\} + \mathbb{1}\left\{\Delta\mathcal{L} \in \overline{\Psi}\left(\mathcal{L} \cup a\right)\right\} + \mathbb{1}\left\{\Delta\mathcal{L} \in \Psi\left(\mathcal{L} \cup a\right), q_{d(\Delta\mathcal{L})} = q^{max}\right\}\right) \cdot \left(P\left\{\mathbf{I}_0\right\} + \sum_{q_k = q^{max}, k \in V} p\left\{\mathbf{I}_k\right\}\right) \quad (17)$$

$$P_{c1:2} = \mathbb{1}\left\{\Delta\mathcal{L} \in \Psi\left(\mathcal{L} \cup a\right), s\left(\Delta\mathcal{L}\right) = i, d\left(\Delta\mathcal{L}\right) = 0\right\} \cdot P\left\{\mathbf{I}_i\right\}, \quad (18)$$

where, $\mathbb{1}(\cdot)$ is an indicator function.

Case 2 (c2): $\mathbf{q}' = \mathbf{q} + \mathbf{I}_j, j \in V$. This case includes two possibilities: (*c2:1*) some SISO link $(\cdot, j, \varnothing)$that is directed to Node j successfully transmits and the source self-generates a new packet; and (*c2:2*) no link transmission affects the queue state and there is a new exogenous packet arrival to Node j.

$$P_{c2:1}\left(j\right) = \mathbb{1}\left\{\Delta\mathcal{L} \in \Psi\left(\mathcal{L} \cup a\right), d\left(\Delta\mathcal{L}\right) = j\right\} P\left\{\mathbf{I}_{s(\Delta\mathcal{L})}\right\}. \quad (19)$$

$$P_{c2:2}\left(j\right) = \left(\mathbb{1}\left\{\Delta\mathcal{L} = \varnothing\right\} + \mathbb{1}\left\{\Delta\mathcal{L} \in \overline{\Psi}\left(\mathcal{L} \cup a\right)\right\} + \mathbb{1}\left\{\Delta\mathcal{L} \in \Psi\left(\mathcal{L} \cup a\right), q_{d(\Delta\mathcal{L})} = q^{max}\right\}\right) \cdot P\left\{\mathbf{I}_j\right\}. \quad (20)$$

Case 3 (c3): $\mathbf{q}' = \mathbf{q} - \mathbf{I}_i, i \in V$. This happens because some link $(i, 0, \cdot)$ destined to the Sink successfully transmits and no new exogenous arrival affects the queues.

$$P_{c3}\left(i\right) = \mathbb{1}\left\{\Delta\mathcal{L} \in \Psi\left(\mathcal{L} \cup a\right), \Delta\mathcal{L} = (i, 0, \cdot)\right\} \cdot \left(P\left\{\mathbf{I}_0\right\} + \sum_{q'_k = q^{max}, k \in V} P\left\{\mathbf{I}_k\right\}\right). \quad (21)$$

Case 4 (c4): $\mathbf{q}' = \mathbf{q} - \mathbf{I}_i + \mathbf{I}_j, i, j \in V, i \neq j$. This case includes two possibilities: (*c4:1*) Some SISO link $(i, j, \varnothing)$ successfully transmits and no change of queue due to new exogenous arrival; and (*c4:2*) link $(i, 0, \cdot)$ successfully transmits and Node j self-generates a new

packet.

$$P_{c4:1}(i,j) = \mathbb{1}\{\Delta\mathcal{L} \in \Psi(\mathcal{L} \cup a), \Delta\mathcal{L} = (i,j,\varnothing)\} \cdot \left(P\{\mathbf{I}_0\} + \sum_{q'_k = q^{max}, k \in V} P\{\mathbf{I}_k\} \right). \quad (22)$$

$$P_{c4:2}(i,j) = \mathbb{1}\{\Delta\mathcal{L} \in \Psi(\mathcal{L} \cup a), \Delta\mathcal{L} = (i,0,\cdot)\} P\left\{\mathbf{I}_j\right\}. \quad (23)$$

Case 5 (c5): $\mathbf{q}' = \mathbf{q} - \mathbf{I}_i + 2\mathbf{I}_j, i, j \in V, i \neq j$. This occurs because the SISO link $(i, j, \varnothing)$ successfully transmits and Node j self-generates a new packet.

$$P_{c5}(i,j) = \mathbb{1}\{\Delta\mathcal{L} \in \Psi(\mathcal{L} \cup a), \Delta\mathcal{L} = (i,j,\varnothing)\} \cdot P\left\{\mathbf{I}_j\right\}. \quad (24)$$

Case 6 (c6): $\mathbf{q}' = \mathbf{q} - \mathbf{I}_i + \mathbf{I}_j + \mathbf{I}_k, i, j, k \in V, i \neq j \neq k$. This occurs because the SISO link $(i, j, \varnothing)$ successfully transmits and a different Node k self-generates a new packet.

$$P_{c6}(i,j,k) = \mathbb{1}\{\Delta\mathcal{L} \in \Psi(\mathcal{L} \cup a), \Delta\mathcal{L} = (i,j,\varnothing)\} P\{\mathbf{I}_k\} + \mathbb{1}\{\Delta\mathcal{L} \in \Psi(\mathcal{L} \cup a), \Delta\mathcal{L} = (i,k,\varnothing)\} P\left\{\mathbf{I}_j\right\}. \quad (25)$$

Therefore, the transition kernel of $\mathbf{q}(t)$ is expressed as Eq.(47).

4.3) *Energy evolution dynamics*: The process $\mathbf{e}(t)$ is dictated by transmission energy and receiving energy consumption incurred during a finished link transmission, regardless of success or failure. In the CT case, the cooperators consume additional energy in receiving the broadcast packet initiated by the source and in conducting CT. The transition kernel of $\mathbf{e}(t)$ is given in Eq.(49).

Given the transition kernel of the component processes, the whole system's transition is derived in Eq.(28)-(30).

5) Expected Total Rewards: During a time Slot, the system obtains a reward $g(\mathbf{s}, a) = 1$ if a packet was delivered to the Sink, and $g(\mathbf{s}, a) = 0$ otherwise. Then, for $\mathbf{s} \in S \setminus S_t$ (S_t are termination states), we have:

$$g(\mathbf{s}, a) \triangleq E[r] \quad (25)$$

$$= \sum_{\substack{l \in \Psi(\mathcal{L} \cup a) \\ d(l)=0}} P\left\{z^l \mid \mathcal{L}, a\right\} \mathbb{1}\{\Psi(\mathcal{L} \cup a) \neq \varnothing\}. \quad (26)$$

$$P\{\mathbf{q}' \mid \mathcal{L}', \mathcal{L}, \mathbf{q}, a\} = \begin{cases} P_{c1:1} + P_{c1:2} & \text{if } \mathbf{q}' = \mathbf{q}, \\ P_{c2:1}(j) + P_{c2:2}(j) & \text{if } \mathbf{q}' = \mathbf{q} + \mathbf{I}_j, j \in V, \\ P_{c3}(i) & \text{if } \mathbf{q}' = \mathbf{q} - \mathbf{I}_i, i \in V, \\ P_{c4:1}(i,j) + P_{c4:2}(i,j) & \text{if } \mathbf{q}' = \mathbf{q} - \mathbf{I}_i + \mathbf{I}_j, i, j \in V, \\ P_{c5}(i,j) & \text{if } \mathbf{q}' = \mathbf{q} - \mathbf{I}_i + 2\mathbf{I}_j, i, j \in V, i \neq j, \\ P_{c6}(i,j,k) & \text{if } \mathbf{q}' = \mathbf{q} - \mathbf{I}_i + \mathbf{I}_j + \mathbf{I}_k, i, j, k \in V, i \neq j \neq k, \\ 0 & \text{otherwise.} \end{cases} \tag{26}$$

$$P\{\mathbf{e}' \mid \mathcal{L}', \mathcal{L}, \mathbf{e}, a\} = \begin{cases} \mathbb{1}\left\{\mathbf{e}' = \mathbf{e} - \mathbf{I}_i e_{tx} - \mathbf{I}_j e_{rx}\right\} & \text{if } \Delta\mathcal{L} = (i, j, \varnothing) \in (\mathcal{L} \cup a)^{so}, j \in V^*, \\ \mathbb{1}\left\{\mathbf{e}' = \mathbf{e} - \mathbf{I}_i e_{init}^{CT} - \sum\limits_{k \in \mathcal{H}(i)} \mathbf{I}_k e_{co}^{CT}\right\} & \text{if } \Delta\mathcal{L} = (i, 0, \mathcal{H}(i)) \in (\mathcal{L} \cup a)^{vo}, i \in V, \\ \mathbb{1}\{\mathbf{e}' = \mathbf{e}\} & \text{if } \Delta\mathcal{L} = \varnothing, \\ 0 & \text{otherwise.} \end{cases} \tag{27}$$

$$\begin{aligned} P\{\mathcal{L}', \mathbf{q}', \mathbf{e}' \mid \mathcal{L}, \mathbf{q}, \mathbf{e}, a\} &= P\{\mathbf{q}' \mid \mathcal{L}', \mathbf{e}', \mathcal{L}, \mathbf{q}, \mathbf{e}, a\} P\{\mathcal{L}', \mathbf{e}' \mid \mathcal{L}, \mathbf{q}, \mathbf{e}, a\} && (28) \\ &= P\{\mathbf{q}' \mid \mathcal{L}', \mathbf{e}', \mathcal{L}, \mathbf{q}, \mathbf{e}, a\} P\{\mathbf{e}' \mid \mathcal{L}', \mathcal{L}, \mathbf{q}, \mathbf{e}, a\} P\{\mathcal{L}' \mid \mathcal{L}, \mathbf{q}, \mathbf{e}, a\} && (29) \\ &= P\{\mathbf{q}' \mid \mathcal{L}', \mathcal{L}, \mathbf{q}, a\} P\{\mathbf{e}' \mid \mathcal{L}', \mathcal{L}, \mathbf{e}, a\} P\{\mathcal{L}' \mid \mathcal{L}, a\} && (30) \end{aligned}$$

And for $\mathbf{s} \in S_t$, $g(\mathbf{s}, a) = 0$. The expected total rewards of the process starting from an initial state $\mathbf{s}$, under the policy $\boldsymbol{\pi}$ is denoted by

$$\mathcal{J}^{\pi}(\mathbf{s}) = \sum_{t=1}^{\infty} g(\mathbf{s}(t), a(t)). \tag{27}$$

6) MDP formulation. A transmission policy is a series of decision rules $\boldsymbol{\pi} = [a(1), a(2), \cdots]$, where $a(t) : \mathcal{S}(t) \to \mathcal{A}(\mathcal{S}(t))$. The maximum lifetime $\mathcal{J}^*(\mathbf{s})$ is given by:

$$\mathcal{J}^*(\mathbf{s}) = \max_{\boldsymbol{\pi}} \mathcal{J}^{\pi}(\mathbf{s}). \tag{28}$$

The optimal lifetime $\mathcal{J}^*(\mathbf{s})$ is the unique solution of the Bellman's optimality equation [51]:

$$\mathcal{J}(\mathbf{s}) = \max_{a} \left\{ g(\mathbf{s}, a) + \sum_{\mathbf{s}'} P\{\mathbf{s}' \mid \mathbf{s}, a\} \ \mathcal{J}(\mathbf{s}') \right\}. \tag{29}$$

A policy $\boldsymbol{\pi}^*$ is optimal if it achieves the maximum expected lifetime for all starting state,

i.e.,

$$\mathcal{J}^{\pi^*}(\mathbf{s}) = \mathcal{J}^*(\mathbf{s}), \forall \mathbf{s} \in \mathcal{S} \setminus \mathcal{S}_t. \tag{30}$$

5.3 Computational Method

Consider that the total energies are non-increasing, we group the states according to the sum energy (in decreasing order), and solve the stages backwards. The transmission sets are computed using the Bron-Kerbosch algorithm [90], which is widely used and referred to as one of the fastest. In each stage, the computation of the energy and queue state spaces is similar to the *Bin-Ball* problem. The *Bin-Ball* problem refers to enumerating the ways of allocating n_1 balls into n_2 bins. In our problem, the "bins" are the nodes, the "balls" are the total energies or queued packets. For instance, the number of ways to allocate n_1 units of energies into n_2 nodes with minimum energy requirement of $\theta = e_{th} + 1$ (in $\mathcal{S} \setminus \mathcal{S}_t$), is given by:

$$\sum_{l=0}^{n_2} (-1)^l \binom{n_2}{l} \binom{n_2 + n_1 - n_2\theta - l(e^{max} + 1 - \theta) - 1}{n_2 - 1}. \tag{31}$$

For an integer m (stage), the set of states S_m is defined as:

$$S_m = \left\{ (\mathcal{L}, \mathbf{e}, \mathbf{q}) \mid \sum_{i \in V} \mathbf{e}_i = m \right\}, \ m = N\theta, \cdots, Ne^{max}. \tag{32}$$

For each S_m and $\mathbf{s} \in S_m$, we have

$$\mathcal{J}^*(\mathbf{s}) = \max_{a \in \mathcal{A}(\mathbf{s})} \left\{ g(\mathbf{s}, a) + \sum_{\mathbf{s}'} P\{\mathbf{s}' \mid \mathbf{s}, a\} \mathcal{J}^*(\mathbf{s}') \right\} \tag{33}$$

$$= \max_{a \in \mathcal{A}(\mathbf{s})} \left\{ g(\mathbf{s}, a) + \sum_{\mathbf{s}' \in S_{N\theta} \cup \cdots \cup S_{m-1}} P\{\mathbf{s}' \mid \mathbf{s}, a\} \mathcal{J}^*(\mathbf{s}') + \sum_{\mathbf{s}' \in S_m} P\{\mathbf{s}' \mid \mathbf{s}, a\} \mathcal{J}^*(\mathbf{s}') \right\}, \ \mathbf{s} \in S_m. \tag{34}$$

Therefore, we formulate a Mixed Integer Linear Programming (MILP) problem (Subproblem-1):

$$\text{Minimize} \quad \sum_{\mathbf{s}\in S_m} \mathcal{J}(\mathbf{s}) \tag{35}$$

$$\text{S.t.} \quad \mathcal{J}(\mathbf{s}) - \sum_{\mathbf{s}'\in S_m} P(\mathbf{s}' \mid \mathbf{s}, a)\,\mathcal{J}(\mathbf{s}') \;\geq\; b(\mathbf{s}, a) \tag{36}$$

$$\mathcal{J}(\mathbf{s}) \in Z^+, \mathbf{s} \in S_m. \tag{37}$$

where, $b(\mathbf{s}, a)$ are obtained from previously computed stages:

$$b(\mathbf{s}, a) = g(\mathbf{s}, a) + \sum_{\mathbf{s}'\in S_{N\theta}\cup\cdots\cup S_{m-1}} P\{\mathbf{s}' \mid \mathbf{s}, a\}\,\mathcal{J}^*(\mathbf{s}'). \tag{38}$$

The computational method is summarized in Alg.1.

Algorithm 4: SSP-MILP Algorithm

```
input:
Nθ = Minimum Sum energy in states S \ S_t;
Ne^max = Maximum Sum energy in states S \ S_t;
J(s) = 0, ∀s ∈ S_t;
output: J(s), ∀s ∈ S \ S_t;
begin
    Find transmission link set using Bron-Kerbosch alg. ;
    m ← Nθ;
    while m ≤ Ne^max do
        Solve Bin-ball problem to obtain S_m.
        Solve MILP for Subproblem-1 to obtain J(s), s ∈ S_m.
        m ← m + 1.
    end
end
```

5.4 Numerical Results

We present some numerical results on the optimal lifetime of the *funnel* topology network as in Fig. 31(a). Besides the computational limitation inherent to MDP, the motivations for choosing a small network are as follows. First, the observation from our previous work [13] shows that under duty-cycling, a large network is typically reduced into isolated sections of small networks in the time domain, to reduce interference and collisions, i.e., only a small

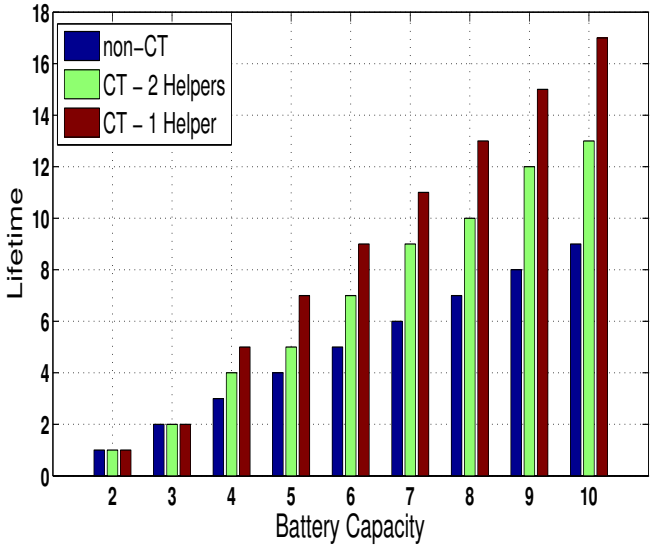

Figure 34. Optimal lifetime for non-CT network and CT network, as battery capacity varies. $N = 4$ **(number of nodes).** $N_H = 1$ **or** 2 **(required number of cooperators).** $e_{th} = 1,\ e_{tx} = e_{rx} = 1,\ e_{init}^{CT} = 1,\ e_{co}^{CT} = 2,\ q^{max} = 1$**.**

portion of a network is awake during a period of time. Second, the topology captures the essence of the *energy hole* problem.

Fig. 34 depicts the optimal lifetime for non-CT and CT networks. We observe the lifetimes are linearly increasing with the battery capacity. We also observe that the performance of CT network is significantly higher than that of the non-CT network. For example, with battery capacity of 10 units, the lifetime improvement factor of CT network is 1.89 with 1 cooperator. The lifetime with larger battery capacities is obtained from linear regression in Fig. 35. The lifetime growth rate w.r.t. battery capacity is 1.0 for non-CT, 1.6 for CT with 2 cooperators, and 2.1 for CT with 1 cooperator.

Fig. 36 shows the computed lifetime for different packet arrival rates (PARs). The PAR[3] is normalized with the packet length, i.e., the number of new exogenous packets per node during a packet duration. The PARs where the curves start to become flat represent the PAR thresholds, beyond which the numerical results are accurate. Fig. 36 demonstrates that our model is accurate for a very large range of arrival rates.

[3]For example, if a node generates a packet every 100 seconds, and the packet transmission time is 100ms, then the PAR is 0.001.

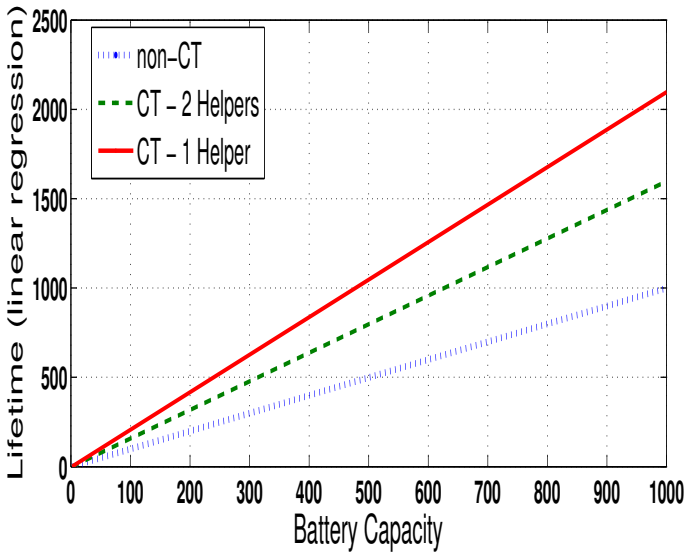

Figure 35. Optimal lifetime for non-CT network and CT network (from linear regression). $N = 4$ **(number of nodes).** $e_{th} = 1,\ e_{tx} = e_{rx} = 1,\ e_{init}^{CT} = 1,\ e_{co}^{CT} = 2,\ q^{max} = 1$**.**

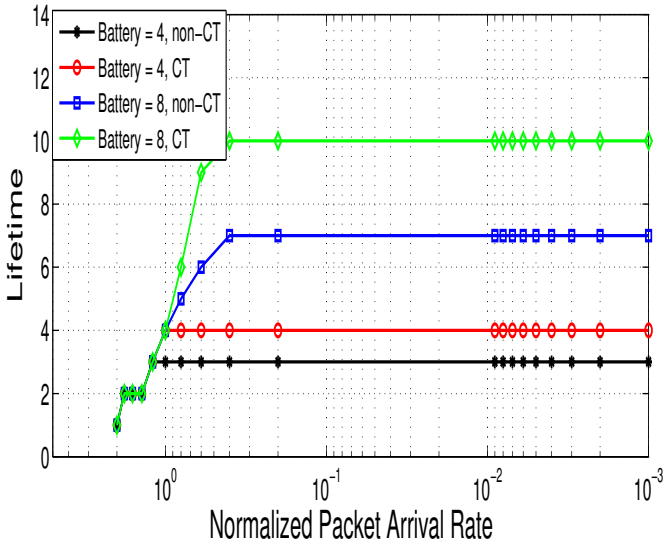

Figure 36. Lifetime for non-CT network and CT network, as the normalized packet arrival rate (PAR) varies. $N = 4,\ N_H = 2.\ e_{th} = 1,\ e_{tx} = e_{rx} = 1,\ e_{init}^{CT} = 1,\ e_{co}^{CT} = 2,\ q^{max} = 1$**.**

5.5 Conclusions

We present and validate a novel MDP framework to model the lifetime of *multihop* wireless sensor networks, for both non-CT and CT networks. The MDP jointly considers MAC layer link constraints, packet transfers in the routing layer, and energy evolution dynamics. A new algorithm that exploits the Stochastic Shortest Path structure and the Mixed Integer

Linear Programming is proposed to efficiently solve the problem.

CHAPTER 6

MODELING OPTIMAL PERFORMANCE OF ENERGY-HARVESTING MULTI-HOP WIRELESS SENSOR NETWORKS

Energy harvesting (EH) enables the next generation of perpetual, sustainable operation of self-powered wireless sensor networks (WSNs). However, a comprehensive multi-hop network model for EH-WSNs has not previously existed. In Chapter 5, we have modeled the lifetime of energy-constrained networks using a MDP model with finite horizon. The problems and performance metrics of EH networks are different with non-EH networks. Because the non-EH nodes depend on a battery, a suitable performance metric is the lifetime, defined as the number of packets delivered upon the first or a portion of nodes' death. Thus, the lifetime is governed by the absorbing states in a controlled dynamic system with finite decision horizon. On the other hand, the lifetime of an EH network is theoretically infinite unless the sensors are broken or destroyed. Therefore, an infinite horizon problem is formulated for analyzing the performance of EH networks.

In this chapter, we propose a Markov decision process model for multi-hop EHWSNs that considers energy harvesting, routing, MAC, and recently introduced cooperative transmission (CT) range extension. We also reformulate the state dynamics using generalized balance equations to improve the accuracy of the model. We will then present a dual linear programming (LP) based algorithm to obtain numerical results on the performance improvement of CT network over non-CT network, in terms of expected total discounted reward.

6.1 System Model and Assumptions

6.1.1 Topology and Link Models

6.1.1.1 Topology Model

The multi-hop network topology is modeled as a directed graph $G = (V, E)$. $V = \{1, \cdots, N\}$ is the set of nodes except the sink, whose ID is 0, and E is the set of links comprising

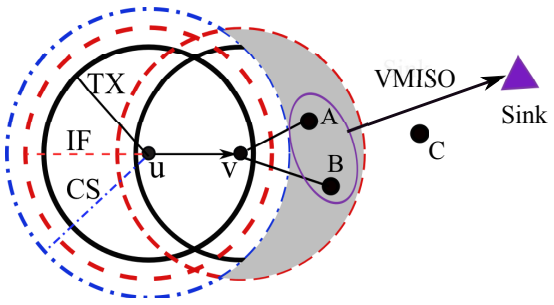

Figure 37. An illustration of interference model and VMISO link. Node v is the receiver of Node u. Node u's hidden nodes in the gray area will interfere v's reception.

both single-input-single-output (SISO) links and VMISO links, i.e., $E = E^{so} \cup E^{vo}$. A link l exists if its source can transmit to its destination through either SISO or CT with cooperators. In the later case, we assume the destination is the Sink. Therefore, a link is represented by the 3-tuple, $\langle s(l), d(l), C(s(l))\rangle \in E$, where $s(l)$ and $d(l)$ are the source and the destination, respectively; $C(s(l))$ is the cooperators of $s(l)$. Note that in the case of SISO link, $C(s(l)) = \varnothing$; and in the case of VMISO link, $d(l) = 0$.

6.1.1.2 Interference Model

A node has three ranges associated with it: the transmission range (TX), the interference range (IF), and the carrier sensing range (CS), as shown in Fig. 37. Similar to [86], we assume that link $(i, j, \cdot)$ interferes with link $(u, v, \cdot)$ if either the distance $dist(i, v) \leq IF(i)$ or $i = v$.

6.1.1.3 Medium Access Control Model

We assume that carrier-sensing-medium-access (CSMA) is performed before a node attempts to transmit. Further, similar to [88], it is assumed that (i) a node cannot transmit and receive at the same time, (ii) a node can transmit if none of its neighbors (in CS range) is transmitting, (ii) link errors result only from collisions due to hidden terminals, and (iii) nodes receive with perfect capture, i.e., a packet is successfully decoded if the receiver and none of its neighbors is transmitting at the start of packet.

6.1.2 Traffic and Energy Models

A mini-time-slotted system is considered, where slots are normalized to integral units $t \in \{1, 2, 3, \cdots\}$. By time t, we refer to the duration between $[t, t+1]$.

6.1.2.1 Traffic Model

The transmission duration of a link $l \in E$ is assumed exponentially distributed with the expectation $\bar{T}_l$, same as in [88] [89]. Note that this assumption is inaccurate, however, it is necessary to make the MDP problem tractable [89]. The memoryless property of the exponential distribution indicates that, given a packet is being transmitted at the beginning of a time slot, it completes within the slot of length ΔT with probability $\beta_l = 1 - e^{-\Delta T/\bar{T}_l}$, regardless of the number of slots it has been transmitting. Making ΔT small enough allows us to assume at most one link can finish transmission during a time slot, i.e., the probability that more than one link finish transmission is $o(\Delta t)$.

The number of exogenous (self-generated) packets at Node i of commodity d (destined to Sink d), $f_i^d(t)$, during any slot t is modeled as a binary random variable (RV), with probability mass function (PMF) $Pr[f_i^d(t) = 1] = \alpha^d(i)$ and $Pr[f_i^d(t) = 0] = 1 - \alpha^d(i)$, where $\alpha^d(i)$ represents the exogenous packet arrival rate, and is assumed *i.i.d.* over time slots.

6.1.2.2 Energy Harvesting Model

The energy harvested at Node i during any slot t is also modeled as a binary RV, which is denoted by $h_i(t) \in \{0, 1\}$. This RV has PMF $Pr[h_i(t) = 1] = \gamma(i)$ and $Pr[h_i(t) = 0] = 1 - \gamma(i)$. Representing the energy harvesting rate, $\gamma(i)$ is assumed *i.i.d.* over time slots. Thus, the energy of Node i evolves as

$$\mathbf{e}_i(t+1) = \min\{\Big(\mathbf{e}_i(t) - e_{com}^{(i,l)}\Big)^+ + h_i(t), e_{max}\}, \tag{39}$$

where, $e_{com}^{(i,l)}$ is the energy consumption of Node i if it participates in a finished link transmission l, and e_{max} is the battery capacity of a node.

6.2 Markov Decision Process Formulation

6.2.1 Network State Space

The network state is defined as $\mathbf{s} \triangleq \{\mathcal{L}, \mathbf{q}, \mathbf{e}\}$ to include the transmission set $\mathcal{L}$, the queuing level $\mathbf{q}$ of each node, and the energy $\mathbf{e}$ of each node. Note that the state space is not the Cartesian product of each component's state space, because they are interactive (e.g. an active link cannot have an empty queue at its source node).

The transmission set $\mathcal{L}(t)$ includes the links that are active (in transmission) at time t. Denote the state space of $\mathcal{L}$ as $\mathbb{L}$. This component includes the collisions in the MAC layer. We denote the links that are free of collision as $\Phi(\mathcal{L}) \subset \mathcal{L}$. $\Phi(\mathcal{L})$ is deterministic given $\mathcal{L}$, and $\Phi = \Phi^{\text{so}} \cup \Phi^{\text{vo}}$.

To find $\mathbb{L}$, it is equivalent to find the matchings of a graph. Given a graph $G = (V, E)$, a matching $M(G)$ in G is a set of non-adjacent edges (i.e., no two edges share a common vertex), implying $\mathcal{L} \in \{M(G)\}$. Further, the MAC layer CSMA adds constraints on $\mathcal{L}$, that for any two links $l_1, l_2 \in \mathcal{L}$, the sources of the two links $(s(l_1), s(l_2))$ must be out of carrier sensing (CS) range of each other. Therefore, $\mathbb{L}$ is determined by the graph G and the binary hearing matrix $\mathbf{H} = [h_{ij}]_{i,j \in V}$ of the network, where the element $h_{i,j} = 1$ if and only if (i.f.f.) Node i and Node j are within CS range of each other. Though enumerating matchings of a graph is *NP-complete*, Bron-Kerbosch algorithm has been shown to be one of the fastest [90] and has been used in this section.

6.2.2 Decision Epochs and Action Space

A decision epoch corresponds to the beginning of a time slot. The set of decision epochs are denoted by $\{1, 2, \cdots, T\}$. When T is finite (infinite), the decision problem is the referred to as a finite (infinite) horizon problem. An action, $a(t)$, is to admit a new link to the "*remaining*" transmission set $\mathcal{L}(t)$, which comprises those links that did not complete transmission during Slot $t-1$. Note that $\mathcal{L}(t) \subset \mathcal{L}(t-1) \cup a(t-1)$. The action space at time t when the system state is $\mathbf{s}(t)$ is represented by

$$\mathcal{A}(\mathbf{s}(t)) = \{l \in E : \mathbf{q}_{s(l)}(t) > 0, l \notin \mathcal{L}(t), \mathcal{L}(t) \cup l \subset \mathbb{L}, E_{\text{suf}}\}, \tag{40}$$

where E_{suf} indicates $\mathbf{e}_i \geq e_{com,}^{(i,l)}, \forall i \in l$. Therefore, a link l can join $\mathcal{L}(t)$ i.f.f. its source has a non-empty queue, $\mathcal{L}(t) \cup l$ is also a transmission set, and, the participating nodes have enough energy. Note that it is assumed at most one link can be admitted to $\mathcal{L}(t)$, because ΔT is small. Also, note that the null set $\varnothing \in \mathcal{A}(\mathbf{s}(t))$. As a result, an action can be either a "CT" link, a "non-CT" link or null (no new transmission).

6.2.3 State Transition Dynamics

6.2.3.1 Transmission set dynamics

: let action $a(t) \in \mathcal{A}(\mathbf{s}(t))$ denote the link admitted the transmission set. Denote $p\left\{z^l(t) \mid \mathcal{L}(t), a(t)\right\}$ as the probability that only link $l \in \mathcal{L}(t) \cup a(t)$ finishes transmission during Slot t, and $p\left\{z^{\varnothing}(t) \mid \mathcal{L}(t), a(t)\right\}$ as the probability that no link finishes transmission during Slot t. The time index is dropped when there is no ambiguity. For abbreviation, we denote the transition kernel as $p\left\{\mathcal{L}' \mid \mathcal{L}, a\right\} := p\left\{\mathcal{L}\left(t+1\right) \mid \mathcal{L}\left(t\right), a\left(t\right)\right\}$.

$$p\left\{z^l \mid \mathcal{L}, a\right\} = \beta_l \prod_{\substack{k \in \mathcal{L} \cup a \\ k \neq l}} \left(1 - \beta_k\right), \forall l \in \mathcal{L} \cup a. \tag{41}$$

$$p\left\{z^{\varnothing} \mid \mathcal{L}, a\right\} = \begin{cases} \prod_{l \in \mathcal{L} \cup a} \left(1 - \beta_l\right) & \text{if } \mathcal{L} \cup a \neq \varnothing, \\ 1 & \text{if } \mathcal{L} \cup a = \varnothing. \end{cases} \tag{42}$$

Define $\mathcal{D}^{(L)} \triangleq \{\mathcal{L} \cup a\} \setminus \mathcal{L}'$, then we can get:

$$p\left\{\mathcal{L}' \mid \mathcal{L}, a\right\} = \begin{cases} p\left\{z^l \mid \mathcal{L}, a\right\} & \text{if } \mathcal{D}^{(L)} = l, \\ p\left\{z^{\varnothing} \mid \mathcal{L}, a\right\} & \text{if } \mathcal{D}^{(L)} = \varnothing, \\ 0 & \text{otherwise.} \end{cases} \tag{43}$$

To express in a uniform form, the evolutions of $\mathbf{q}$ and $\mathbf{e}$ are governed by the following balance equations:

$$\psi^{(i)}(t+1) = \psi^{(i)}(t) + \mathbf{R}^{(i)}\mathbf{M}^{(i)}(t)\Gamma^{(i)}(t) + \sigma^{(i)}(t), \tag{44}$$

where, $i \in \{q, e\}$, $\psi^{(q)}$ represents $\mathbf{q}$, and $\psi^{(e)}$ represents $\mathbf{e}$.

6.2.3.2 *Queue length dynamics*

In Eq. (44), $\mathbf{M}^{(q)}$ is a $|E| \times |E|$ diagonal matrix. The diagonal element $\mathbf{M}_l^{(q)} = 1$ if the transmission of link l is *completed* and *successful*[1], and $\mathbf{M}_l^{(q)} = 0$ otherwise. Note that it is assumed $\sum_{l \in E} \mathbf{M}_l^{(q)} \leq 1$, i.e., at most one link can finish transmission. $\Gamma^{(q)}$ is the transmission schedule vector, which satisfies $\Gamma_l^{(q)} = 1, \forall l \in \mathcal{L} \cup a$ and $\Gamma_l^{(q)} = 0$ otherwise. $\mathbf{R}^{(q)}$ is the $N \times |E|$ routing matrix, whose element in ith row and lth column is

$$r_{il}^{(q)} = \begin{cases} 1 & \text{if } d(l) = i \text{ and Node } i \text{ is not the sink,} \\ -1 & \text{if } s(l) = i, \\ 0 & \text{otherwise.} \end{cases} \tag{45}$$

$\sigma^{(q)}$ is an $N \times 1$ vector representing the number of self-generated packets, and $\sigma_i^{(q)} = f_i$.

Let $\mathbf{I}_i$ represent a vector with its ith element being 1 and other elements being 0, $1 \leq i \leq N$, and let $\mathbf{I}_0$ be the zero vector. Denote $V^{(q)}(t)$ as the nodes whose queue is not full at time t, and define the difference

$$\mathcal{D}^{(q)} = \begin{cases} \mathbf{q}' - \mathbf{q} & \text{if } \mathcal{D}^{(L)} = \varnothing, \\ \mathbf{q}' - \mathbf{q} + \mathbf{I}_{s(\mathcal{D}^{(L)})} - \mathbf{I}_{d(\mathcal{D}^{(L)})} & \text{if } \mathcal{D}^{(L)} \in \Phi^{\text{so}}\{\mathcal{L} \cup a\}, \\ \mathbf{q}' - \mathbf{q} + \mathbf{I}_{s(\mathcal{D}^{(L)})} & \text{if } \mathcal{D}^{(L)} \in \Phi^{\text{vo}}\{\mathcal{L} \cup a\}. \end{cases} \tag{46}$$

Then consider exogenous packet arrivals, the queue status is updated as follows:

$$p\{\mathbf{q}' \mid \mathcal{L}', \mathcal{L}, \mathbf{q}, a\} = \begin{cases} \prod_{i \in V} \left(\alpha_i \mathbb{1}\left\{ \mathcal{D}_i^{(q)} = 1 \right\} + (1 - \alpha_i) \mathbb{1}\left\{ \mathcal{D}_i^{(q)} = 0, i \in V^{(q)} \right\} \right) \\ \qquad \text{if } \mathcal{D}^{(L)} \in \{\Phi^{\text{so}}\{\mathcal{L} \cup a\}, \Phi^{\text{vo}}\{\mathcal{L} \cup a\}, \varnothing\}, \\ 0 \qquad \text{otherwise.} \end{cases} \tag{47}$$

where $\mathbb{1}\{\cdot\}$ is the indicator function.

[1] A finished transmission, while always consuming energy, is not necessarily successfully decoded by the receiver, because of collision due to hidden terminals; in case of failure, the packet remains in the queue of the transmitter.

6.2.3.3 *Energy evolutions*

using analysis similar to queue in *(2)*, denote $V^{(e)}(t)$ as the nodes whose battery is not full at time t, and define

$$\mathcal{D}^{(e)} = \begin{cases} \mathbf{e}' - \mathbf{e} & \text{if } \mathcal{D}^{(L)} = \varnothing, \\ \mathbf{e}' - \mathbf{e} + \mathbf{I}_{s(\mathcal{D}^{(L)})} \cdot e_{tx} + \mathbf{I}_{d(\mathcal{D}^{(L)})} \cdot e_{rx} & \text{if } \mathcal{D}^{(L)} \in E^{\text{so}}, \\ \mathbf{e}' - \mathbf{e} + \mathbf{I}_{s(\mathcal{D}^{(L)})} e_{init}^{\text{CT}} + \sum\limits_{k \in C(\mathcal{D}^{(L)})} \mathbf{I}_k e_{co}^{\text{CT}} & \text{if } \mathcal{D}^{(L)} \in E^{\text{vo}}. \end{cases} \tag{48}$$

Then, consider the influence of energy harvesting, we get

$$p\left\{\mathbf{e}' \mid \mathcal{L}', \mathcal{L}, \mathbf{e}, a\right\} = \begin{cases} \prod\limits_{i \in V} \left(h_i \mathbb{1}\left\{\mathcal{D}_i^{(e)} = 1\right\} + (1 - h_i)\, \mathbb{1}\left\{\mathcal{D}_i^{(e)} = 0, i \in V^{(e)}\right\}\right) \\ \qquad\qquad \text{if } \mathcal{D}^{(L)} \in \{E^{\text{so}}, E^{\text{vo}}, \varnothing\}, \\ 0 \qquad\qquad \text{otherwise.} \end{cases} \tag{49}$$

6.2.3.4 *System dynamics*

the transition matrix of the system states $\mathbf{s} \triangleq \{\mathcal{L}, \mathbf{e}, \mathbf{q}\}$ can be obtained by the following theorem.

Theorem 6.2.1 *The transition kernel of the system, $p\{\mathbf{s}'|\mathbf{s}, a\}$, is equal to the product of Eq.*(43)*,* (47) *and* (49)*.*

Proof According to the chain rule, $p\{\mathbf{s}'|\mathbf{s}, a\}$ can be expressed as $p(\mathbf{q}'|A) \cdot p(\mathbf{e}'|B) \cdot p(\mathcal{L}'|C)$, where $A = \{(\mathcal{L}', \mathbf{e}', \mathcal{L}, \mathbf{q}, \mathbf{e}, a)\}$, $B = \{(\mathcal{L}', \mathcal{L}, \mathbf{q}, \mathbf{e}, a)\}$, and $C = \{(\mathcal{L}, \mathbf{q}, \mathbf{e}, a)\}$. Further, since $\mathbf{q}'$ and $(\mathbf{e}', \mathbf{e})$ are conditionally independent, given $(\mathcal{L}', \mathcal{L}, \mathbf{q}, a)$, the first element in the product, $p(\mathbf{q}'|A)$, is reduced to Eq.(47). Applying similar arguments to $p(\mathbf{e}'|B)$ and $p(\mathcal{L}'|C)$, Theorem 6.2.1 is proved.

6.2.4 Performance Criterion and Reward Function

Let $v_T^{\pi}(\mathbf{s})$ denote the expected total reward, when an initial state $\mathbf{s}$ and a policy π (a series of decisions) are given, and the decision-making horizon length T is a random variable:

$$v_T^{\pi}(\mathbf{s}) = \lim_{T\to\infty} \mathbb{E}_{\mathbf{s}}^{\pi}\left[\mathbb{E}_T\left\{\sum_{t=1}^{T} r\left(\mathbf{s}(t), a(t)\right)\right\}\right]. \tag{50}$$

The definition of the reward function, $r(\mathbf{s}, a)$, depends on application requirements and can be subjective to network designers. We define two reward functions as follows. In Eq. (51), a unit of reward is obtained if a packet is successfully received by the Sink. Eq. (52) is a weighted sum of the rewards from delivered packet, and the penalty from a QoS degradation (e.g. S_D are states where any node's energy drops to zero).

$$r^{(1)}(\mathbf{s}, a) = \sum_{\substack{l\in\Phi(\mathcal{L}\cup a)\\ d(l)=0}} P\left\{z^l \mid \mathcal{L}, a\right\} \mathbb{1}\left\{\Phi(\mathcal{L}\cup a) \neq \varnothing\right\}, \tag{51}$$

$$r^{(2)}(\mathbf{s}, a) = \omega_1 r^{(1)}(\mathbf{s}, a) - \omega_2 \mathbb{1}\left\{\mathbf{s} \in S_D\right\}. \tag{52}$$

Since the state space and the action space are finite, with a finite reward function, Eq. (50) can be expressed as:

$$v_{\lambda}^{\pi}(s) = \mathbb{E}_s^{\pi}\left\{\sum_{t=1}^{\infty} \lambda^{t-1} r\left(\mathbf{s}(t), a(t)\right)\right\}, \tag{53}$$

where it is assumed that T is geometrically distributed with parameter λ, $0 \leq \lambda < 1$. Thus, the expected value of T is $1/(1-\lambda)$. The parameter λ is the discount factor, which measures the present value of one unit of reward received one period in the future [51].

6.2.5 Optimality Equations

The optimality equation for the expected total discounted reward criteria given an initial state, a.k.a. the Bellman's equation, is given as follows:

$$v_{\lambda}^{*}(\mathbf{s}) = \max_{a\in\mathcal{A}(s)}\left\{r\left(\mathbf{s}, a\right) + \sum_{\mathbf{s}'} \lambda p\left\{\mathbf{s}' \mid \mathbf{s}, a\right\}\ v_{\lambda}^{*}\left(\mathbf{s}'\right)\right\}. \tag{54}$$

6.3 Computational Method

The following theorem provides the basis for a linear programming (LP) approach to solve the MDP problem. The proof can be found in [51].

Theorem 6.3.1 *Suppose there exists a* $\mathbf{v}$*, for which* $\mathbf{v} \geq \mathbb{T}(\mathbf{v})$*, then* $\mathbf{v} \geq \mathbf{v}^*_\lambda$*.* $\mathbb{T}$ *is the nonlinear operator defined as:* $\mathbb{T}(\mathbf{v}) \equiv \sup_{all\ a}\{\mathbf{r}_a + \lambda \mathbf{P}_a \mathbf{v}\}$.

From the observation in Theorem 6.3.1, the primal LP is constructed as follows:

Primal LP:

$$\text{Minimize} \quad \sum_{\mathbf{s}\in S} \eta(\mathbf{s}) v(\mathbf{s}) \tag{55}$$

$$\text{s.t.} \quad v(\mathbf{s}) - \sum_{\mathbf{s}'\in S} \lambda P\left(\mathbf{s}' \mid \mathbf{s}, a\right) v(\mathbf{s}') \quad \geq \quad r(\mathbf{s}, a) \tag{56}$$

for all $a \in \mathcal{A}(\mathbf{s})$, and all $\mathbf{s} \in S$. $\eta(\mathbf{s})$ are chosen to be positive scalars that satisfy $\sum_{\mathbf{s}\in S} \eta(\mathbf{s}) = 1$.

However, it is more informative to solve this model using its dual LP [51], which has less rows in the constraints matrix.

Dual LP:

$$\text{Maximize} \quad \sum_{\mathbf{s}\in S} \sum_{a\in\mathcal{A}(\mathbf{s})} r(\mathbf{s}, a) x(\mathbf{s}, a) \tag{57}$$

$$\text{s.t.} \sum_{a\in\mathcal{A}(\mathbf{s})} x(\mathbf{s}, a) - \sum_{\mathbf{s}'\in S} \sum_{a\in\mathcal{A}(\mathbf{s}')} \lambda P\left(\mathbf{s} \mid \mathbf{s}', a\right) x(\mathbf{s}', a) = \eta(\mathbf{s}) \tag{58}$$

and $x(\mathbf{s}, a) \geq 0$ for $a \in \mathcal{A}(\mathbf{s})$ and $\mathbf{s} \in S$.

Note that the primal LP has $\sum_{\mathbf{s}\in\mathcal{S}} |\mathcal{A}(\mathbf{s})|$ rows and $|\mathcal{S}|$ columns, while the dual LP has $|\mathcal{S}|$ rows and $\sum_{\mathbf{s}\in\mathcal{S}} |\mathcal{A}(\mathbf{s})|$ columns. In [91], it is shown that the value function for each state in the primal LP is equal to the dual price [2] corresponding to the constraint associated with the state in the dual LP. Thus, the value function associated with a given initial state of the primal LP is obtained by firstly solving the dual problem and then finding the dual price of the corresponding constraint.

[2] The dual price (a.k.a. shadow price) of a constraint is instantaneous change in the objective function by relaxing the constraint by one unit.

6.4 Numerical Results

We present some numerical results on the expected total discounted reward of the 2-hop *funnel* topology network (Node A, B, C and the Sink), as in Fig. 37. Besides the computational limitation inherent to MDP, the motivation for choosing a small network is as follows. It is observed from our previous work [13] that under duty-cycling, a large network is typically reduced into isolated small networks in the time domain, to reduce interference and collisions. This observation renders the possibility to analyze a small tree topology towards the whole network. The reward function in Eq. (51) is used for plotting Figs. 38, 39 and 40, while Eq. (52) is used for Fig. 41.

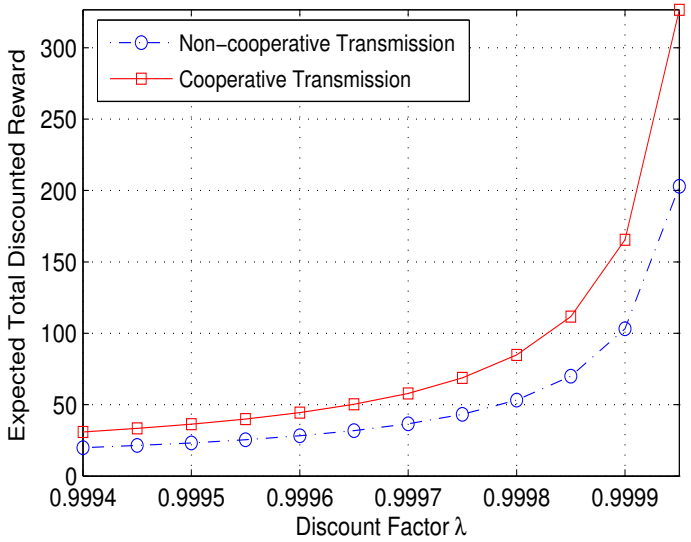

Figure 38. The effect of discount factor λ. $\alpha = 0.1$, $\gamma = 0.01$, $e_{max} = 4$, $q_{max} = 1$.

Fig. 38 shows the expected total discounted reward of non-CT and CT networks, versus different discount factors λ. The decision-making horizon is indicated by $1/(1-\lambda)$ time units. The system parameters are $\alpha = 0.1$, $e_{max} = 4$, $q_{max} = 1$, $e_{tx} = e_{rx} = e_{init}^{\mathrm{CT}} = 1$, and $e_{co}^{\mathrm{CT}} = 2$, where e_{tx} and e_{rx} represent transmitting/receiving energy, e_{init}^{CT} represents the energy consumption of initiating CT, and e_{co}^{CT} is the energy consumption of a cooperator. We observe that the rewards increase as λ increases due to an increase in the number of decision epochs, which allows prolonged operation of the network in the optimal states

prescribed by the optimal policy. While CT network always outperforms non-CT network (55% to 61% improvement), the curve of the CT network also grows with a steeper rate.

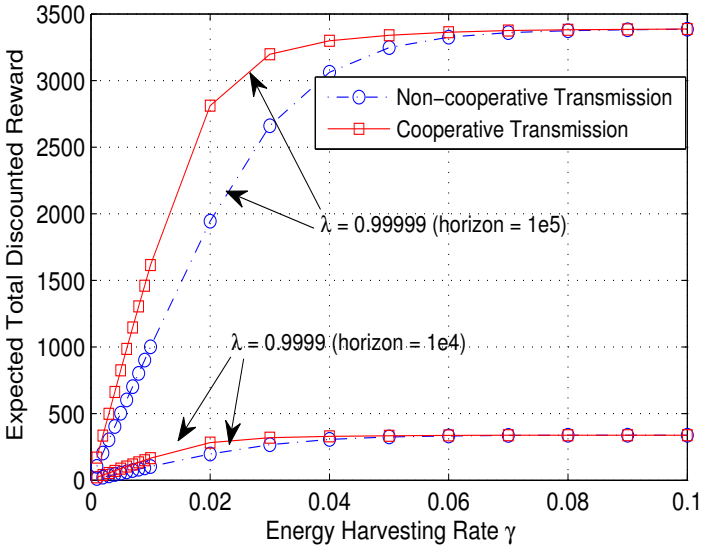

Figure 39. The effect of energy harvesting rate γ. $\alpha = 0.1$, $\lambda = 0.9999$ or 0.99999, $e_{max} = 4$, $q_{max} = 1$.

Fig. 39 depicts the expected total discounted reward of non-CT and CT networks, versus energy harvesting rate γ, with $\lambda = 0.9999$ or $\lambda = 0.99999$. Other system parameters are the same as used in Fig. 38. We observe that for both non-CT and CT network, the rewards increase linearly when γ is below 0.01. Then the curves grow with a slower rate, before the performances of non-CT and CT networks start to converge when the value of γ reaches a threshold value γ_{th}. For $\lambda = 0.9999$, $\gamma_{th} = 0.04$, and for $\lambda = 0.99999$, $\gamma_{th} = 0.07$. This threshold is related to both energy harvesting rate and battery capacity. High harvesting rate, with which packet transmission opportunities are less constrained by energy level, diminishes the benefits of CT. However, in practice, when harvesting rate is not large enough, the CT network still provides a significant gain over the non-CT network, as shown in the figure.

Fig. 40 shows the expected total discounted reward of non-CT and CT networks, versus exogenous packet arrival rate α, with $q_{max} = 1$ or $q_{max} = 2$. The system parameters are $\lambda = 0.9999$, $\gamma = 0.02$. It can be seen that when the offered traffic load (α) increases while

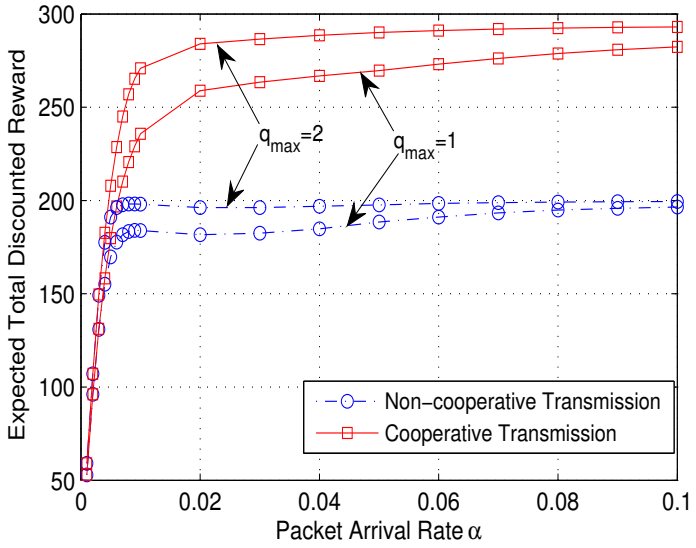

Figure 40. The effect of packet arrival rate α. $\lambda = 0.9999$, $\gamma = 0.02$, $e_{max} = 4$.

not saturating the networks, the rewards show a linear increase. When α is large enough, the rewards are bottlenecked by the queue capacity. We also observe that the reward of non-CT shows slight instability between $\alpha = 0.01$ and 0.02, in between the rewards slightly decrease, for both $q_{max} = 1$ and $q_{max} = 2$, which we did not explain. However, the CT network does not show this behavior.

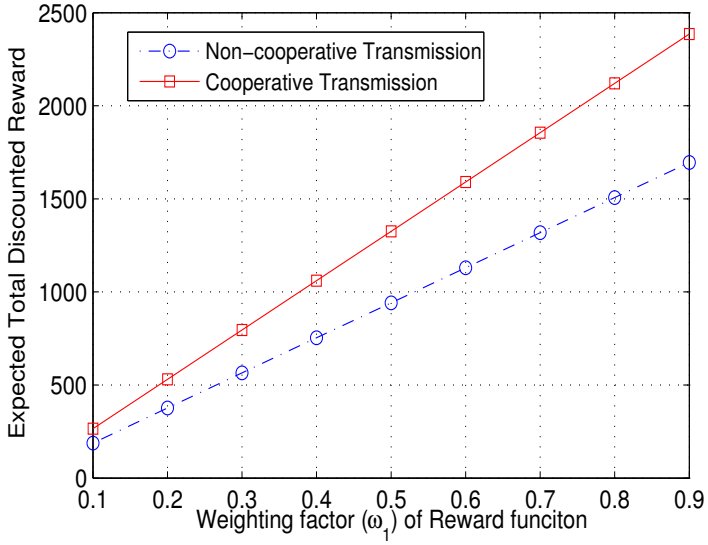

Figure 41. The effect of weight factor ω_1. $\lambda = 0.99999$, $\gamma = 0.02$, $e_{max} = 4$.

Fig. 41 gives an example that the calculated benchmark of performance is highly affected by he choice of reward function. The network designer can choose a reward function according to a particular QoS requirement. The x-axis is the preference weighting factor ω_1 in the reward function in Eq. (52). Note that $\omega_2 = 1 - \omega_1$ represents the significance of an occurrence of QoS degradation. When a certain application deems a state with a node having zero energy as a severe situation, both non-CT and CT network will be conservative in initiating a packet transmission, limiting the packets delivered in a given time horizon. On the other hand, the value functions increase as the significance relaxes. Again, CT network still outperforms non-CT network both in magnitude and rate in all cases.

6.5 Conclusions

A comprehensive network model for energy-harvesting multi-hop WSN is presented to encompass energy harvesting, routing, MAC and cooperative transmission. The expected total discounted reward model allows one to formulate different performance metrics of interest. Numerical results evaluate the sensitivity of several network parameters on the optimal reward of non-CT and CT networks. Deriving the approximate optimal policy is among some of the future directions.

CHAPTER 7

THZ PULSE-LEVEL BEAM-SWITCHING MAC WITH ENERGY CONTROL (TRPLE)

Terabit-per-second (Tbps) short-range communication in the Terahertz (THz) Band (0.1-10 THz) is envisioned as a key wireless technology in the next decade [17] [18] [19] [20]. Though much research has been recently performed towards channel modeling, antenna design and transceiver design [18], the protocol design in the system level is still unsolved. In this chapter, we introduce pulse-level beam-switching and pulse repetition for energy control (TRPLE), and present the first system design and stochastic analysis with directional MAC for THz networks. TRPLE is designed to tailor to the peculiarities of the THz channel and the expected capability of THz transceivers.

As introduced in Chapter 2 and shown in Fig. 42, the peculiarities of the THz Band limit its range compared to 60 GHz or ultra-wideband (UWB), and distinguish TeraNets from conventional wireless systems. Specifically, the absorption loss makes THz channel strongly frequency-selective and lossy. In the context of such a THz channel, and in contrast to conventional MACs that tackle contention and interference management, the new direction of MAC design for TeraNets will target scheduling transmission over either line-of-sight (LOS) or directed NLOS, and utilize the pulse-level beam-switching capability enabled by on-board large antenna arrays.

In the rest of this chapter, we will first describe the assumptions on the modulation scheme and device capability. Then, the details of TRPLE MAC protocol will be presented to solves the neighbor discovery, transmission scheduling, and energy control. Based on the protocol, analytical investigations for single user data rate and network throughput will be performed, followed by numerical evaluation.

7.1 Pulse-level Beam Switching: Physical Layer Vision

In this section, we further motivate TRPLE and describe the expected physical layer and the transceiver structure. To our knowledge, the implications of pulse-level beam-switching on the upper layer protocols have not been investigated. Also, we note that multi-band carrier-modulation is theoretically possible, but impractical due to nonexistence of a supportive digital processor.

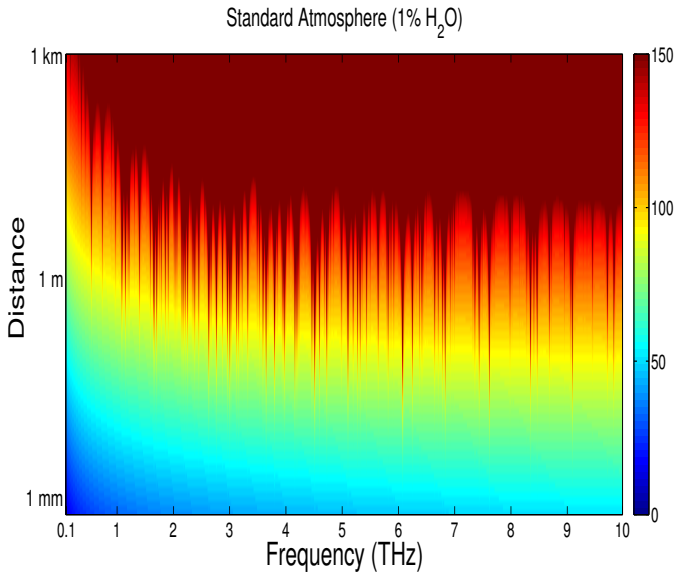

Figure 42. Path loss (in dB) in THz Band v.s. distances and frequencies. The peaks are caused by molecular absorption.

Impulse radio with TS-OOK: we assume an impulse radio, which generates pulses which are extremely narrow in time, as demonstrated in [27] [28]. The modulation considered is Time-spread On-off-keying (TS-OOK) [30], which can be supported by current technology. In TS-OOK, the logical "1" is encoded with a pulse, and the logical "0" is encoded with silence, as in traditional OOK. The distinction of TS-OOK is that as the channel is frequency-selective (even without multi-path) due to molecular absorption, the gap between consecutive pulses to the same user must be adequately large to tolerate pulse-broadening by the channel, so that equalization is not needed.

Narrow beamwidth: in light of graphene-based nano-antennas [26], we assume that all the THz radios are equipped with electronically steerable antenna arrays. Therefore,

directivity can be achieved at both the transmitter and the receiver. With high directivity, transmission-beam is narrow enough to illuminate only one user path, making negligible interference on other users and thus rendering a "pseudo-wired" abstraction of the wireless links [71].

User multiplexing: in an indoor picocell that has one access point (AP) and a number of users, it is assumed that the AP can multiplex users in fast time by illuminating beams to users one at a time, as in Fig. 43. Recently, the concept and analysis of beamscanning capability of graphene-based antannas at THz have been presented [29], which however did not specify the scanning frequency. Following the notably property that graphene conductivity can be easily tuned by electric field effect [29] [92], taking one step further we reasonably envision that in all-graphene devices, beams can be switched at nearly pulse-level with sufficiently small switching time.

Energy control: in THz Band, the transceiver has limited capabilities in power control and coherent detection. Thus, we assume all pulses have the same power. Further, we assume transmitter pulse shaping is not practical because of too much overhead and channel state information (CSI) aging is severe due to poor transmitter self-coherence. It is also assumed that receiver equalization is not practical because signal processing takes too much time compared with the time scale of Terahertz signal. Coherent receivers require correlators, suffering from burden of channel estimation for large antenna arrays and synchronization errors. Because of these assumptions, we consider an energy detection (ED) receiver that collects energy from the pulses. Thus, the AP controls the transmission-energy by modulating the number of repeated pulses to users.

7.2 THz Pulse-level beam-switching with energy control (TRPLE)

In this section, we describe the principles of the proposed THz Pulse-level Beam-switching with Energy control (TRPLE), designed upon the emitter and detector as discussed in Section II. We consider a typical indoor picocell, where the access point (AP) communicates

with a group of users. In addition to line-of-sight (LOS) transmission whenever possible, the presence of blockage foresees directed non-LOS (NLOS) transmission [18]. In this context, we present the MAC protocol to solve three problems: (1) neighbor discovery, (2) transmission scheduling, and (3) energy control.

7.2.1 Pulse-level Beamscanning Neighbor Discovery

The purpose of neighbor discovery in the THz network is to identify users along with the best beam direction to reach them. The best direction should be along the direct path in the LOS case and the strongest path in the NLOS case. Similar to [71] [93] , we assume that nodes are placed on a two-dimensional plane, and we do not consider variation in the beam pattern over the elevation angle. We expect that typically communication does not occur over the whole sphere, and infrequent activities can be solved by localization schemes.

Following a spatial scan-based approach, the AP points the thin beam rotationally into all possible directions. Existing works for narrow-band systems require the beam to dwell in one direction sending an entire packet and waiting for the acknowledgment, before being able to steer to another direction, incurring substantial delay. In contrast, ultrashort-pulse modulation in THz opens the door to pulse-level beam-switching, in which scanning is interleaved in pulse. Fig. 43 depicts the scanning process, where different beam directions are illuminated by beams of different colors. The key benefit is the abilities to scan all directions in one packet time, thanks to the interleaved pulses destined to different directions.

We note that there is a minimum requirement on the pulse separation for the same direction (user), T_s, as in Fig. 43. Firstly, the pulse separation T_s must be larger than the delay spread (DS) of the channel. The DS is a function of both multipath DS and DS caused by molecular absorption. With the considered narrow beamforming, the multipath part is quite diminished. The pulse separation must be long enough to allow echoes from one pulse to die off at the target user before the next pulse arrives. One-hundred-femtosecond-long first-order derivative of Gaussian pulse is assumed.

Fig. 44 shows the signal to inter-symbol interference ratio (SIR) varied over different

pulse separations in terms of the number of pulse lengths, where the inter-symbol interference accounts for 120 precursor pulses and 120 postcursor pulses. The SIR increases as the pulse separation increases, and exceeds 10 dB for all distances from 1 m to 10 m, when the pulse separation is 100 times of pulse length. Thus, with a safe margin we assume $T_s = 100T_p = 10$ picoseconds. Further, we validate T_s by looking at the total number of directions. Assuming 5^o degree beam-width, minimum 72 beams are required to cover all possible directions, and this number is less than 100 - the maximum number of pulses within T_s.

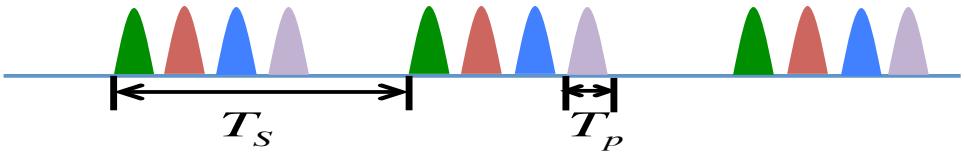

Figure 43. llustration of pulse-level beam-switching.

During scanning, users acquire the best beam towards them. In next packet time, users feedback to the AP using a thin beam in the same interleaved fashion as in the AP scanning phase, For each user, the start time of sending its first pulse is according to the beam index corresponding to the direction it receives from. After feedback, the AP builds an occupancy cache table in its own memory, which is one-to-one mapping of user's ID and its beam direction. Since it is not necessary that all directions are occupied, the AP then allocates transmission sequence for the users, which will synchronize to their allocated time slot.

7.2.2 Transmission Scheduling and Energy Control

In THz networks, MAC protocols mainly focus on "scheduling," as opposed to conventional "fighting for access." Tailored to the pulse generator and energy detection receiver, MAC also performs "energy control" by deciding the number of pulses needed to reach the users. Note that a receiver at far distance may need to collect energy from more than one pulse to decode a bit "1."

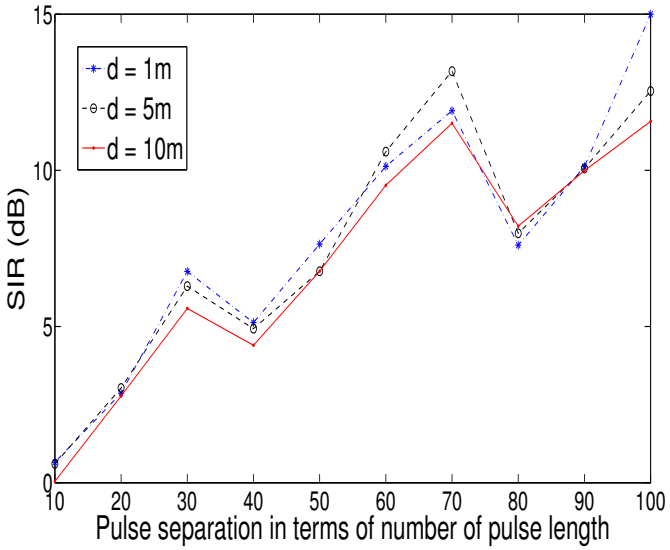

Figure 44. Signal to inter-symbol interference ratio v.s. Pulse separation

7.2.2.1 Energy Control

In the downlink (DL), to guarantee a certain received single-to-noise ratio (SNR), the AP controls the transmission energy by modulating the number of repeated pulses N, which is user dependent. In particular, N depends on the transmit-receiver (TR) separation d, LOS or NLOS path, total path length r, and angle of incidence ψ, i.e., $N = func\{d, \text{LOS/NLOS}^1, r, \psi\}$. More details will be presented in Section IV. Similar arguments apply to the uplink (UL) transmission, where users control the number of pulses sent to the AP.

7.2.2.2 Frame Structure

As in Fig. 45, a MAC frame is composed of a POLL period, a DL period and a UL period. During the POLL period, the AP learns the traffic demand of the users and then schedules the DL and UL transmissions. As an illustrative example in Fig. 45, all the three users have DL demand, while only User 2 and User 3 have UL demand; the far user (User 1) requires 4 pulses to decode "1," while the middle user (User 2) and the near user (User 3) require 2 and 1 pulses to decode "1," respectively. In this particular example, the data rate ratio

[1]Whether a path is LOS or NLOS can be practically learned by, among others, the polarization diversity approach [94].

among the three users is 1 : 2 : 4. We present general analyses for the data rates in next section.

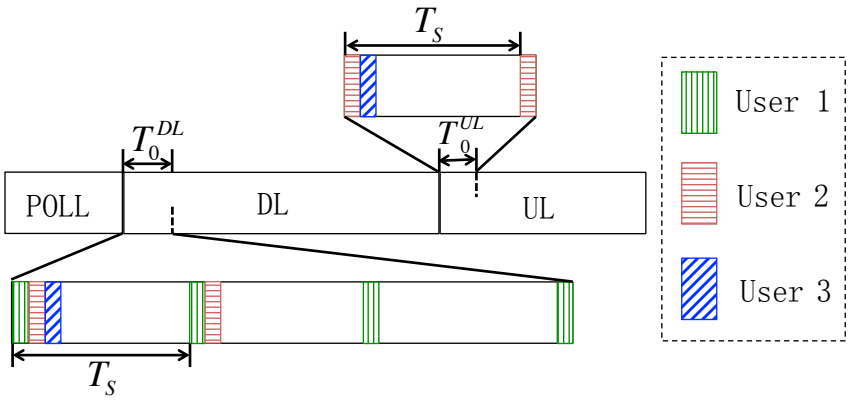

Figure 45. MAC frame structure.

7.3 Stochastic Analysis of TRPLE

In this section, we present stochastic analyses to quantify the data rate of an arbitrary user and the network throughput achievable under TRPLE. In this section, we focus on the downlink analysis.

We assume that the transmitter generates a Gaussian pulse [30], which can be expressed as

$$p(t) = \frac{A_0}{\sqrt{2\pi}\sigma} e^{-(t-t_0)^2/(2\sigma^2)}. \tag{59}$$

The power spectrum density (PSD) of the n-th[2] derivative of a Gaussian pulse is given by

$$S^{(n)}(f) = A_0^2 (2\pi f)^{2n} e^{-(2\pi\sigma f)^2}. \tag{60}$$

7.3.1 LOS/NLOS Channel Model

We first present our channel model. Extending the LOS model in [70], we consider both LOS and NLOS. The PSD of the channel is given by

$$|H(f,\psi,r)|^2 = \left(\frac{c}{4\pi f r}\right)^2 e^{-k(f)r} L(f,\psi), \tag{61}$$

[2]The first derivative is used in this section.

where the term $\left(\frac{c}{4\pi fr}\right)^2$ is the spreading loss, c is the speed of light, f is the frequency, r is the total path length, $e^{-k(f)r}$ is the molecular absorption loss originated from the excitation of molecular by EM waves at specific frequency computed by the Beer-Lamber Law. Detailed calculation of $k(f)$ can be found in [70]. In Eq. 61, $L(f,\psi)$ is the rough surface reflection loss that characterizes the loss in the case of NLOS, and is expressed as

$$L(f,\psi) = \begin{cases} \rho^2_{rough}(f,\psi) & \text{if NLOS,} \\ 1 & \text{if LOS.} \end{cases} \tag{62}$$

$\rho_{rough}(f,\psi)$ is the reflection coefficient, which depends on the frequency f and the angle of incidence ψ. According to Kirchhoff theory, the reflection coefficient of a rough surface can be obtained as the product of the smooth surface reflection and the Rayleigh roughness factor, as follows

$$\rho_{rough}(f,\psi) = \rho_{smooth}\exp\left[-2\left(2\pi\frac{f}{c}\sigma_h \sin\psi\right)^2\right], \tag{63}$$

where, ρ_{smooth} is the reflection coefficient if the surface were smooth, σ_h is the standard deviation of the height distribution, and, ψ is the angle of incidence.

Without loss of generality, consider the Transverse Electric (TE) part of the EM wave, the smooth surface reflection coefficient is derived from the Fresnel equations:

$$\rho_{smooth} = \frac{\cos\psi - \sqrt{n_t^2 - \sin(\psi)}}{\cos\psi + \sqrt{n_t^2 - \sin(\psi)}}, \tag{64}$$

where n_t is the refractive index. In this section, we use the measured results σ_h = 0.05e-3 and $n_t = 1.922 + 0.057\,j$ [95].

7.3.2 Energy Modulation and Conditional Data Rate

We next determine the number of pulses that a given user of total path length r requires to successfully detect the symbol. First, the received signal power of a single pulse is given by

$$P_0(r,\psi) = \int_B S^{(1)}(f)\left(\frac{c}{4\pi fr}\right)^2 e^{-k(f)r} L(f,\psi)\,\mathrm{d}f. \tag{65}$$

Then, accounting for the antenna array gain, G_T and G_R, the received signal power of total N_p pulses is given by

$$P(r, \psi) = N_p G_T G_R P_0(r, \psi). \tag{66}$$

On the other hand, the noise power is obtained as

$$W(r) = \int_B N_o(f, r) \mathrm{d}f = k_B \int_B T_{noise} \, \mathrm{d}f, \tag{67}$$

where k_B stands for Boltzmann constant, and T_{noise} refers to the equivalent noise temperature.

Hence, the minimum number of pulses to guarantee an decoding threshold θ is determined as

$$N_p(r, \psi) = \min_n \{n : \frac{P(r)}{W(r)} \geq \theta\} = \left\lceil \frac{\theta K_B \int_B T_{noise} \, \mathrm{d}f}{G_{tx} G_{rx} \int_B S^{(1)}(f, r) (\frac{c}{4\pi f r})^2 e^{-k(f) r} L(f, \psi) \, \mathrm{d}f} \right\rceil. \tag{68}$$

Accordingly, the maximum data rate conditioned on the total path length r and angle of incidence, ψ, is obtained as

$$\Upsilon(r, \psi) = \frac{1}{T_s N_p(r, \psi)}. \tag{69}$$

Note that in the case of LOS, ψ is NULL.

7.3.3 Data Rate of An Arbitrary User

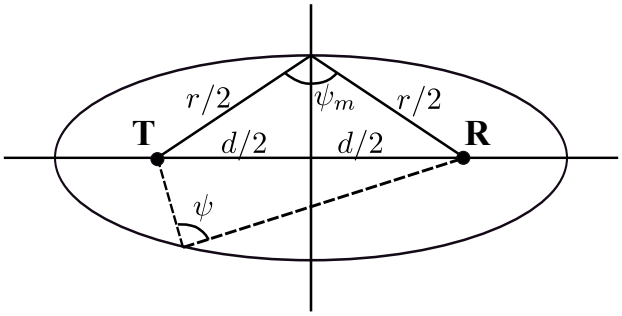

Figure 46. Illustration of angle of incidence, given d and r.

We now consider the data rate conditioned on T-R separation d. In the LOS case, $r = d$. In the NLOS case ($r > d$), the propagation time τ_i of the NLOS path is larger than the

LOS propagation time τ_0, which equals to d/c. We can introduce a maximum path delay, τ_m such that $\tau_0 \leq \tau_i < \tau_m$, and assume that reflectors are uniformly distributed in space. Conditioned on the T-R separation d, the probability distribution function (PDF) of the normalized total path delay τ, i.e., sum of the incident path and the reflected path, is given by [96]

$$f_{\hat{\tau}}(\hat{\tau}|d) = \frac{2\hat{\tau}^2 - 1}{\beta\sqrt{\hat{\tau}^2 - 1}}, \quad 1 \leq \hat{\tau} < \hat{\tau}_m, \tag{70}$$

where $\beta = \hat{\tau}_m\sqrt{\hat{\tau}_m^2 - 1}$, and $\hat{\tau}_m = \tau_m/\tau_0 = \tau_m c/d$. The total path length r is linearly proportional to $\hat{\tau}$, $r = \hat{\tau}d$. Therefore, the PDF of the total path length is obtained as

$$f_r(r|d) = \frac{2(r/d)^2 - 1}{d\beta\sqrt{(r/d)^2 - 1}}, \quad d \leq r < \hat{\tau}_m d. \tag{71}$$

We now consider the rate of User i, conditioned on d, by averaging over r and ψ. The conditional mean of the rate is given by

$$\mathbb{E}\left[\Upsilon_i|d\right] = p_0\mathbb{E}\left[\Upsilon_i^{(0)}|d\right] + p_1\mathbb{E}\left[\Upsilon_i^{(1)}|d\right], \tag{72}$$

where, the expectations are taken over r and ψ, the first component represents the case that user i is a LOS user, and, the second component, a NLOS user. p_0 and p_1, which are related to shadowing, are the probabilities of being a LOS or a NLOS user.

In the LOS case, $r = d$. Thus, we have

$$\mathbb{E}\left[\Upsilon_i^{(0)}|d\right] = \Upsilon_i^{(0)}(d). \tag{73}$$

In the NLOS case, we have

$$\mathbb{E}\left[\Upsilon_i^{(1)}|d\right] = \int_d^{\tau_m c} f_r(r|d)\int_0^{\psi_m} f_\psi(\psi|r,d)\Upsilon_i^{(1)}(r,\psi)\,\mathrm{d}\psi\,\mathrm{d}r. \tag{74}$$

We assume that the angle of incidence is uniformly distributed between 0 and the maximum ψ_m, given (d, r), i.e.,

$$f_\psi(\psi|r,d) = \begin{cases} \dfrac{1}{\psi_m} & 0 \leq \psi \leq \psi_m, \\ 0 & \text{otherwise}, \end{cases} \tag{75}$$

where $\psi_m = \arcsin(d/r)$, as illustrated in Fig. 46.

Finally, we substitute (73) (74) into (72).

Remark: p_0 and p_1 can be determined by log-normal distribution with a threshold, similar to the shadowing model. Using the cumulative distribution function (CDF) of a log-normal random variable $\ln\mathcal{N}(\mu, \sigma^2)$, we get

$$p_0 = 1 - p_1 = \frac{1}{2}\text{erfc}\left(-\frac{\ln x_0 - u}{\sigma\sqrt{2}}\right), \tag{76}$$

where erfc$(\cdot)$ is the complementary error function, and x_0 is the threshold determining whether the beam is LOS or NLOS.

7.3.4 Throughput of a THz Network

Taking the stochastic geometry approach, we assume that users are distributed according to a Poisson point process (PPP), with intensity λ. Thus, the number of users inside any bounded region $A \in \mathbb{R}^{dim}$, $N(A)$, follows the Poisson distribution

$$\mathbb{P}[N(A) = k] = \frac{(\lambda A)^k e^{-\lambda A}}{k!}. \tag{77}$$

In a PPP network, consider the ith user, which is ith nearest neighbor to the AP. The distance between User i and the AP (T-R separation) follows the generalized Gamma distribution

$$f_{D_i}(d) = d^{2i-1}(\lambda\pi)^i \frac{2}{\Gamma(i)} e^{(-\lambda\pi d^2)}, \quad d \geq 0. \tag{78}$$

Then, averaging over the distribution of d yields

$$\mathbb{E}[\Upsilon_i] = \int_0^{d_m} f_{D_i}(d)\mathbb{E}[\Upsilon_i|d]\ \mathrm{d}d. \tag{79}$$

With some straightforward manipulations, we have

$$\mathbb{E}[\Upsilon_i] = \int_0^{d_m} (X + YZ)\,\mathrm{d}d, \tag{80}$$

where,

$$X = p_0 f_{D_i}(d)\Upsilon_i^{(0)}(d) \tag{81}$$

$$Y = \frac{p_1 f_{D_i}(d)}{\tau_m c \sqrt{\tau_m^2 c^2 - d^2}} \tag{82}$$

$$Z = \int_d^{\tau_m c} \frac{2r^2 - d^2}{\sqrt{r^2 - d^2} \arcsin(d/r)} \int_0^{\arcsin(d/r)} \Upsilon_i^{(1)}(r, \psi) \, \mathrm{d}\psi \, \mathrm{d}r \tag{83}$$

As the AP performs user multiplexing in the downlink by illuminating beams to users one at a time, the network throughput is the summation of rates of the scheduled users. Finally, the network throughput can be expressed as

$$\Upsilon = \sum_{k=1}^{K} \left\{ \mathbb{P}\left[N(A) = k\right] \sum_{i=1}^{k} \mathbb{E}\left[\Upsilon_i\right] \right\}, \tag{84}$$

where K is a sufficiently large number.

7.4 Numerical Results

In this section, we present numerical results for the achievable data rate of a single arbitrary user. As THz communication relies on directional transmission through a LOS path or a directed NLOS path, we evaluate two types of users separately. The main parameters used in the numerical evaluation are as follows: the pulse length is 100 femto-seconds, the per-pulse energy is 100 femto-joules, the noise power is -75 dBm, the decoding SNR threshold is 20 dB, and the antenna gains are $G_T = G_R = 35$ dB or 40 dB.

Fig. 47 - Fig. 49 show the data rates of the LOS and NLOS users. In Fig. 47, the data rates of a LOS user are plotted versus different LOS distances $d \in$ [1m, 60m]. As the distances increase, the overall path loss surges and thus the data rates show a decreasing trend. The curve is not smooth because of the ceiling operator in Eq. (68). Specifically, at 1 m $< d <$ 23 m, the data rate is 100 Gbps, while the data rates reduce sharply to 50 Gbps, 33 Gbps and 25 Gbps for distances of 24 m $< d <$ 32 m, 33 m $< d <$ 38 m, and 39 m $< d <$ 43 m, respectively. The rate is constant at 100 Gbps at near distances (1 m $< d <$ 23 m) because the strongly frequency selective channel requires a minimum separation of consecutive pulses to the same user, and also because pulse-based modulation

has maximum 1bit/symbol. Although theoretically, more advanced modulation (such as MQAM) may increase the date rate on an order of magnitude, compact THz radios that support those modulation are not foreseen to exist in the very near future.

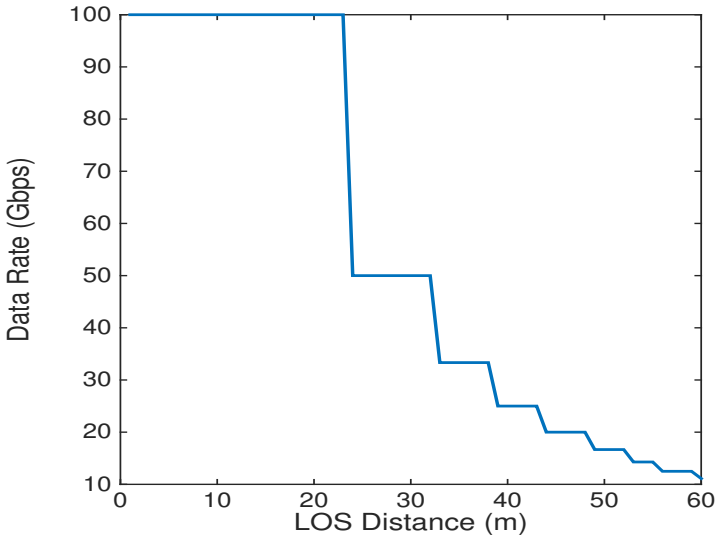

Figure 47. LOS user (antenna gain 35dB).

Fig. 48 shows the data rates of NLOS users as a function of total path length r and the angle of incidence (AOI) ψ, with antenna gain (AG) of 35 dB. The rates dwindle with increased distance, and depend on the AOI. Under the same path length r, larger AOIs incur less reflection loss and thus allow higher rates. Also, it is observed that the rates are less sensitive to AOIs as the distance increases. Specifically, with 35 dB AG, only users at 6 m and nearer can support the rate of 100 Gbps. Among other methods, using larger AG to increase rates is more practical than increasing pulse power, considering Graphene-based compact large antenna arrays.

Comparing Fig. 48 and Fig. 49,, with 5 dB increase in AG, even the users at 20 m can support at least 50 Gbps. Meanwhile, the users nearer than 17 m can always achieve 100 Gbps regardless of the AOI. Again, the non-smoothness of the curves in Fig. 48 and Fig. 49 is due to the ceiling operator in Eq.(68).

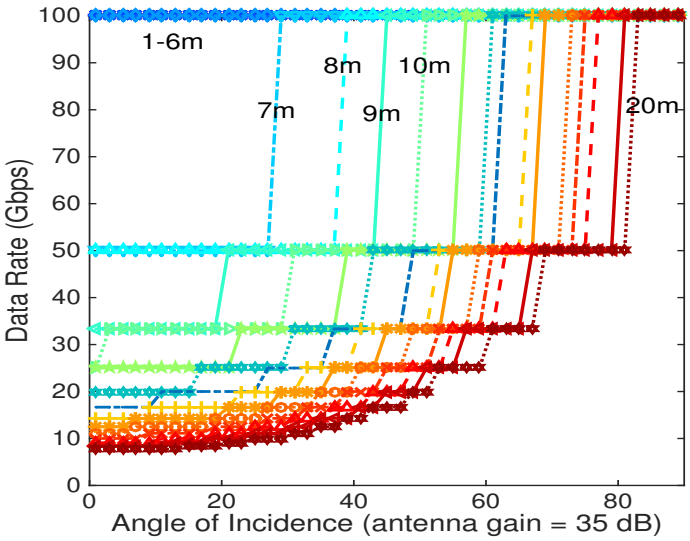

Figure 48. NLOS user (antenna gain 35dB).

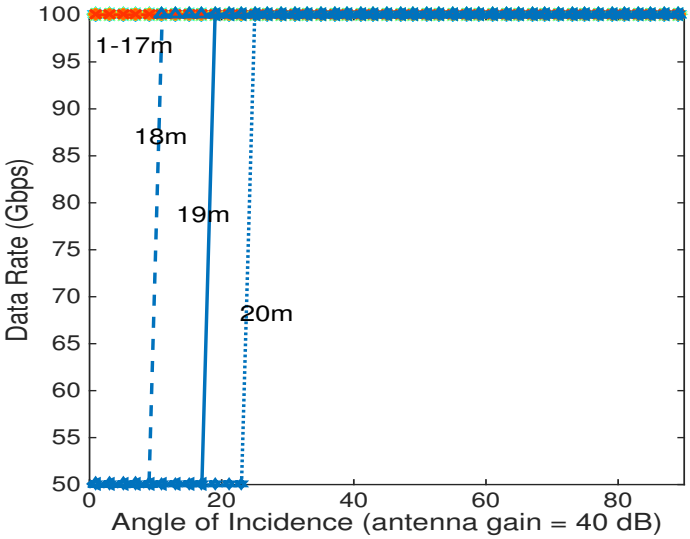

Figure 49. NLOS user (antenna gain 40dB).

7.5 Conclusions

We present the first MAC protocol (TRPLE) to enable "macro-scale" communication in Terahertz networks. Tailored to THz channel and the expected capability of THz radios, TRPLE utilizes "pulse-level" beam-switching of compact large Graphene-antenna arrays to perform transmission through either the line-of-sight (LOS) path or the directed NLOS path. Assuming "pseudo-wired" THz wireless links, TRPLE solves neighbor discovery and

transmission scheduling with fast interleaved pulse beams, and controls the transmission-energy according to users' locations. For the downlink, analytical study is presented to evaluate the achievable data rates of an arbitrary user as well as the network throughput. We found that the minimum pulse separation at the receiver to avoid inter-symbol interference, which is defined by the molecular absorption of THz channel, limits the single-user data rate to 100 Gbps.

CHAPTER 8

TRPLE OPTIMIZATION

The Terahertz Pulse-level Beam-switching MAC with Energy control (TRPLE) proposed in Chapter 7 provides the data rate up to 100 Gbps for an arbitrary user. The ceiling rate at 100 Gbps is limited by the defined minimum "pulse separation" to tolerate the delay spread predominately caused by the molecular absorption of THz channel. However, considering the energy detection receiver, the inter-symbol interference (ISI) does not always cause destructive effects; this leaves us a degree of freedom to optimize the pulse separation while maintaing the desired received energy. In this chapter, we present an enhanced design by optimizing the pulse separation, in terms of the inter-pulse separation (IPS) and the inter-symbol separation (ISS). Following a review of the previous pulse separation design, we then optimize IPS and ISS by evaluating the received symbol energy numerically, because of the lack of a closed form expression for the THz channel. Though it is possible to jointly optimize the IPS and the ISS, for simplicity we opt to optimize them sequentially.

8.1 Previous Design of TRPLE

The previous design for TRPLE in Chapter 7 does not optimize the inter-pulse separation (IPS) and inter-symbol separation (ISS); it simply applies same separation to multi-pulse users, i.e., the IPS always equals 100 times of the pulse-width and there is no distinction between ISS and IPS in Chapter 7. Fig. 50 depicts the single pulse user (green) and the two-pulse user (red), where for the green user, 4 symbols "1" are shown, and for the red user, a symbol "1" and a symbol "0" are shown. The pulse separation of 100 is selected to guarantee that the signal to interference ratio (SIR) requirement is met, i.e., $SIR \geq 12$ dB, for a one-pulse user. The universal pulse separation of $100T_p$ reduces the complexity at the receiver, especially for synchronization, at the expense of suboptimal throughput due to the lack of optimization over inter-pulse separation.

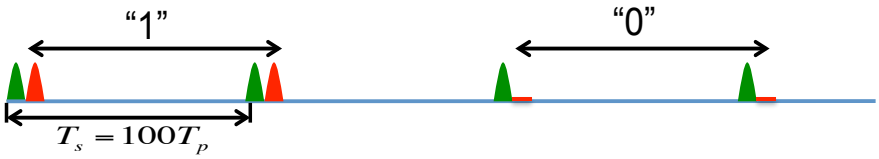

Figure 50. Illustration of the single pulse user (green) and the two-pulse user (red)

8.2 Optimization of IPS and ISS

In this chapter, we aim to reduce the IPS for a multi-pulse user and ISS by numerically evaluating the received energy as a function of IPS and ISS.

8.2.1 Illustration of IPS and ISS

The IPS and ISS are illustrated in Fig. 51 and Fig. 52. Recall that for a single-pulse user a symbol “1” is represented by a pulse followed by a time gap to accommodate the delay spread, such that the pulse and the gap define the ISS, and a symbol “0” is represented by the absence of a pulse. In Fig. 51, for the single pulse user, the ISS is the symbol period. Fig. 52 depicts the multiple pulse user scenario (2, in this example), where a single “1” symbol is represented by 2 pulses separated by the inter-pulse separation (IPS) as shown in Fig. 52, similar to the ISS in the single-pulse user. The symbol “0” for the two-pulse user is the same length as the symbol “1”, but contains no pulses.

Figure 51. Illustration of the single pulse user, 2 symbol-“1” (green), and 2 symbol-“0” (red)

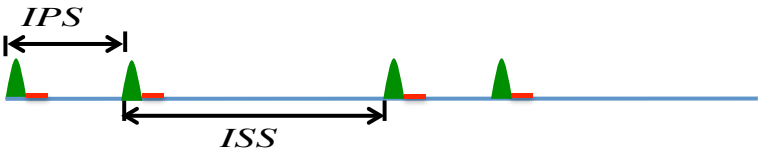

Figure 52. Illustration of the multiple pulses user, 2 symbol-“1” (green), and 2 symbol-“0” (red)

In our considered picocell with maximum range of 10m, the relationship between the number of pulses and the served distance in the LOS case is displayed in Table. 4. Thus

in the following discussions, we will mainly show the results for users that require up to 3 pulses to successfully decode.

Table 4. Number of Pulse v.s. Distance Served

Number of pulses	Distances (AG = 35 dB)	Distances (AG = 40 dB)
1	1 - 23 m	1 - 65 m
2	24 - 32 m	66 - 88 m
3	33 - 38 m	89-105 m

8.2.2 Receiver Model

In THz communications, among other types of modulation, femtosecond-long pulse-based modulation has been proposed to capture the expected capabilities of THz signal generator and detectors [30]. Within this context, a receiver architecture must have ultra compact size, ultra-low power and ultra-low complexity. Following this trend, we assume that the received signal is the superposition of the transmitted pulse responses, i.e., we assume a linear receiver. Due to practical considerations, it is assumed that each pulse incurs a random independent pulse jitter, τ_k, at the receiver. In particular, we make the following assumption regarding the randomness of the jitter:

a.1) Uniformly distributed from 0 to 10% pulse-width, i.e., $\tau_k \in (0, 0.1T_p), \forall k$

a.2) One Pulse-width T_p captures 95% of the pulse energy E_p

a.3) All pulses within a symbol jitter independently, i.e., τ_k, are independent

a.4) Each symbol has independent jitter

According to above assumptions, the received signal in the absence of ISS is denoted as

$$S(t) = \sum_{k=0}^{N-1} P(t + kT_{IPS} + \tau_k) * h(t) \tag{85}$$

where $P(t)$ is the first derivative of a Gaussian pulse, $h(t)$ is the transfer function of the THz channel, N is the number of the pulses within a symbol, T_{IPS} is the inter-pulse separation, and τ_k are independent uniformly distributed jitter for each pulse within a symbol.

Then, the received energy considering ISS can be expressed as

$$E_{RX}^{\text{w/ ISI}} = \int \left(\sum_{q=0}^{M} S(t + qT_{ISS}) \right)^2 dt \tag{86}$$

where T_{ISS} represents the inter-symbol separation, and M is a large number (e.g., 50) representing the number of interfering symbols.

8.2.3 Optimization of IPS

In this section, we evaluate the the normalized received symbol energy, R_n, as a function of the inter-pulse separation (IPS). The R_n is defined as the ratio between the received symbol energy with ISI and the received symbol energy without ISI. Clearly, a choice of IPS that is smaller but just large enough to allow $R_n \approx 1$ is desirable.

$$R_n = \frac{E_{RX}^{\text{w/ ISI}}}{E_{RX}^{\text{w/o ISI}}} \tag{87}$$

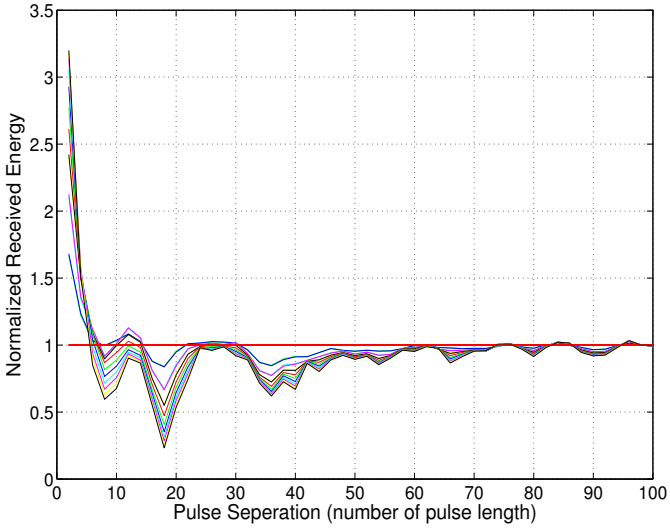

Figure 53. 5% **Percentile of Normalized RX Symbol Energy v.s. IPS**

Fig. 53 shows the 5% percentile of the normalized received symbol energy as the IPS increases, that is 5% of the trials have energy below the plotted curves, i.e., 95% percent of the cases are above the curves; each curve represent a different distance that is among [8m, 20m]. The IPS of $100T_p$ at the right end of the figure is the choice of TRPLE in

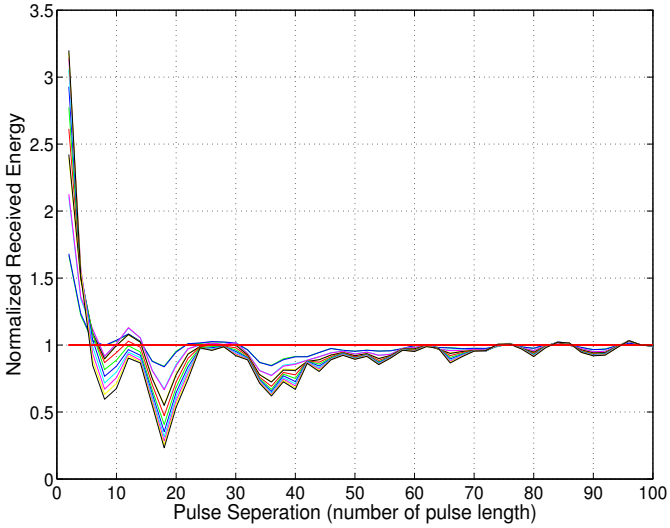

Figure 54. Average Normalized RX Symbol Energy v.s. IPS

Chapter 7. Fig. 54 shows the average over all the trials. Comparing Fig. 53 and Fig. 54, we note that the difference between the average and the 5% percentile is minimum.

From Fig. 53 and Fig. 54, it is also observed that for pulse separation larger than a half pulse length, the curves are almost overlapping. This suggests that the normalized received symbol energy is less sensitive to the distance, and the choice of IPS is independent of the locations of the users. An implication to the MAC layer is that the MAC layer does not need to manage IPS for each individual user, instead it can use the same IPS for all the users in the considered distance range.

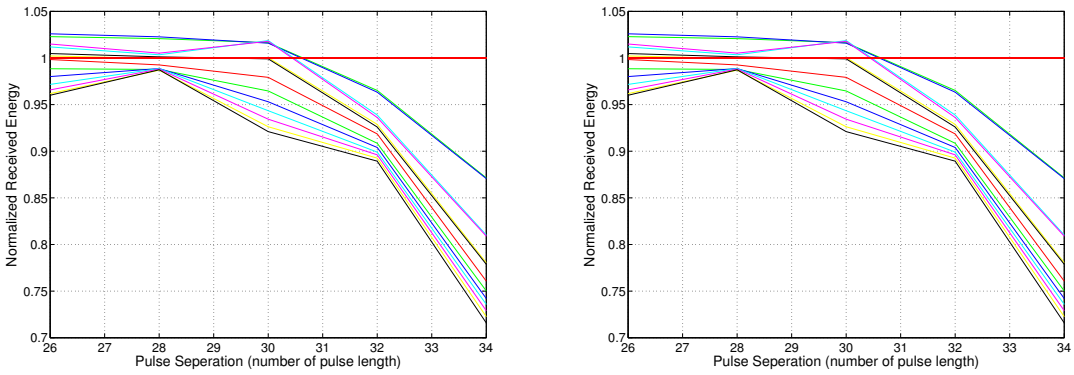

(a) Zoomed-in 5% Percentile (b) Zoomed-in Average

Figure 55. Zoomed-in plots of Normalized RX Energy v.s. IPS

We observe that the normalized received symbol energy still approaches "1", even at the IPS around $30T_p$, cutting the $100T_p$ by two thirds. To give an specific choice, Fig. 55 zooms in Fig. 53 and Fig. 54 in a small range of IPS centered around $30T_p$, from which we can choose IPS as $28T_p$. This means the received symbol energy when IPS equals $28T_p$ is comparable to that when PS equals $100T_p$ as chosen in Chapter 7. Moreover, for some distances, the normalized received symbol energy exceeds "1"; this is because the ISI combines constructively so that the received symbol energy is higher than when ISI is not present.

8.2.4 Optimization of ISS

Based on the optimized inter-pulse separation, we next aim to reduce the inter-symbol separation (ISS) for all users that require two or more pulses to decode. To motivate the necessity and show the feasibility for reducing the ISS, Fig. 56 illustrates the received pulses (red curves) of a two-pulse user and the leakage from the previous pulses (blue curves), for different cases of ISS, i.e., ISS = 100 and ISS = 50. As compared in Fig. 56(a) and Fig. 56(b), the magnitude of the leakage does not show noticeable increase as the ISS decreases by half (i.e., from 100 to 50). It is also seen that the RX pulse waveforms are noise-like. Therefore, we can reduce ISS without incurring too much interference, because RX pulse autocorrelation resembles white noise autocorrelation.

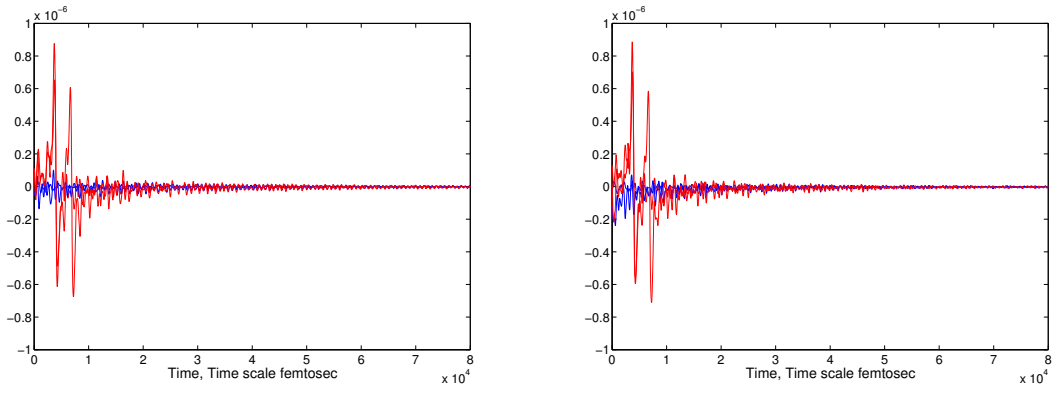

(a) ISS = 100 pulse-width (b) ISS = 50 pulse-width

Figure 56. Illustration of received pulses of a two-pulse user and interference from leakage.

To determine the optimal ISS, we next define two criteria, as follows

(1) Normalized Energy (NE) Criterion

$$R_n = \frac{E_{RX,1}^{\text{w/ ISI}}}{E_{RX,1}^{\text{w/o ISI}}} \approx 1 \tag{88}$$

(2) Signal to Interference Ratio (SIR) Criterion

$$SIR \approx \frac{E_{RX,1}^{\text{w/ ISI}}}{E_{RX,0}^{\text{w/ ISI}}} \geq SIR_{th} \tag{89}$$

The normalized energy (NE) criterion as shown in Eq. (88) ensures that the received symbol "1" energy is comparable to that when ISI is absent. The signal to interference ratio (SIR) criterion as shown in Eq. (89) ensures that the SIR exceeds a certain threshold in order to successfully decode. Note that the denominator is (89), $E_{RX,0}^{\text{w/ ISI}}$, is the received symbol "0" energy, which is equivalent to the ISI, because symbol "0" is transmitted as silence. Also note that when Eq. (88) is satisfied, $\frac{E_{RX,1}^{\text{w/ ISI}}}{E_{RX,0}^{\text{w/ ISI}}} = \frac{E_{S+I}}{E_I} \approx \frac{E_S}{E_I} = \text{SIR}$. Therefore, we would prefer a choice of ISI that meets both criteria.

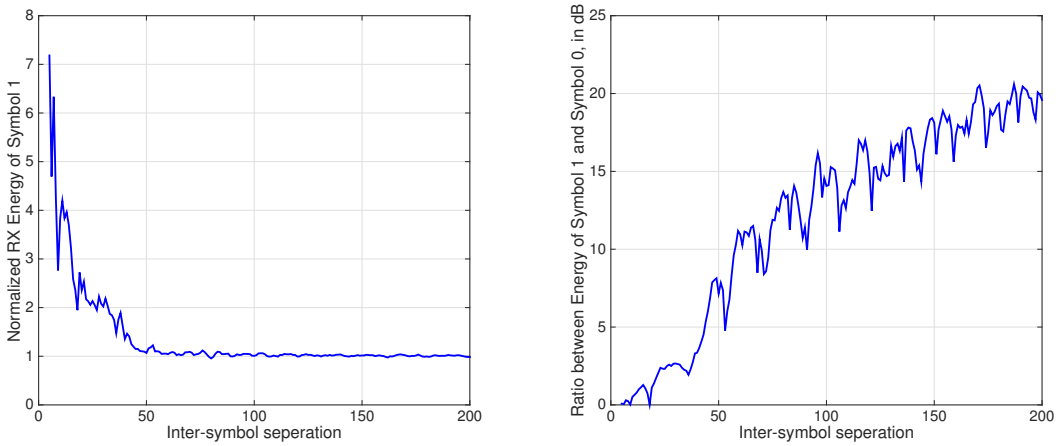

(a) $R_n = \frac{E_{RX,1}^{\text{w/ ISI}}}{E_{RX,1}^{\text{w/o ISI}}}$ (b) $SIR \approx \frac{E_{RX,1}^{\text{w/ ISI}}}{E_{RX,0}^{\text{w/ ISI}}}$

Figure 57. 1-pulse user: R_n, *SIR* v.s. ISS.

Fig. 57 shows, for the 1-pulse user, the trends of the normalized received symbol "1"

energy (R_n) in dB and the signal to interference ratio (SIR) in dB as the inter-symbol separation (ISS) increases. It is observed that when we select ISS as $60T_p$, both the NE criterion and the SIR criterion have been met.

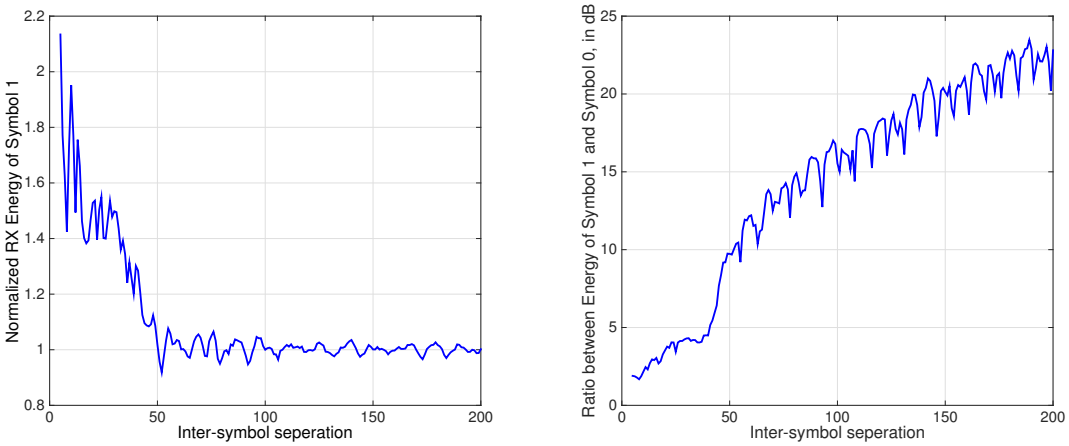

(a) $R_n = \frac{E_{RX,1}^{\text{w/ ISI}}}{E_{RX,1}^{\text{w/o ISI}}}$ (b) $SIR \approx \frac{E_{RX,1}^{\text{w/ ISI}}}{E_{RX,0}^{\text{w/ ISI}}}$

Figure 58. 2-pulse user: R_n, *SIR* v.s. ISS.

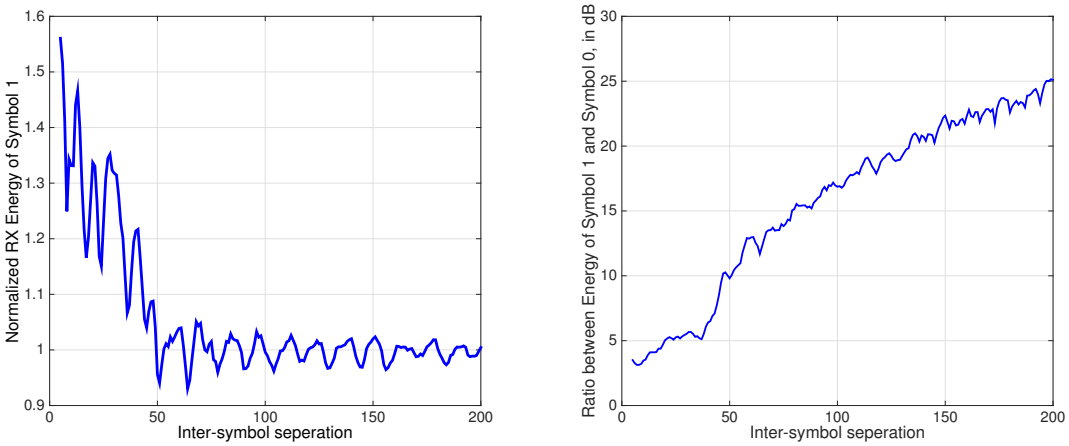

(a) $R_n = \frac{E_{RX,1}^{\text{w/ ISI}}}{E_{RX,1}^{\text{w/o ISI}}}$ (b) $SIR \approx \frac{E_{RX,1}^{\text{w/ ISI}}}{E_{RX,0}^{\text{w/ ISI}}}$

Figure 59. 3-pulse user: R_n, *SIR* v.s. ISS.

The cases for the 2-pulse user and the 3-pulse user are shown in Fig. 58 and Fig. 59, respectively. Similar to the arguments above, for both the 2-pulse user and the 3-pulse user, we can select ISS as $60T_p$, same as the 1-pulse user.

Users that require more than 3 pulses are those that are NLOS and thus utilize the strongest reflect path for communication. Similar numerical analysis have been performed, and same arguments as above still apply to the NLOS users.

In summary, after the optimization steps of IPS and ISS, we select, $IPS = 28T_p$ and $ISS = 60T_p$.

8.3 MAC Protocol Design

8.3.1 Data Transmission Scheduling

Due to the separate considerations for IPS and ISS, the transmission scheduling in the MAC needs some revision from the previous TRPLE design in Chapter 7. As mentioned in Section 8.2.3, IPS of around $30T_p$ are preferable; to relax the synchronization requirement, the MAC will choose $IPS = 30T_p$, and $ISS = 60T_p = 2IPS$. Therefore, the transmission channel can be devided into 30 sub-channels; each sub-channel is composed of equally spaced (with $30T_p$) pulse "*virtual positions*." The 30 sub-channels relate to each other by shifting in time in the units of pulse-width.

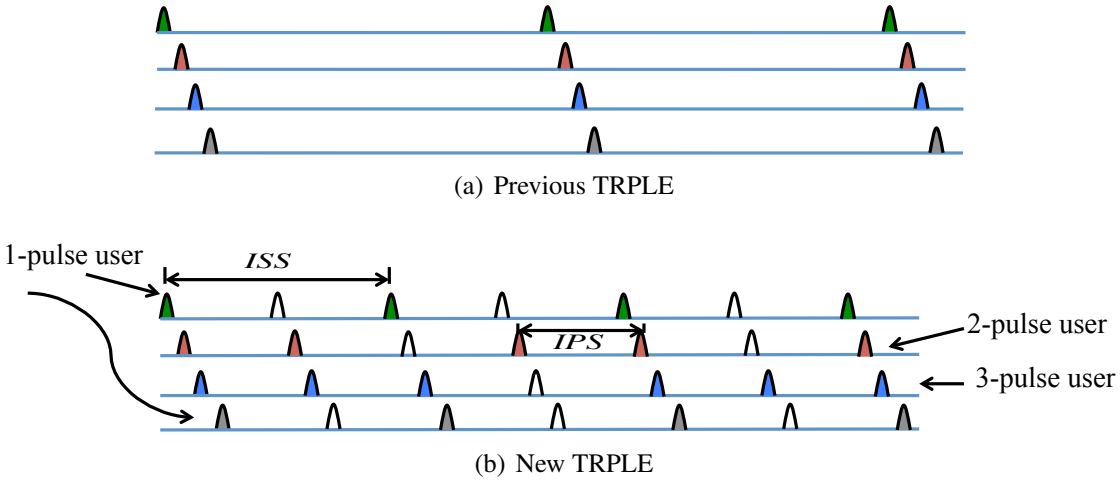

Figure 60. Comparison of MAC layer transmission scheduling.

Fig. 60 gives an example of the data transmission for 4 users, i.e., two 1-pulse users, one 2-pulse user and one 3-pulse user, where Fig. 60(a) represents the previous design, and Fig. 60(b) illustrates the new transmission scheduling that tailors to the optimized IPS

and ISS. As compared in Fig. 60 in the same time scale, the new MAC data transmission gains greater efficiency against the previous design, thanks to the reduced IPS and ISS. In particular, Fig. 60(b) depicts 4 sub-channels. All sub-channels are shifted in different time slots. Commonly, each sub-channel is characterized by equally spaced pulse "*virtual positions*", and the "filled" pulses denote actual transmission (symbol "1" or "0"). Note that users that require different number of pulses have different "filled" pattern.

8.3.2 Beam Acquisition

It is seen from Section 8.3.1 that beam acquisition is required before the data transmission may begin. The mission of beam acquisition is to identify users along with the best beam direction to reach them. Our previous design follows a spatial scan-based approach, where the AP points the narrow beam rotationally into all possible directions. Assuming nodes are placed on a two-dimensional plane and assuming 5^o narrow beam, 72 directions need to be scanned. The beam-width in scanning phase is the same as in data phase. Since $100T_p$ was taken as the minimum pulse separation, these 72 directions can be scanned within the interval of two consecutive pulses destined to the same direction. However, since both the AP and the users use thin beams this method suffers from long scanning time especially when there are only a few number of users. Also, these directions can not be completely scanned in the interval of the new IPS, which is only $30T_p$. In addition, to incorporate 3D scanning yet to keep the scanning time low, in this section we will take different beam-widths for scanning and data, respectively.

One question is how wide should the beams be? Fig. 61 shows beam-width selection schemes for scanning and data transmission. Specifically, Fig. 61(a) shows one possible beam orientation, where three radios are shown to have approximate alignment with the AP. After the coarse alignment, a refinement process can be used to allow the pairs to achieve better alignment and narrow their beams to have higher gain, as shown in Fig. 61(c). Note that the concept of the two-stage scanning process is similar to other methods in 60 GHz, such as [93]. The notable difference of TRPLE-based scanning is that packets for different

users are interleaved in pulse, i.e., scanning for all the directions are done in one packet time, as opposed to concatenated packet transmission in conventional directional schemes.

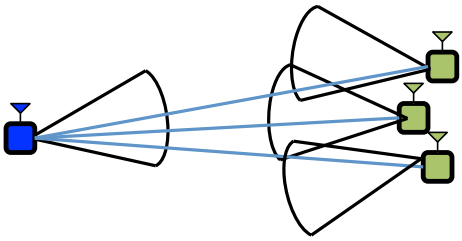

(a) Single broader beam at the AP for users acquisition.

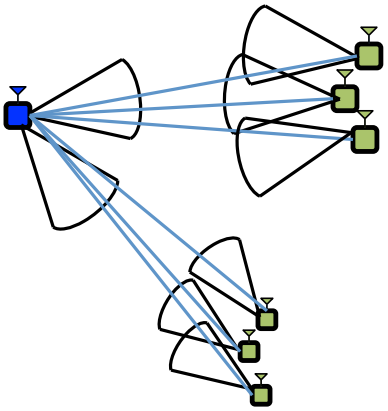

(b) Multiple broader beams at the AP for users acquisition.

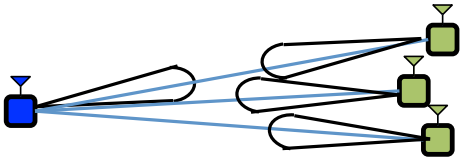

(c) Full alignment and narrow beam for data transmission.

Figure 61. Beam-width selection schemes for scanning and data.

Enabled by Graphene antenna subarrays, multiple steered beams would increase the probability of the coarse beam alignment, as shown in Fig. 61(b). We consider this unique feature for the AP, which can afford the complexity of higher number of subarrays than a user. In this example, the AP can discover two "clusters" of users at the same time by forming two broader beams. The non-aligned radios could switch their beam positions again, so more pairs could become aligned approximately. After that, the beam refinement

process within the coarse direction range will be initiated until the AP is accurately aligned with each of the user, i.e, using all subarrays to form one beam.

Beam-scanning can be sequential or randomized, and there exists a tradeoff between user acquisition complexity and communication robustness, in terms of beam-width choice. This topic is out of the scope of this chapter, and related discussion about this issue can be found in existing studies [93] [97].

8.4 Numerical Results

In this section, we present numerical results for the optimized design for TRPLE, in terms of the achievable data rates of an arbitrary single user. We evaluate LOS users and NLOS users separately. As in Chapter 7, the main parameters used in the numerical evaluation are as follows: the pulse length is 100 femto-seconds, the per-pulse energy is 100 femto-joules, the noise power is -75 dBm, the decoding SNR threshold is 20 dB, and the antenna gains (AG) are $G_T = G_R = 35$ dB or 40 dB.

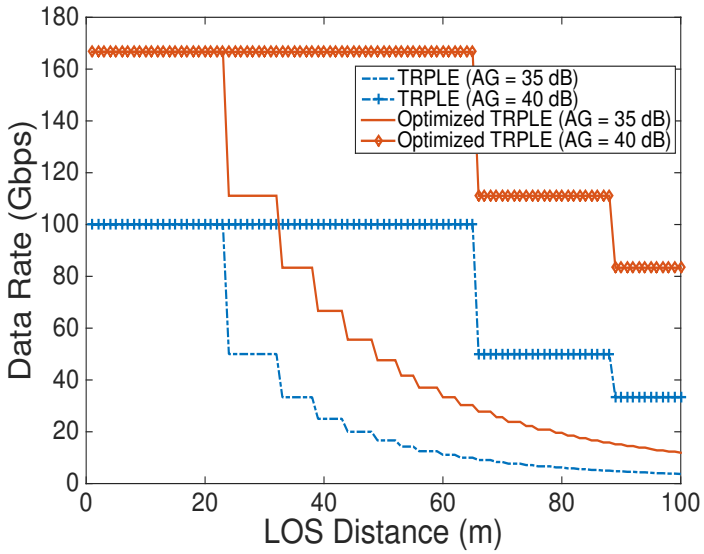

Figure 62. LOS user.

Fig. 62 shows the data rates of LOS users as a function of the distance, for both TRPLE and its optimization with antenna gains (AG) of 35 dB or 40 dB. With the optimized TRPLE, at antenna gain of 40 dB, the users at 65 m and nearer achieve the data rate of 167

Gbps, which is 67% improvement over the maximum rate in the TRPLE without IPS/ISS optimization. This rate is constant due to the selection of inter-symbol separation (ISS) and that all users need only 1 pulse to decode. On the other hand, with a smaller AG of 35 dB, the dates show a faster decreasing trend with distance. However, the optimized TRPLE (red curves) provides improved data rates compared with TRPLE without IPS/ISS optimization; the improvement ratio increases as the distance increases. For example, at AG of 40 dB, the rate improvement is 67% at 1 m $< d <$ 65 m, 122% at 66 m $< d <$ 88 m, and, 150% at 89 m $< d <$ 100 m. This is because the reduction in symbol duration increases as the number of pulses within a symbol increases. The curves are non-smooth due to the ceiling function in Eq. (68) that forces the number of pulses to be an integer.

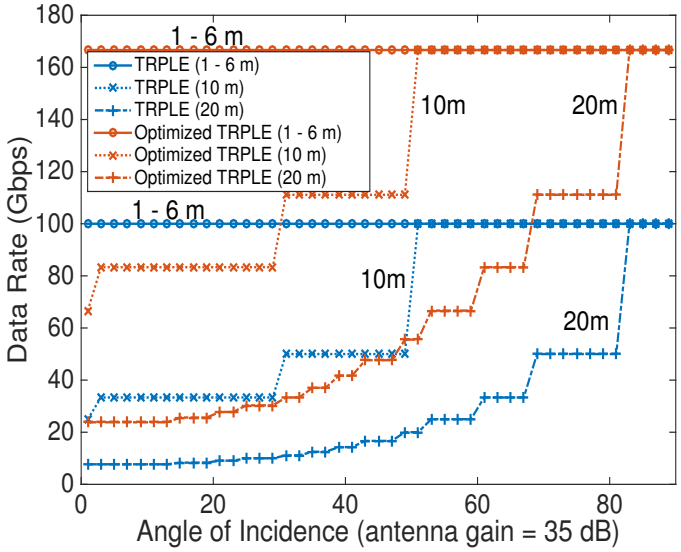

Figure 63. NLOS user data rates (antenna gain 35 dB).

Fig. 63 shows the data rates of NLOS users as a function of total path length r and the angle of incidence (AOI) , with antenna gain of 35 dB. Similar to what we have observed for the previous TRPLE design in Chapter. 7, the data rates decrease with increased distance, and depend on the AOI, where larger AOIs allow higher rates due to less reflection loss. Again, the non-smoothness of the curves in Fig. 63 is due to the ceiling operator in

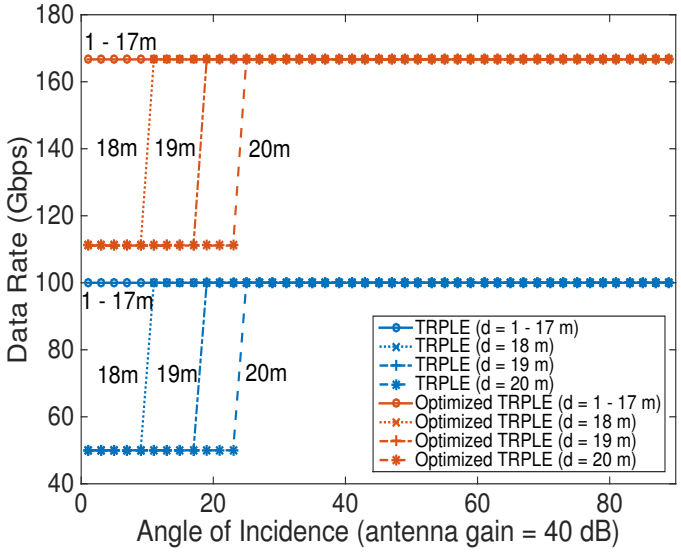

Figure 64. NLOS user data rates (antenna gain 40 dB).

Eq. (68). The users at 6 m or nearer can achieve the maximum date rate (167 Gbps). Moreover, the data rates for NLOS users also benefit from IPS/ISS optimization for the TRPLE protocol. To quantify the the improvement ratio with IPS/ISS optimization, we observe a range of 67% to 210% improvement compared with TRPLE without optimization. In addition, longer distance users experience higher improvement ratios.

With higher antenna gain, at 40 dB, Fig. 64 depicts the data rates of NLOS users with different distance and AOI. It is observed that the higher antenna gain significantly reduces the variability of the data rates for both the distance and the AOI. Under optimized TRPLE, users at 17 m and nearer achieve the maximum data rate of 167 Gbps. Moreover, the NLOS users experience the minimum rate of 111 Gbps when the distance is 20 m.

8.5 Conclusions

Careful design of the inter-pulse separation (IPS) and inter-symbol separation (ISS) are essential to the data rate performance of pulse-based Terahertz communication. In this chapter, we optimize the IPS and ISS by defining several criteria and numerally evaluating the impacts of those parameters. In particular, we define the normalized energy criterion and SIR criterion to justify that at $IPS = 30T_p$ guarantees comparable received energy as

$IPS = 100T_p$, and that $IPS = 60T_p$ provides sufficiently high SIR. The revisions of TR-PLE MAC protocol have been presented to explore the reduced IPS and ISS. In addition, different beam acquisition schemes based on pulse interleaving have been discussed. Numerical results show that considering 20 meters range the maximum data rate of 167 Gbps can be achieved for the majority of users, while the minimum of 111 Gbps is guaranteed as the worst case.

CHAPTER 9

CONCLUSIONS AND SUGGESTED FUTURE WORKS

This dissertation has focused on designing and analyzing novel medium access control (MAC) protocols for two types of wireless networks: (1) duty-cycling cooperative multi-hop wireless sensor networks (MHWSNs), and (2) single-hop Terahertz networks (TeraNets). For MHWSNs, the specific contributions include alleviating the "energy-hole" problem with an on-demand scheduling MAC (OSC-MAC) that combines cooperative transmission (CT) and duty cycling, and developing a comprehensive analytical framework that considers MAC in multi-hop settings both without and with CT. For TeraNets, the contributions include the MAC protocol (TRPLE), which captures the peculiarities of THz Band channel and takes advantage of electrical beam-steering capabilities of large antenna arrays. In Sections 9.1, 9.2 and 9.3, we review the most important claims of the dissertation. The suggested future works are listed in Section 9.4.

9.1 Scalable Scheduling Duty Cycle MAC (OSC-MAC) for Multi-hop Multi-flow WSNs

We have designed the first scalable on-demand scheduling duty cycle cooperative MAC protocol (OSC-MAC) that incorporates both energy conserving (*duty cycling*) and energy balancing (*cooperative transmission*) schemes to overcome the "energy hole," the general problem that limits the lifetime of a Multi-hop wireless sensor networks.

- Existing MAC protocols have not sufficiently enhanced the lifetime of a multi-hop WSN due to their inability to solve the "energy-hole" problem. The proposed OSC-MAC addresses the spatio-temporal challenges of performing CT in an asynchronous duty cycling network.

- OSC-MAC shows scalability in various network scenarios including concurrent multi-hop multi-flow traffic, random and grid topologies, with and without a mobile Sink.

Even with control packet energy accounted for, OSC-MAC still produces about 80%–200% longer lifetime, compared with the state-of-the-art MAC protocols, in all the considered multi-hop network scenarios.

- While all the MAC protocols we considered benefitted in terms of lifetime from the mobility of the Sink, OSC-MAC benefits most, because of its flexibility in duty cycle schedules.

- We further obtained the following two insights regarding lifetime of multi-hop WSNs, by investigating both lifetime and energy efficiency for different routing protocols jointly with the MAC. First, we found a general example that a seemingly advantageous routing algorithm evaluated without consideration of the MAC) does not necessarily lead to better lifetime, mainly because the MAC layer captures many complex aspects of energy consumption besides transceiving, including collision, overhearing and idle listening, while analysis of a routing scheme typically examines only transmission and reception energy consumption. Second, energy efficiency and lifetime should be jointly considered to quantitatively evaluate a WSN, because a general example shows that, for a network under different protocols, the significant difference in lifetime may not be inferred from the energy efficiency (in terms of energy consumption per packet); the latter may appear indistinguishable even under different protocols.

9.2 Unified Analytical Model for Multi-hop EC and EH WSNs

We created a Markovian decision process (MDP) framework for analysis of multihop wireless sensor networks (MHWSNs) to bound the network performance of both energy constrained (EC) networks and energy harvesting (EH) networks, both with and without relay cooperation.

- The model provides the fundamental performance limit that a MHWSN can theoretically achieve, under the general constraints from medium access control (MAC), routing, and energy harvesting.

- Existing studies have been limited to point-to-point transmission, single-hop networks without routing, or multi-hop networks that overlook MAC costs; in contrast, the proposed model encompasses these protocol aspects including MAC link admission, packet transfers between sensors, energy consumption and replenishment, and cooperative transmission.

- We observe that the analyses for EC and EH networks fall into two branches of MDP theory, which are finite-horizon processes and infinite-horizon processes, respectively. The performance metrics for EC and EH networks are different. For EC networks, an appropriate metric is the network lifetime; for EH networks, an appropriate metric is, e.g., the network throughput. The model is flexible enough to allow formulating different performance metrics. To efficiently solve the models with high dimension, for the EC networks, we propose a novel computational algorithm by taking advantage of the stochastic shortest path (SSP) structure of the problem; for the EH networks, we propose a dual linear programming (DLP) based algorithm by considering the sparsity of the transition matrix.

- Under the unified MDP framework, numerical results demonstrate the impact of the different network parameters, such as packet arrival rate, energy harvesting rate etc., on the optimal network performance. The analyses also show the advantages of cooperation for the optimal performance, in both EC and EH networks.

9.3 Pulse-level Beam-Switching MAC with Energy Control (TRPLE) for Picocell TeraNets

We presented the first joint PHY/MAC design and stochastic analysis with directional MAC for THz networks that relies on pulse-level beam-switching and pulse repetition for energy control (TRPLE).

- Existing directional MACs for cellular, broad-band, and WIFI based multi-hop wireless networks operating at lower radio frequency bands cannot be used for TeraNets, because they do not capture the peculiarities of the THz channel. With a focus on "macro-scale" communication in TeraNets, TRPLE utilizes time-division pulse interleaving for both beam acquisition and data transmission.

- Our system design is based on the advancements in Graphene-based electronics, including the novel plasmonic nano-antennas, compact plasmonic pulse generators and detectors, and nano-antenna arrays with scanning capability. Specially, two aspects distinguish TRPLE form existing studies. First, TRPLE explores "pulse-level" beam-switching to point to all directions in one packet time, whereas existing protocols dwell the beam in one direction for an entire packet time before switching to another. Second, TRPLE focuses on pulse-based transmission scheduling due to the "pseudo-wired" nature of THz channel and the expected capabilities of THz devices, as opposed to channel contention and interference management in existing studies.

- To our knowledge, pulse-based directional transmission has not been explored in system design in THz networks and the implications of pulse-level beam-switching on the upper layer protocols have not been investigated before this dissertation. Filling this gap, the TRPLE protocol solves neighbor discovery transmission scheduling and energy control, while capturing the peculiarity of THz channel (we extend the existing LOS channel to include both LOS and NLOS channel) and the expected THz transceiver capabilities.

- Our design is the first work to optimize the inter-pulse separation (IPS) and inter-symbol separation (ISS) in pulse-based THz communication. We found the optimal IPS and ISS using normalized received energy criterion and SIR criterion. Under our assumptions the numerical results show that considering a 20 meters range TRPLE provides the maximum data rate of 167 Gbps for the majority of users, while the minimum of 111 Gbps is guaranteed as the worst case.

9.4 Suggested Future Works

The following is a list of several interesting open problems that are topics for future research.

1. Further optimization for TRPLE. The current TRPLE design is particularly suitable when the number of users is smaller than the available TDMA slots. When the number of users is large, one option that may avoid lowering the data rate is to explore "1"s only channel allocation. The reasoning is as follows: in the current TRPLE design, a) a beam points to a direction even if it is transmitting "silence," and b) the receiver does not distinguish whether the beam is transmitting "silence" or simply pointing to another direction. Therefore, under "1"s only channel allocation, the beam points to a direction only if "1" is supposed to be transmitted, otherwise, the beam can serve another direction if "0" is supposed to be transmitted. Though this is a novel way of statistical time-division multiplexing scheme in pulse level, intelligent synchronize scheme should be carefully devised.

2. Usage of reflective mirror. Due to the high reflective loss of indoor materials, we propose to design and use a reflective mirror mounted on the ceiling as supplementary to LOS propagation. There is typically clearance between the ceiling and the tops of the partitions, which enables an approach where a ceiling-mounted AP steers a very narrow beam parallel to the ceiling, hitting a ceiling-mounted mirror with facets. A strategically placed mirror would reflect the beam in a downward direction to the

receiver. The challenges reside in acquiring the receiver location through the mirror reflection, which could be obtained through a MAC protocol able to learn the location and steer the beam to the strongest NLOS path.

3. Utilization of relay nodes. In the small-cell systems, there might be obstacles between a source and a destination. Resorting to relay nodes to translate direct transmission into multi-hop transmissions is an option, as in 60 GHz MACs. In contrast to traditional relay communication even in 60 GHz, the highly directional beams in THz Band system poses new challenges for relay selection, nodes transmission and reception alignment. The above ideas about adapting beamwidth to scanning and communication will be jointly considered with a relay scheme. Also the controls of the coverage by different routing options will be investigated in the context of relay communication.

BIBLIOGRAPHY

[1] I. Akyildiz, W. Su, Y. Sankarasubramaniam, and E. Cayirci, "Wireless sensor networks: a survey," *Computer Networks*, vol. 38, no. 4, pp. 393 – 422, 2002.

[2] J. Li and P. Mohapatra, "An analytical model for the energy hole problem in many-to-one sensor networks," *in Proc. IEEE VTC*, 2005.

[3] W. Ye, J. Heidemann, and D. Estrin, "An energy-efficient MAC protocol for wireless sensor networks," *in Proc. IEEE INFOCOM*, 2002.

[4] "IEEE Std 802.11b-1999 (R2003)," *LAN/MAN Standards Committee of the IEEE Computer Society, IEEE-SA Standards Board*, 2003.

[5] Y. Sun, S. Du, O. Gurewitz, and D. B. Johnson, "DW-MAC: a low latency, energy efficient demand-wakeup MAC protocol for wireless sensor networks," *in Proc. ACM MobiHoc*, 2008.

[6] J. W. Jung and M. A. Ingram, "Residual-Energy-Activated Cooperative Transmission (REACT) to Avoid the Energy Hole," *in Proc. IEEE ICC*, pp. 1–5, 2010.

[7] J. N. Laneman, D. N. C. Tse, and G. W. Wornell, "Cooperative diversity in wireless networks: Efficient protocols and outage behavior," *IEEE Trans. Information Theory*, vol. 50, no. 12, pp. 3062–3080, 2004.

[8] J. W. Jung and M. A. Weitnauer, "On using cooperative routing for lifetime optimization of multi-hop wireless sensor networks: Analysis and guidelines," *IEEE Trans. Commun.,*, no. 99, pp. 1–11, 2013.

[9] V. Sharma, U. Mukherji, V. Joseph, and S. Gupta, "Optimal energy management policies for energy harvesting sensor nodes," *Wireless Comm., IEEE Trans. on*, vol. 9, no. 4, pp. 1326–1336, 2010.

[10] Z. Wang, A. Tajer, and X. Wang, "Communication of energy harvesting tags," *Communications, IEEE Transactions on*, vol. 60, pp. 1159–1166, April 2012.

[11] Y. Chen, Q. Zhao, V. Krishnamurthy, and D. Djonin, "Transmission Scheduling for Optimizing Sensor Network Lifetime: A Stochastic Shortest Path Approach," *IEEE Trans. Signal Processing*, vol. 55, pp. 2294 –2309, may 2007.

[12] H. Jung, Y. J. Chang, and M. A. Ingram, "Experimental range extension of concurrent cooperative transmission in indoor environments at 2.4ghz," in *MILCOM*, 2010.

[13] J. Lin and M. A. Ingram, "SCT-MAC: A Scheduling Duty Cycle MAC protocol for Cooperative Wireless Sensor Networks," *in Proc. ICC*, June 2012.

[14] J. W. Jung and M. A. Ingram, "Using range extension cooperative transmission in energy harvesting wireless sensor networks," *Communications and Networks, Journal of*, vol. 14, no. 2, pp. 169–178, 2012.

[15] J. Lin and M. A. Ingram, "OSC-MAC: Duty Cycle Scheduling and Cooperation in Multi-hop Wireless Sensor Networks," *in Proc. IEEE WCNC*, April 2013.

[16] S. Cherry, "Edholm's law of bandwidth," *Spectrum, IEEE*, vol. 41, no. 7, pp. 58–60, 2004.

[17] M. Koch, "Terahertz communications: A 2020 vision," in *Terahertz Frequency Detection and Identification of Materials and Objects* (R. Miles, X.-C. Zhang, H. Eisele, and A. Krotkus, eds.), NATO Science for Peace and Security Series, pp. 325–338, Springer Netherlands, 2007.

[18] R. Piesiewicz, T. Kleine-Ostmann, N. Krumbholz, D. Mittleman, M. Koch, J. Schoebel, and T. Kurner, "Short-range ultra-broadband terahertz communications: Concepts and perspectives," *Antennas and Propagation Magazine, IEEE*, vol. 49, no. 6, pp. 24–39, 2007.

[19] J. Federici and L. Moeller, "Review of terahertz and subterahertz wireless communications," *Journal of Applied Physics*, vol. 107, no. 11, pp. 111101–111101–22, 2010.

[20] K.-C. Huang and Z. Wang, "Terahertz terabit wireless communication," *Microwave Magazine, IEEE*, vol. 12, no. 4, pp. 108–116, 2011.

[21] I. F. Akyildiz, J. M. Jornet, and M. Pierobon, "Nanonetworks: a new frontier in communications," *Communications of the ACM*, vol. 54, no. 11, pp. 84–89, 2011.

[22] R. Choudhury, X. Yang, R. Ramanathan, and N. Vaidya, "On designing mac protocols for wireless networks using directional antennas," *Mobile Computing, IEEE Transactions on*, vol. 5, no. 5, pp. 477–491, 2006.

[23] R. Ramanathan, J. Redi, C. Santivanez, D. Wiggins, and S. Polit, "Ad hoc networking with directional antennas: a complete system solution," *IEEE JSAC*, vol. 23, no. 3, pp. 496–506, 2005.

[24] T. Korakis, G. Jakllari, and L. Tassiulas, "Cdr-mac: A protocol for full exploitation of directional antennas in ad hoc wireless networks," *Mobile Computing, IEEE Transactions on*, vol. 7, no. 2, pp. 145–155, 2008.

[25] J. Pujol, J. Jornet, and J. Pareta, "Phlame: A physical layer aware mac protocol for electromagnetic nanonetworks," in *INFOCOM Workshops*, pp. 431–436, 2011.

[26] M. Tamagnone, J. Gomez-Diaz, J. R. Mosig, and J. Perruisseau-Carrier, "Reconfigurable terahertz plasmonic antenna concept using a graphene stack," *Applied Physics Letters*, vol. 101, no. 21, p. 214102, 2012.

[27] W. Knap, F. Teppe, N. Dyakonova, D. Coquillat, and J. Łusakowski, "Plasma wave oscillations in nanometer field effect transistors for terahertz detection and emission," *Journal of Physics: Condensed Matter*, vol. 20, no. 38, p. 384205, 2008.

[28] L. Vicarelli, M. Vitiello, D. Coquillat, A. Lombardo, A. Ferrari, W. Knap, M. Polini, V. Pellegrini, and A. Tredicucci, "Graphene field-effect transistors as room-temperature terahertz detectors," *Nature materials*, vol. 11, no. 10, pp. 865–871, 2012.

[29] M. Esquius-Morote, J. Gomez-Diaz, and J. Perruisseau-Carrier, "Sinusoidally modulated graphene leaky-wave antenna for electronic beamscanning at thz," *Terahertz Science and Technology, IEEE Transactions on*, vol. 4, pp. 116–122, Jan 2014.

[30] J. Jornet and I. Akyildiz, "Information capacity of pulse-based wireless nanosensor networks," in *IEEE SECON*, pp. 80–88, June 2011.

[31] J. Polastre, J. Hill, and D. Culler, "Versatile low power media access for wireless sensor networks," *in Proc. ACM SenSys*, pp. 95–107, 2004.

[32] M. Buettner, G. V. Yee, E. Anderson, and R. Han, "X-MAC: a short preamble MAC protocol for duty-cycled wireless sensor networks," *in Proc. ACM SenSys*, vol. 55, no. 11, pp. 307–320, 2006.

[33] Y. Sun, O. Gurewitz, and D. B. Johnson, "RI-MAC: a receiver-initiated asynchronous duty cycle MAC protocol for dynamic traffic loads in wireless sensor networks," in *Proc. of the 6th ACM conference on Embedded network sensor systems*, SenSys '08, pp. 1–14, ACM, 2008.

[34] A. Sendonaris, E. Erkip, and B. Aazhang, "User cooperation diversity. part ii. implementation aspects and performance analysis," *IEEE Trans. Commun.*, vol. 51, no. 11, pp. 1939–1948, 2003.

[35] J. Luo, R. Blum, L. Cimini, L. Greenstein, and A. Haimovich, "Decode-and-forward cooperative diversity with power allocation in wireless networks," *Wireless Communications, IEEE Transactions on*, vol. 6, no. 3, pp. 793–799, 2007.

[36] T. Rappaport, *Wireless Communications: Principles and Practice*. Upper Saddle River, NJ, USA: Prentice Hall PTR, 2001.

[37] L. Badia, M. Levorato, F. Librino, and M. Zorzi, "Cooperation techniques for wireless systems from a networking perspective," *Wireless Communications, IEEE*, vol. 17, no. 2, pp. 89–96, 2010.

[38] P. Liu, Z. Tao, S. Narayanan, T. Korakis, and S. S. Panwar, "CoopMAC: A Cooperative MAC for Wireless LANs," *IEEE J. Sel. Areas in Commun.*, vol. 25, no. 2, pp. 340–354, 2007.

[39] B. Zhao and M. Valenti, "Practical relay networks: a generalization of hybrid-arq," *Selected Areas in Communications, IEEE Journal on*, vol. 23, no. 1, pp. 7–18, 2005.

[40] M. Gokturk, O. Gurbuz, and E. Erkip, "Recomac: A cross-layer cooperative network protocol for wireless ad hoc networks," in *New Technologies, Mobility and Security (NTMS), 2012 5th International Conference on*, pp. 1–7, 2012.

[41] S. Moh and C. Yu, "A Cooperative Diversity-Based Robust MAC Protocol in Wireless Ad Hoc Networks," *IEEE Trans. Parallel and Distributed Systems*, vol. 22, no. 3, pp. 353–363, 2011.

[42] Y. Zhou, J. Liu, L. Zheng, C. Zhai, and H. Chen, "Link-Utility-Based cooperative MAC protocol for Wireless Multi-hop Networks," *IEEE Trans. Wireless Commun.*, vol. 10, no. 3, pp. 995–1005, 2011.

[43] G. Jakllari, S. V. Krishnamurthy, M. Faloutsos, P. V. Krishnamurthy, and Ö. Erçetin, "A framework for distributed spatio-temporal communications in mobile ad hoc networks.," in *INFOCOM*, 2006.

[44] H. Jiao, M. Ingram, and F. Li, "A cooperative lifetime extension mac protocol in duty cycle enabled wireless sensor networks," *in Proc. IEEE MILCOM*, pp. 896 –901, 2011.

[45] X. Wu, G. Chen, and S. K. Das, "Avoiding energy holes in wireless sensor networks with nonuniform node distribution," *Parallel and Distributed Systems, IEEE Transactions on*, vol. 19, no. 5, pp. 710–720, 2008.

[46] L. An-Feng, W. Xian-you, and G. Wei-hua, "Research on energy hole problem for wireless sensor networks based on alternation between dormancy and work," in *Young Computer Scientists, 2008. ICYCS 2008. The 9th International Conference for*, pp. 475–480, 2008.

[47] J. Lian, K. Naik, and G. B. Agnew, "Data capacity improvement of wireless sensor networks using non-uniform sensor distribution," *International Journal of Distributed Sensor Networks*, vol. 2, no. 2, pp. 121–145, 2006.

[48] W. Wang, V. Srinivasan, and K.-C. Chua, "Using mobile relays to prolong the lifetime of wireless sensor networks," in *Proceedings of the 11th annual international conference on Mobile computing and networking*, pp. 270–283, ACM, 2005.

[49] J. Lian, L. Chen, K. Naik, T. Otzu, and G. Agnew, "Modeling and enhancing the data capacity of wireless sensor networks," *IEEE Monograph on Sensor Network Operations*, pp. 91–138, 2004.

[50] A. Kansal, J. Hsu, S. Zahedi, and M. B. Srivastava, "Power management in energy harvesting sensor networks," *ACM Trans. Embed. Comput. Syst.*, vol. 6, Sept. 2007.

[51] M. L. Puterman, *Markov Decision Processes: Discrete Stochastic Dynamic Programming*. New York, USA: John Wiley & Sons., 1994.

[52] F. Iannello, O. Simeone, and U. Spagnolini, "Optimality of myopic scheduling and whittle indexability for energy harvesting sensors," in *Information Sciences and Systems (CISS), 2012*.

[53] D. Niyato, E. Hossain, M. M. Rashid, and V. K. Bhargava, "Wireless sensor networks with energy harvesting technologies: a game-theoretic approach to optimal energy management," *Wireless Communications, IEEE*, vol. 14, no. 4, pp. 90–96, 2007.

[54] L. Qiu, Y. Zhang, F. Wang, M. K. Han, and R. Mahajan, "A general model of wireless interference," in *Proceedings of the 13th Annual ACM International Conference on Mobile Computing and Networking*, MobiCom '07, (New York, NY, USA), pp. 171–182, ACM, 2007.

[55] J.-H. Chang and L. Tassiulas, "Energy conserving routing in wireless ad-hoc networks," *in Proc. IEEE INFOCOM*, vol. 1, pp. 22–31, 2000.

[56] L. Huang and M. J. Neely, "Utility optimal scheduling in energy harvesting networks," in *Proc. of the 12th ACM International Symposium on Mobile Ad Hoc Networking and Computing*, p. 21, ACM, 2011.

[57] M. Bhardwaj and A. Chandrakasan, "Bounding the lifetime of sensor networks via optimal role assignments," in *INFOCOM 2002. Twenty-First Annual Joint Conference of the IEEE Computer and Communications Societies. Proceedings. IEEE*, vol. 3, pp. 1587–1596 vol.3, 2002.

[58] H. Zhang and J. Hou, "On deriving the upper bound of α-lifetime for large sensor networks," in *Proceedings of the 5th ACM international symposium on Mobile ad hoc networking and computing*, MobiHoc '04, (New York, NY, USA), pp. 121–132, ACM, 2004.

[59] W.-J. Huang, Y.-W. Hong, and C.-C. Kuo, "Lifetime maximization for amplify-and-forward cooperative networks," *Wireless Comm., IEEE Trans. on*, vol. 7, no. 5, pp. 1800–1805, 2008.

[60] S. Ikki and M. Ahmed, "Performance analysis of adaptive decode-and-forward cooperative diversity networks with best-relay selection," *Communications, IEEE Trans. on*, vol. 58, no. 1, pp. 68–72, 2010.

[61] J. W. Jung and M. Ingram, "On the Optimal Lifetime of Cooperative Routing for Multi-hop Wireless Sensor Networks," *in Proc. IEEE WCNC*, April 2013.

[62] M. J. Fitch and R. Osiander, "Terahertz waves for communications and sensing," *Johns Hopkins APL technical digest*, vol. 25, no. 4, p. 348355, 2004.

[63] T. Kleine-Ostmann and T. Nagatsuma, "A review on terahertz communications research," *Journal of Infrared, Millimeter, and Terahertz Waves*, vol. 32, no. 2, pp. 143–171, 2011.

[64] "Ieee 802.15 wireless personal area networks-terahertz interest group," .

[65] T. Rappaport, J. Murdock, and F. Gutierrez, "State of the art in 60-ghz integrated circuits and systems for wireless communications," *Proceedings of the IEEE*, vol. 99, pp. 1390–1436, Aug 2011.

[66] F. Alsaadi and J. Elmirghani, "Mobile multigigabit indoor optical wireless systems employing multibeam power adaptation and imaging diversity receivers," *Optical Communications and Networking, IEEE/OSA Journal of*, vol. 3, pp. 27–39, January 2011.

[67] A. Ashok, M. Gruteser, N. Mandayam, J. Silva, M. Varga, and K. Dana, "Challenge: Mobile optical networks through visual mimo," in *Proceedings of the Sixteenth Annual International Conference on Mobile Computing and Networking*, MobiCom '10, (New York, NY, USA), pp. 105–112, ACM, 2010.

[68] J. Lee, Y. Chen, and Y. Huang, "A low-power low-cost fully-integrated 60-ghz transceiver system with ook modulation and on-board antenna assembly," *Solid-State Circuits, IEEE Journal of*, vol. 45, pp. 264–275, Feb 2010.

[69] P.-Y. Chen, C. Argyropoulos, and A. Alu, "Terahertz antenna phase shifters using integrally-gated graphene transmission-lines," *Antennas and Propagation, IEEE Transactions on*, vol. 61, pp. 1528–1537, April 2013.

[70] J. Jornet and I. Akyildiz, "Channel modeling and capacity analysis for electromagnetic wireless nanonetworks in the terahertz band," *Wireless Communications, IEEE Transactions on*, vol. 10, no. 10, pp. 3211–3221, 2011.

[71] R. Mudumbai, S. Singh, and U. Madhow, "Medium access control for 60 ghz outdoor mesh networks with highly directional links," in *INFOCOM 2009, IEEE*, pp. 2871–2875, April 2009.

[72] J. M. Jornet, J. C. Pujol, and J. S. Pareta, "Phlame: A physical layer aware {MAC} protocol for electromagnetic nanonetworks in the terahertz band," *Nano Communication Networks*, vol. 3, no. 1, pp. 74 – 81, 2012.

[73] P. Wang, J. M. Jornet, M. A. Malik, N. Akkari, and I. F. Akyildiz, "Energy and spectrum-aware {MAC} protocol for perpetual wireless nanosensor networks in the terahertz band," *Ad Hoc Networks*, vol. 11, no. 8, pp. 2541 – 2555, 2013.

[74] T. Winter and P. Thubert, "RPL: IPv6 Routing Protocol for Low Power and Lossy Networks," in *draft-ietf-roll-rpl-19*, Sep. 2011.

[75] B. Villaverde, R. De Paz Alberola, S. Rea, and D. Pesch, "Experimental Evaluation of Beacon Scheduling Mechanisms for Multihop ieee 802.15.4 Wireless Sensor Networks," *in Proc.nternational Conference on Sensor Technologies and Applications (SENSORCOMM)*, 2010.

[76] G. Anastasi, A. Falchi, A. Passarella, M. Conti, and E. Gregori, "Performance measurements of motes sensor networks," in *Proceedings of the 7th ACM international*

symposium on Modeling, analysis and simulation of wireless and mobile systems, MSWiM '04, (New York, NY, USA), pp. 174–181, ACM, 2004.

[77] F. Tong, W. Tang, R. Xie, L. Shu, and Y.-C. Kim, "P-MAC: A Cross-Layer Duty Cycle MAC Protocol Towards Pipelining for Wireless Sensor Networks," *in Proc. IEEE ICC, 2011*.

[78] G. Jakllari, S. Krishnamurthy, M. Faloutsos, P. Krishnamurthy, and O. Ercetin, "A cross-layer framework for exploiting virtual miso links in mobile ad hoc networks," *Mobile Computing, IEEE Transactions on*, vol. 6, no. 6, pp. 579–594, 2007.

[79] S. M. Alamouti, "A simple transmit diversity technique for wireless communications," *Selected Areas in Communications, IEEE Journal on*, vol. 16, no. 8, pp. 1451–1458, 1998.

[80] S. Haykin and M. Moher, *Modern Wireless Communication*. Upper Saddle River, NJ, USA: Prentice-Hall, Inc., 2004.

[81] K. Fall, "A delay-tolerant network architecture for challenged internets," *in Proc. SIGCOMM*, 2003.

[82] "Ns2 networks simulator," .

[83] G. Bianchi, "Performance analysis of the ieee 802.11 distributed coordination function," *IEEE J. Sel. Areas in Commun.*, vol. vol.18, pp. pp.535 –547, Mar 2000.

[84] H. Dai and R. Han, "A node-centric load balancing algorithm for wireless sensor networks," in *Global Telecommunications Conference, 2003. GLOBECOM'03. IEEE*, vol. 1, pp. 548–552, IEEE, 2003.

[85] J. Luo, J. Panchard, M. Pirkowski, M. Grossglauser, and J.-P. Hubaux, "Mobiroute: Routing towards a mobile sink for improving lifetime in sensor networks," in *Distributed Computing in Sensor Systems* (P. Gibbons, T. Abdelzaher, J. Aspnes, and R. Rao, eds.), vol. 4026 of *Lecture Notes in Computer Science*, pp. 480–497, Springer Berlin Heidelberg, 2006.

[86] B. Nardelli and E. Knightly, "Closed-form Throughput Expressions for CSMA Networks with Collisions and Hidden terminals," *in Proc. IEEE INFOCOM*, pp. 2309 –2317, march 2012.

[87] F. Liu, J. Lin, Z. Tao, T. Korakis, E. Erkip, and S. Panwar, "The Hidden Cost of Hidden Terminals," *in Proc. IEEE ICC*, vol. vol., no. no., pp. pp.1–6, 2010.

[88] R. Boorstyn, A. Kershenbaum, B. Maglaris, and V. Sahin, "Throughput Analysis in Multihop CSMA Packet Radio Networks," *IEEE Trans. Commun.*, vol. 35, pp. 267 – 274, mar 1987.

[89] V. Bui, W. Zhu, A. Botta, and A. Pescape, "A Markovian Approach to Multipath Data Transfer in Overlay Networks," *IEEE Trans. Parallel and Distributed Sys.*, vol. 21, no. 10, pp. 1398 –1411, 2010.

[90] C. Bron and J. Kerbosch, "Algorithm 457: finding all cliques of an undirected graph," *Commun. ACM*, vol. 16, no. 9, pp. 575–577, 1973.

[91] S. Stidham Jr, "Optimal control of markov chains," in *Computational Probability*, pp. 325–363, Springer, 2000.

[92] Y.-J. Yu, Y. Zhao, S. Ryu, L. E. Brus, K. S. Kim, and P. Kim, "Tuning the graphene work function by electric field effect," *Nano letters*, vol. 9, no. 10, pp. 3430–3434, 2009.

[93] J. Ning, T.-S. Kim, S. V. Krishnamurthy, and C. Cordeiro, "Directional neighbor discovery in 60 ghz indoor wireless networks," *Perform. Eval.*, vol. 68, pp. 897–915, Sept. 2011.

[94] F. Yildirim and H. Liu, "A cross-layer neighbor-discovery algorithm for directional 60-ghz networks," *Vehicular Technology, IEEE Transactions on*, vol. 58, pp. 4598–4604, Oct 2009.

[95] R. Piesiewicz, T. Kleine-Ostmann, N. Krumbholz, D. Mittleman, M. Koch, and T. Kurner, "Terahertz characterisation of building materials," *Electronics Letters*, vol. 41, pp. 1002–1004, Sept 2005.

[96] J. Liberti and T. Rappaport, "A geometrically based model for line-of-sight multipath radio channels," in *Vehicular Technology Conference*, pp. 844–848 vol.2, 1996.

[97] X. An, R. Venkatesha Prasad, and I. Niemegeers, "Impact of antenna pattern and link model on directional neighbor discovery in 60 ghz networks," *Wireless Communications, IEEE Transactions on*, vol. 10, pp. 1435–1447, May 2011.

VITA

Jian Lin received the B.S. degree in Information and Science Engineering from Southeast University, Nanjing, China, in 2007, and the M.S. degree in Electrical and Computer Engineering from Polytechnic Institute of New York University, NY, in 2009. In 2010, he joined Smart Antenna Research Laboratory (SARL) in Georgia Institute of Technology as a graduate research assistant, under the supervision of Prof. Mary Ann Weitnauer (Ingram).

Jian Lin's doctoral research work addressed MAC protocol design and analysis for multi-hop wireless sensor network, and Terahertz network that is envisioned as the key picocell wireless network in the next five to ten years. He was a system engineering intern at Qualcomm, San Diego, CA, in 2013, and a research intern at Intel Labs, Hillsboro, OR, in 2012. During his graduate in Georgia Tech, he was awarded the Management of Technology (MOT) Certificate from Scheller College of Business, in 2015.